Small Soil Column Investigation of Soil-Geotextile Capillary Barrier Systems

by

Nathan Evan Thompson, B.S.

Thesis

Presented to the Faculty of the Graduate School of

The University of Texas at Austin

in Partial Fulfillment

of the Requirements

for the Degree of

Master of Science in Engineering

The University of Texas at Austin

August 2009

Small Soil Column Investigation of Soil-Geotextile Capillary Barrier Systems

Approved by
Supervising Committee:

Jorge G. Zornberg

Robert B. Gilbert

Dedication

To my parents, Jim and Sheila, and my sister, Katie.

Acknowledgements

I would like to thank my advisor, Dr. Jorge Zornberg, for giving me the opportunity to pursue this study and providing support throughout my time at UT. I would also like to thank Dr. Bob Gilbert for reviewing this thesis. Finally, thanks to the Zornberg research group—Ranjiv Gupta, Kuo-Hsin Yang, Jeff Kuhn, Brian Freilich, Michael Plaisted, Julio Zambrano, Yucao Tang, Chris Pickles, Michael Alfortish (honorary) and others—for lending a hand with lab work, talking through a research issue, or even building a shed in the middle of a Texas summer.

August 2009

Abstract

Small Soil Column Investigation of Soil-Geotextile Capillary Barrier Systems

Nathan Evan Thompson, M.S.E.

The University of Texas at Austin, 2009

Supervisor: Jorge G. Zornberg

Geotextiles are often incorporated in engineered structures—including landfill liners and covers, earthen dams, retaining walls, and roads—to perform the separation, filtration, and/or drainage functions. Under unsaturated conditions typical of such structures, a capillary break may form at the interface between soil and geotextile. If the break is unplanned, the resulting build-up of moisture may be detrimental to the structure. Conversely, properly designed geotextile capillary barriers have the potential for many positive applications. Design information, including a complete framework for analysis and an accepted laboratory characterization approach, is lacking. The primary objectives of this study were to investigate geotextile capillary barrier performance with a simple laboratory model and propose a framework for complete analysis of a geotextile capillary barrier life cycle.

Soil columns were designed to allow the formation and breakthrough of a geotextile capillary barrier to be observed. Materials used in the columns were obtained from a capillary barrier system currently under construction at the Rocky Mountain Arsenal in Denver, CO. Hydraulic characterization of the soil and geotextile were performed in the lab. Eleven column tests were completed for this study—soil compaction and applied flow rate were varied to investigate their effect on capillary barrier response. Analysis was approached within a proposed framework covering each stage of a capillary barrier life cycle.

While there was considerable scatter in the test results, important insight was gained. The geotextile capillary barrier performed consistently. Conditions near the interface at breakthrough were similar between tests, regardless of soil compaction or applied flow rate, and were predicted adequately with the laboratory characterization. Storage capacity of the capillary barrier decreased with increasing relative compaction. A framework for analysis, from which the entire capillary barrier response may be modeled, was developed. Application of this model allowed for identification of weaknesses and recommendations for future work.

Table of Contents

List of Tables

List of Figures

Chapter 1: Introduction

1.1 MOTIVATION

Geotextiles are often incorporated in engineering applications to perform the separation, filtration, and/or drainage functions. Typical applications include paved and unpaved roads, landfill liners and covers, earthen dams, and retaining walls. Design information for many of these applications is well documented (Steward et al. 1977, Holtz et al. 1995, Koerner 2005). An important assumption in commonly applied design standards is that soil in contact with the geotextile is fully saturated. However, the engineering applications in which geotextiles are most commonly used are under unsaturated state for a majority of their design life.

Coarse materials such as a sand, gravel, or geotextiles are often placed to aid drainage, either by acting as a filter or providing an increase in total drainage capacity. Under saturated conditions, the coarse material behaves adequately. If the soil is in an unsaturated state, however, the coarse material may create a temporary barrier to water flow. This type of barrier, in which a coarser material impedes flow from an adjacent finer material, is termed a capillary barrier, or capillary break. Unwanted creation of a capillary break can lead to detrimental behavior due to a build-up of moisture, such as instability of a cover system or at the facing of reinforced walls or slopes.

As understanding of the capillary break phenomenon has improved, systems utilizing a capillary barrier as an important aspect of design have become more commonplace. Example applications include landfills, where a capillary barrier may be constructed as part of a cover system to prevent moisture flow from entering underlying

layers, and roadways, where a capillary barrier may be relied upon to prevent frost heave resulting from upward flow of moisture into subgrade material.

Nonwoven geotextiles, with a pore structure similar to that of coarse, uniform gravel, have been shown to be effective in creating a capillary barrier (Iryo and Rowe 2003, Bouazza et al. 2006, Krisdani et al. 2006, Bathurst et al. 2007, McCartney et al. 2005, McCartney et al. 2008). However, little progress has been made in identifying the parameters of a soil-geotextile system that most significantly affect capillary barrier performance. Understanding these parameters is imperative for accurate, efficient design. Using published studies and design procedures currently available, a designer would find it impossible to specify with confidence a particular geotextile product or characteristics of the adjacent soil, e.g., compaction effort and placement water content. While the potential benefits of designing geotextile capillary barriers are being increasingly recognized for applications such as landfill covers and roadways (Gabr et al. 2006, Bouazza et al. 2006a), design information is lacking.

In addition to a lack of standard approach or information for design, there is a major need for simpler, more economically feasible laboratory testing used to characterize capillary barrier performance. While a full-scale field section is currently required by current U.S. regulatory agencies to demonstrate conformance of a proposed alternative landfill cover, i.e., a cover incorporating a capillary barrier, preliminary laboratory testing focused on basic design parameters could be available commercially. Laboratory studies currently found in the literature are too complex and typically not economically feasible due to equipment cost and long testing times.

1.2 RESEARCH OBJECTIVES

Considering the uncertainty in the current state of practice regarding design of geotextile capillary barriers, and the need for improved laboratory characterization and testing methods, the primary objectives of this research project were to:

1) investigate geotextile capillary barrier performance with a simple, more practical test that makes progress toward a commercially feasible setup,
2) develop the framework for a model used to describe the overall process of unsaturated flow, formation of capillary barrier, storage, and breakthrough,
3) investigate the effect of cover soil relative compaction on capillary barrier performance, and
4) investigate the effectiveness of current unsaturated laboratory characterization methods in predicting soil-geotextile capillary barrier behavior.

Laboratory tests were conducted using comparatively small soil columns designed to facilitate observation of the flow of water through a soil profile. As a constant flow rate was applied at the top of the columns, the progression of a moisture front was monitored with sensors taking periodic measurements of volumetric water content. Failure of the capillary barrier, referred to as breakthrough, was detected using a rain gauge tipping bucket placed beneath the column to measure outflow. The columns were designed to model a geotextile capillary barrier that may be constructed as part of a landfill cover system. Soil and geotextiles used for the models tested were obtained from a capillary barrier system in an existing evapotranspirative landfill cover currently under construction in the western United States, at the Rocky Mountain Arsenal in Denver, CO.

A general testing plan was developed to address the research objectives. This testing plan evolved as the project progressed and observations about the column setup lead to variations in setup conditions. The effect of relative compaction on capillary barrier response was investigated. Applied flow rate was varied to gain insight on the testing time required to obtain meaningful results. In addition to gaining insight into flow behavior of a capillary barrier system, analysis of test results also focused on conditions present at breakthrough; namely, soil suction present at the geotextile-soil interface, the vertical profile of volumetric moisture content, and the total storage capacity of the capillary barrier system. Results from the tests also allowed an assessment of the accuracy of available laboratory characterization techniques in predicting capillary barrier performance.

1.3 ORGANIZATION OF THESIS

This thesis is organized into six chapters. Following this introduction, background information is presented in Chapter 2. Geotextiles and their traditional uses are introduced, as is the capillary break phenomenon. Principles of unsaturated hydraulic characterization and their relevance to the prediction of capillary barrier are discussed, and a brief review of previous column testing is given.

Chapter 3 focuses on the materials, methods and instrumentation used as part of the experimental testing program. Properties and characterization of the soil are first presented. Next, an overview of relevant geotextile properties and unsaturated behavior is provided. Details on the design, construction, and use of the columns tested are also included in Chapter 3.

Results from each column test are presented in Chapter 4, and analysis of this data is contained in Chapter 5. Analysis is presented within the framework of a model encompassing each aspect of capillary barrier performance. Experimental results from this testing program are compared to expected results based on the literature whenever possible. Additionally, the expected and observed effect of relative compaction of the overlying soil layer are investigated.

Chapter 6 contains a summary of the work completed as part of this study, conclusions made, a note on the applicability of the results of this study to practice, and recommendations for future research.

Chapter 2: Background Information

Background information relevant to this project's objectives, materials and procedures is presented in Chapter 2. Basic information on geotextiles and their most common, traditional applications are first provided. Next, the capillary break application is introduced. After a discussion of relevant hydraulic characterization principles and methods, the application of this characterization to capillary barriers is presented. Finally, an overview of experimental testing programs similar to that completed as part of this study is presented.

2.1 GEOTEXTILES OVERVIEW

Geosynthetics are defined as planar products manufactured from polymeric material, which are used with soil, rock, or other geotechnical engineering-related material as an integral part of a man-made project, structure, or system (Zornberg and Christopher 2007). Initial uses of "geosynthetics" in North America, early 1900s, consisted of stabilization of roads constructed over soft subgrades in the southern United States with cotton mats. Modern manufacturing techniques make it possible to create polymeric materials with desired characteristics in a quality-controlled environment. This combined with a better understanding of geosynthetic behavior and important design principles has resulted in increased performance and improved cost-effectiveness.

Types of geosynthetics are numerous and continuously changing as new applications are developed in engineering practice. An exhaustive list is not practical, but the most commonly seen geosynthetics are as follows:

- geotextiles
- geomembranes

- geogrids
- geosynthetic clay liners (GCLs)
- geocomposites
- geocells
- erosion control products

This project focuses solely on geotextiles. A geotextile is defined as a permeable geosynthetic made of textile materials. Among the different geosynthetic products, geotextiles are manufactured with the widest range of properties. Their versatility makes them potentially applicable to a large number of applications.

The polymers used in the manufacture of geotextile fibers include the following, listed in order of decreasing use: polypropylene (≈85%), polyester (≈12%), polyethylene (≈2%), and polyamide (≈1%) (Koerner 2005). The most common types of filaments used in the manufacture of geotextiles include monofilament, multifilament, staple filament and slit-film. If fibers are twisted or spun together, they are known as a yarn.

The filaments, fibers, or yarns are formed into geotextiles using either woven or nonwoven methods. Figure 2.1 shows a number of typical geotextiles. Woven geotextiles are manufactured using traditional weaving methods and a variety of weave types: plain weave, basket weave, twill weave and satin weave. Nonwoven geotextiles are manufactured by placing and orienting the filaments or fibers onto a conveyor belt, which are subsequently bonded by needle punching or by melt bonding.

Common terminology associated with geotextiles includes machine direction, cross machine direction, and selvage. Machine direction refers to the direction in the plane of the fabric in line with the direction of manufacture. Conversely, cross machine direction refers to the direction in the plane of fabric perpendicular to the direction of

manufacture. The selvage is the finished area on the sides of the geotextile width that prevents the yarns from unraveling.

Figure 2.1: View of different types of geotextiles

The primary functions of geotextiles have traditionally included separation, filtration, reinforcement, and drainage. A certain geotextile product can perform different functions and conversely, the same function may often be performed by different types of geotextiles. In addition to their primary function, geotextiles can perform one or more secondary functions. For example, a geotextile can provide separation of two dissimilar soils, but it may also provide filtration as a secondary function by minimizing the build-

up of excess pore water pressure in the soil beneath the separator. A brief overview of functions typically performed by geotextiles highlights their versatility.

Separation is the introduction of a flexible porous geotextile placed between dissimilar materials so that the integrity and the functioning of both materials remains intact for the life of the structure or is improved (Koerner 2005). When a coarse material, e.g., stone aggregate, is placed on fine-grained soil, the boundary between the two layers diminishes over time. Migration occurs when fine soil enters the aggregate pore space, thereby hurting the drainage capability of the coarse layer. Simultaneously, intrusion occurs when the coarse material moves into the fine layer, thereby lowering the strength of the coarse layer. Placing a geotextile to perform the separation function addresses both of these concerns.

Filtration is defined as the equilibrium geotextile-soil system that allows for adequate liquid flow with limited soil loss across the plane of the geotextile over a service lifetime compatible with the application under consideration (Koerner 2005). The structure of the geotextile should be open enough to allow a desired amount of liquid flow, but tight enough to prevent major soil migration through the geotextile. As the flow of liquid is perpendicular to the plane of the geotextile, filtration refers to the cross plane hydraulic conductivity, or permittivity, defined as:

$$\psi = \frac{k_n}{t} \tag{2.1}$$

where ψ is the permittivity, k_n is the cross-plane hydraulic conductivity, and t is the geotextile thickness at a specified normal pressure. The important property for soil retention design is the apparent opening size (AOS), a measure of the pore sizes in a

geotextile. More specifically, AOS refers to the opening size at which 95% of all pore spaces are smaller. This value is compared to soil particle size characteristics. The coarser sized particles eventually create a filter bridge, which in turn retains the finer-sized particles, building a stable upstream soil structure. In addition to ensuring adequate liquid flow and upstream soil retention, proper filtration design ensures that no long-term clogging occurs.

Reinforcement is the synergistic improvement in a total system's strength created by the introduction of a geotextile into a pavement layer (Koerner 2005). Several mechanisms may contribute to a strength increase, but the general improvement is due to the geotextile's tensile benefit to the surrounding soil.

Drainage refers to the ability of geotextiles (typically thick, nonwoven geotextiles) to provide an avenue for flow of water within the plane of the geotextile. Drainage capability of the geotextile is quantified by its transmissivity, defined as:

$$\theta = k_p * t \tag{2.2}$$

where θ is the transmissivity, k_p is the in-plane hydraulic conductivity, and t is the geotextile thickness at a specified normal pressure.

2.2 CAPILLARY BREAK EFFECT

While geotextiles are typically placed in engineering structures—such as roadways, landfill liners and covers, earthen dams, embankments and retaining walls—to perform the functions discussed in Section 2.1, unexpected consequences may result if unsaturated conditions are not considered in design. Indeed, these engineering structures

spend a majority of their design life in an unsaturated state. Under unsaturated conditions, coarse materials tend to be less conducive to flow than fine materials. Capillary forces in a fine material increase with suction, holding moisture in the finer material's pores and making flow across an interface to a coarser material less likely. As a result, a coarse material placed adjacent to a fine material forms a capillary barrier, or capillary break. This coarse material does not have to be soil—research has shown that nonwoven geotextiles may also create a capillary barrier (Iryo and Rowe 2003, McCartney et al. 2005).

A capillary break forming at the soil-geotextile interface in a retaining wall or reinforced slope may result in a decrease in shear strength, leading to poor performance if unsaturated conditions are not adequately considered in design. Richardson (1997) observed a sliding failure in the side slope of a landfill cover system that was likely due to increased degree of saturation induced by a capillary break. Similar observations have been made elsewhere in lab and numerical studies (Iryo and Rowe 2006). Ignoring unsaturated conditions prevalent in pavement edge drain systems may result in the edge drain retarding rather than providing a path for water flow, thereby keeping the water in the pavement section and increasing its detrimental effects (Stormont and Zhou 2005). Instability may occur due to build-up of water near the facing of retaining walls or slopes.

While ignoring unsaturated conditions may result in undesirable behavior, a capillary barrier may be used effectively when appropriately designed. A capillary barrier located at the bottom of a landfill cover system increases the total amount of moisture storage available for a given cover height, providing opportunities for more economical cover design. In roadways, laboratory work has shown that geotextile capillary barriers may be used effectively to mitigate frost heave and its detrimental effects on pavements (Henry 1996).

The terms “capillary barrier” and “capillary break” are generally interchangeable in the literature. However, using “barrier” may be misleading, as the effect is only temporary. As suction decreases, i.e., as water content increases, capillary forces decrease. At a certain suction, termed the “breakthrough suction”, capillary forces are no longer strong enough to prevent flow from entering the adjacent coarse material. Accordingly, an important design parameter for a capillary barrier system is the breakthrough suction. In general, the lower the breakthrough suction, the stronger the capillary barrier, as it is maintained over a wider range of suction.

Until breakthrough, a certain volume of water is retained above the geotextile as a result of formation of the capillary barrier. This volume of water is termed the storage capacity. The effectiveness of a given capillary barrier system may also be measured by its storage capacity, with a larger capacity indicating a stronger capillary barrier. Stormont and Morris (1998) present a method to estimate storage capacity based on an expected suction profile developed in the soil layer and the water retention characteristics of the soil. Suction profiles for a variety of flow conditions are reviewed—if the water retention characteristics of the soil are known, a suction profile may be converted to moisture content, which allows for calculation of the storage capacity when integrated over the full volume of the cover soil.

2.3 HYDRAULIC CHARACTERIZATION OF UNSATURATED SOIL AND GEOTEXTILES

A common assumption in design standards dealing with flow is that soil is fully saturated. Flow characteristics in a porous medium are much more complex under unsaturated conditions. Of particular importance is the variation in hydraulic conductivity when air is present in pore spaces, i.e., desaturation has occurred. Soils

experience a drop in hydraulic conductivity of several orders of magnitude over the range of suction, or negative pore pressures, typically seen in the field. An adequate understanding of the variation in hydraulic conductivity for a given soil type under expected moisture conditions is essential for effective design.

2.3.1 Water Retention Curve

The relationship between hydraulic conductivity and matric suction is typically estimated empirically from the soil's water retention curve (WRC). The WRC is a measure of the amount of moisture present in the available pore spaces, most commonly represented by volumetric moisture content or degree of saturation, over a desired range in matric suction. Several laboratory methods are available for obtaining the WRC for either a soil or a geotextile, as discussed later in this chapter.

The amount of moisture in a soil at any given time depends on the capillary forces developed in its network of pores. Smaller pore sizes develop higher capillary forces, therefore requiring higher suctions to drain, and vice versa for larger pore sizes. Therefore, the amount of water present in soil at a given matric suction is dependent upon the soil's particle size distribution and soil structure. Figure 2.2 provides a general representation of the WRCs for various soil types.

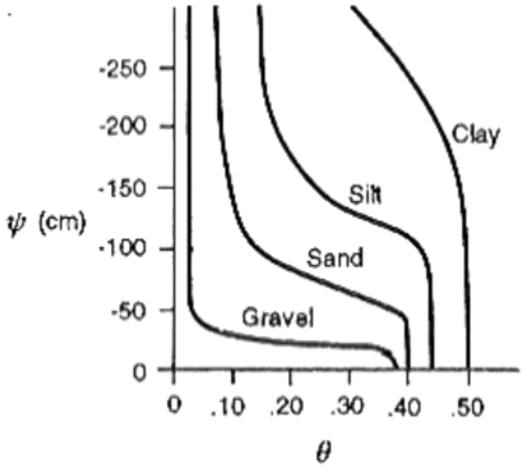

Figure 2.2: Effect of soil texture on the soil WRC (Stephens 1996)

The air entry suction of a soil, at which air is introduced into the pore system and the soil becomes unsaturated, increases with decreasing particle size. The decrease in moisture content with increasing suction after the air entry suction is reached is gradual for a well-graded material (with a wide range in particle sizes). However, for a material like gravel—coarse, with fairly uniform pore sizes—the decrease in water content is very sharp after reaching the air entry suction. A nonwoven geotextile behaves like a gravel of relatively small particle size. It typically has fairly uniform pore sizes, resulting in a sharply defined WRC.

Several laboratory methods are available for obtaining a soil WRC. This discussion primarily focuses on methods employed for the laboratory characterization performed as part of this research project. Other methods are touched on briefly. The general approach to obtaining a WRC is to apply increments of suction over the range of interest, allow the moisture in the system to equilibrate, and determine the moisture

content at equilibrium. Each moisture content-suction value represents a point on the WRC.

Retention curves for soils with a significant amount of fines typically span a large range in applied suction. Often, multiple types of tests are required to cover the complete range of suction desired. Low suction, up to around 10 kPa, is commonly covered with the hanging column method. Several methods may be used to cover the range of suction from 10 kPa to around 500 kPa—in this research project, the pressure plate method was used. For higher suctions, ranging to over 100,000 kPa, thermodynamic methods are typically employed.

The hanging column method involves application of suction created by changing the height between a soil sample and a water reservoir. The use of a Büchner funnel allows a sample placed atop a saturated porous plate to remain in hydraulic contact with a water source. The suction head applied to the sample equals to the difference in elevation between the top of the porous plate and the surface of the water reservoir. For each applied suction increment, a moisture content is obtained for the soil sample, representing a point on the WRC. Flow measurements are typically taken during the duration of the test and, after obtaining a moisture content destructively at the end of the test, incremental moisture contents are back-calculated. Physical limitations related to the required height between soil specimen and reservoir limit applicability of the hanging column to the lower end of the suction range.

The pressure plate method employs the axis translation technique to impose varying levels of suction. Air pressure is applied to a sample contained in a pressure vessel and in hydraulic contact with a low pressure source, typically a water reservoir, at the sample base. The difference in air and water pressures results in an applied suction of the same magnitude. Range of the pressure source used and construction of the pressure

vessel typically control the magnitude of applied suctions available via the pressure plate testing method. As in the hanging column method, suction is applied incrementally and a moisture content is obtained for each increment.

Thermodynamic methods involve placing a soil sample in a closed environment of known relative humidity and associated suction, allowing the system to come to hydraulic equilibrium, and obtaining a water content of the soil specimen. The target relative humidity is commonly reached using salt solutions. Thermodynamic methods require the soil specimen to equilibrate to a total suction, as opposed to a matric suction applied in the two physical methods described previously. High ranges of suction may be reached by lowering the system's relative humidity to an appropriate level.

As a nonwoven geotextile is a highly porous material with largely uniform pore sizes, characterization of its unsaturated behavior requires application of a much smaller range in suction than seen with soils containing a significant amount of fines. Several cases in the literature present a full geotextile WRC developed with only a hanging column test (Stormont et al. 1997, Iryo and Rowe 2003, McCartney et al. 2005, McCartney et al. 2008).

However, some characteristics of nonwoven geotextiles present special challenges when running a hanging column test. The water retention curve is very steep due to uniformity in pore sizes—often the geotextile will go from near saturation to the residual water content in less than a 0.5 kPa change in suction. It is difficult to apply multiple suction increments confidently over such a narrow range using the typical hanging column setup. There are questions about the adequacy of hydraulic contact created by placing a confining weight atop a geotextile specimen resting on the fritted glass disc of a Büchner funnel. For the drying curve, it is difficult to reach saturation without the presence of free water, not actually contained in the geotextile pore structure, prior to

application of the first suction increment. Finally, the total pore volume of a typical geotextile specimen tested is very small due to the thickness, making control of losses from the system extremely important considering that a required equilibration time of up to 72 hours for a given suction increment is found in the literature (Bouazza et al. 2006b).

Other methods have been used to obtain the geotextile WRC, including a suction plate apparatus and a controlled outflow capillary pressure cell (Iryo and Rowe 2003). The simplest test found in the literature was first reported in Lafleur et al. (2000), where a capillary rise test was used to develop the geotextile water retention curve. A 50 cm long specimen was hung with the bottom 2 cm submerged in a water reservoir. Allowing the system to reach hydraulic equilibrium results in a linear distribution of suction throughout the geotextile specimen, as shown in the schematic provided in Figure 2.3.

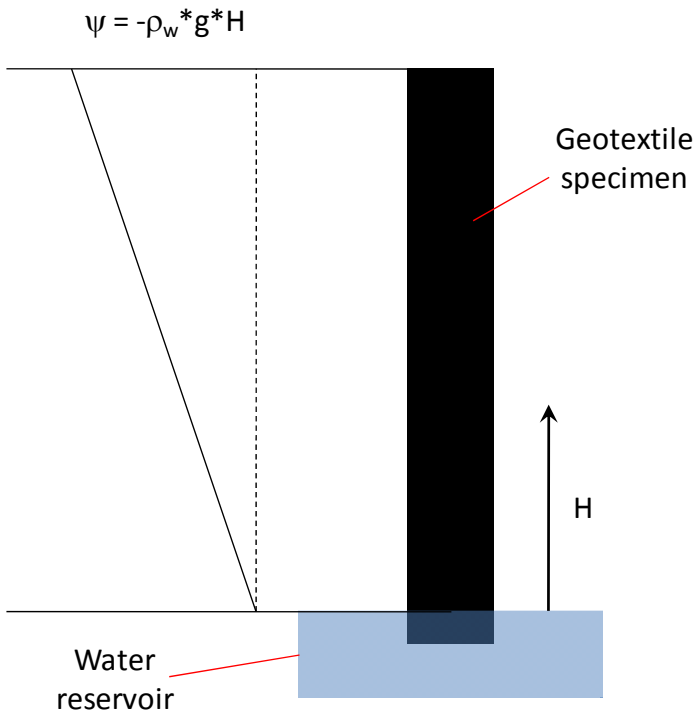

Figure 2.3: Capillary rise test schematic

The system was allowed to come to hydraulic equilibrium for 72 hours, after which the portion of the geotextile specimen above the water reservoir is quickly cut into strips. Water contents were determined for strips of geotextile by drying overnight. Each water content was assumed to correspond to the average suction present in the geotextile strip at equilibrium, equal to the height above the water reservoir. Data obtained via the capillary rise test compared favorably to results obtained via a suction cell apparatus for the same material. Similar results are shown elsewhere in the literature (Stormont and Ramos 2004, Krisdani et al. 2006, Krisdani et al. 2008).

Regardless of the particular laboratory method used to obtain the retention characteristics of a nonwoven geotextile, results presented in the literature are notably consistent. Figure 2.4 presents data for both the drying and wetting curves collected from the literature and presented in Iryo and Rowe (2003). Data is presented from nonwoven geotextiles of differing polymer type, thickness, apparent opening size, to name a few properties. However, the water retention characteristics are quite consistent. In most cases, water and air entry values lie between 0 and 2 kPa suction, an extremely narrow range when considered in contrast to the fine soil to which the geotextile is compared in capillary barrier system analysis. Similar results have been obtained in more recent studies (McCartney et al. 2005, McCartney et al. 2008, Krisdani et al. 2008).

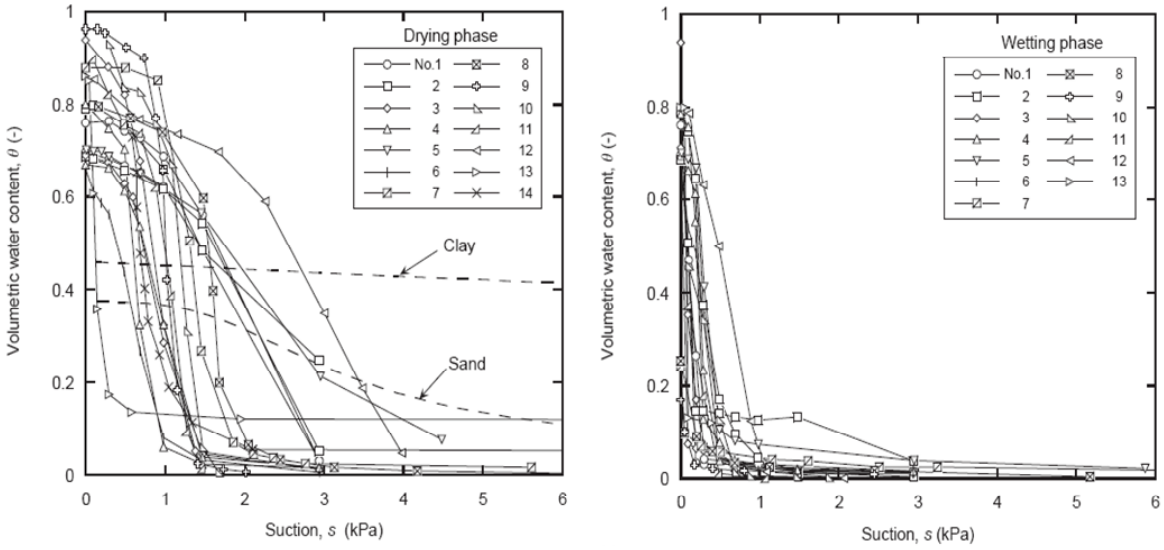

(a) (b)

Figure 2.4: Nonwoven geotextile water retention data presented in Iryo and Rowe (2003)

After obtaining the retention data from various laboratory methods for either soil or geotextile, the next step is to fit a curve to the data using one of several published methods. Perhaps the most commonly used method is the van Genuchten function:

$$\theta = \theta_r + (\theta_s - \theta_r)[1 + (\alpha_{vG}\psi)^{N_{vG}}]^{-\left(1-\frac{1}{N_{vG}}\right)} \quad (2.3)$$

where α_{vG} and N_{vG} are fitting parameters. The van Genuchten fitting method has been shown to be adequate for both soil and geotextiles (Iryo and Rowe 2003, McCartney et al. 2005, McCartney et al. 2008).

2.3.2 Hydraulic Conductivity Function

Decrease of moisture in a soil or geotextile's pore structure results in a decreased area of flow available, i.e., a more tortuous flow path, thus lowering the material's hydraulic conductivity. The quantified relationship between hydraulic conductivity and suction for a given soil is called the hydraulic conductivity function, or K-function. While it is possible to obtain data for the full K-function experimentally, testing methods are complex, often difficult to analyze and prone to significant experimental error (McCartney 2007). The most common approach to defining the K-function for a soil involves obtaining the saturated hydraulic conductivity in the laboratory and using it, along with the soil's water retention characteristics, as inputs for a predictive model.

Most models may generally be viewed as a function of the saturated hydraulic conductivity of the soil and the relative percentage of available pore space that is actually filled with water. The general form is as follows (McCartney 2007):

$$\frac{K(\theta)}{K_s} = \left(\frac{\theta - \theta_r}{\theta_s - \theta_r}\right)^b \left(\frac{\int_0^\theta \frac{dx}{\psi^{2-r}(x)}}{\int_0^1 \frac{dx}{\psi^{2-r}(x)}}\right)^m \tag{2.4}$$

where b, r, and m are empirical constants related to the pore structure of the soil and x is defined for integration (McCartney 2007). The van Genuchten-Mualem model uses the N parameter obtained by fitting the van Genuchten model to the soil water retention data, along with assumptions for b, r and m made by Mualem (1976), to define the K-function:

$$K(\theta) = K_s \sqrt{\frac{\theta - \theta_r}{\theta_s - \theta_r}} \left[1 - \left(1 - \left(\frac{\theta - \theta_r}{\theta_s - \theta_r}\right)^{1-N_{vG}}\right)^{\frac{1}{1-N_{vG}}}\right]^2 \tag{2.5}$$

An exponential model proposed by Gardner (1958) is simple and easily differentiable, with an empirical factor α that depends on the soil pore distribution:

$$K(\psi) = K_s e^{-\alpha\psi} \tag{2.6}$$

Studies of the accuracy of modeled K-functions with those determined experimentally, while limited in number, show a significant amount of scatter for soil data (McCartney 2007). No particular model has been shown to clearly outperform others, and the modeled K-function should be considered a preliminary estimation of the soil's actual unsaturated behavior. Iryo and Rowe (2003) observed similar scatter when comparing predicted versus experimentally observed data for nonwoven geotextiles. However, they concluded that the van Genuchten-Mualem model may be used to reasonably model a nonwoven geotextile's unsaturated behavior.

2.4: PREDICTION OF CAPILLARY BARRIER PERFORMANCE

The breakthrough suction for a capillary barrier depends on the water retention properties of each material, expressed by a soil or geotextile WRC and/or K-function. The suction profile is continuous across any material interface. In the case of vertical flow in a horizontally layered system, e.g., a modeled capillary barrier system, if a coarser material is significantly less conducive to flow than the overlying soil, a capillary break will occur. A comparison of the K-functions between two adjacent materials shows the suction value at which the capillary break effect is expected to occur.

Figure 2.5 shows the plotted K-functions and associated predictions of breakthrough suction values presented in McCartney et al. (2005). The point at which the K-function of the coarser material, either nonwoven geotextile or sand in this case, crosses under that of the finer material, a silt in this study, represents the breakthrough suction. At any suction higher than the crossing point, the coarser material is significantly less conducive to flow than the finer material—therefore, flow of water across the material interface will be prevented, resulting in the observed capillary barrier effect. Subsequent experimental tests confirmed the accuracy of the predicted breakthrough suctions. Similar results were found in Stormont and Clifford (1999), who found a breakthrough suction consistently between 5 and 20 mm in column tests with a silty sand overlying a pea gravel. This closely matches the predicted breakthrough suction, shown at the intersection of the K-functions for pea gravel and silty sand, respectively, in Figure 2.6.

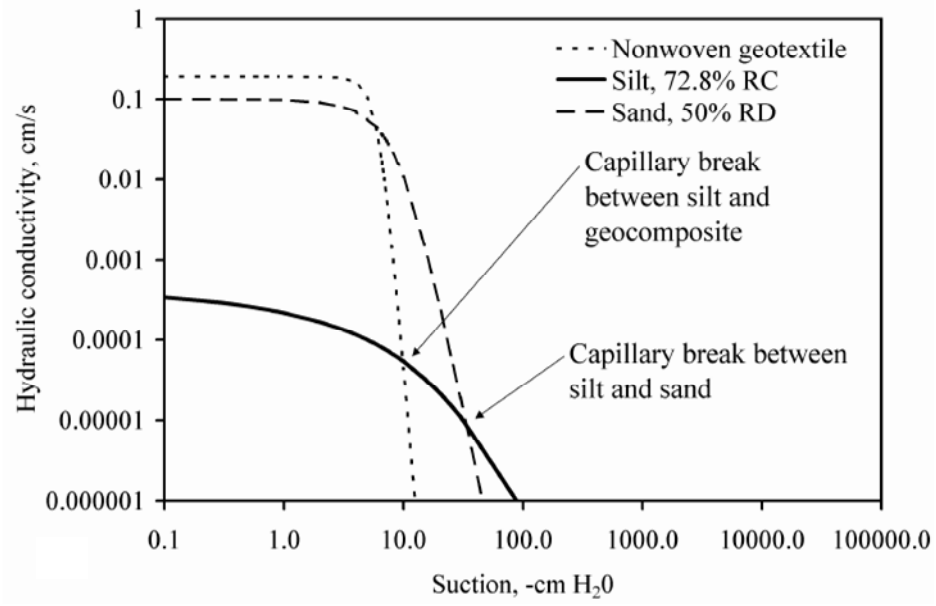

Figure 2.5: Predicted breakthrough suction from McCartney et al. (2005)

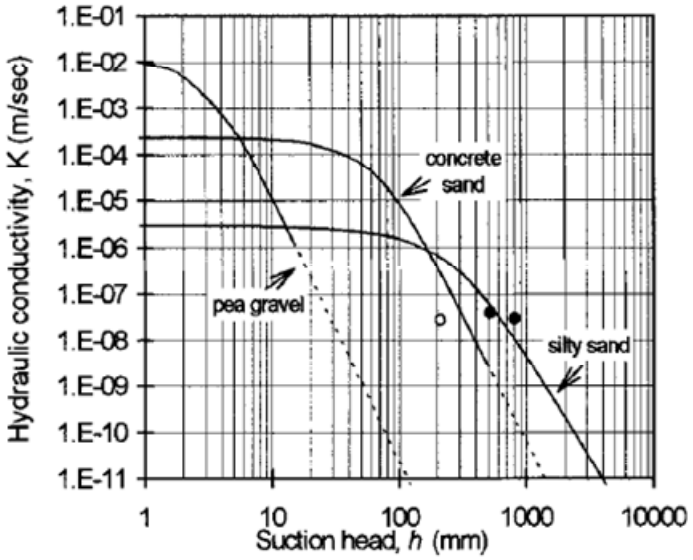

Figure 2.6: Predicted breakthrough suction from Stormont and Anderson (1999)

2.5 COLUMN TESTING TO ASSESS CAPILLARY BARRIER PERFORMANCE

Soil columns have been used to test a capillary barrier model in the laboratory. Stormont and Anderson (1999) investigated the performance of various soil combinations in creating a capillary barrier. Their model was compacted into clear plexiglass columns of 20 cm diameter and 100 cm height. A peristaltic pump was used to pump the required low flow rate into a cup sitting atop the column. Inside the cup were the ends of wicks made with filter paper—these wicks extended out from the cup and were used to distribute the applied flow evenly across the top of the column. Tensiometers were located at five elevations along the soil column to monitor the progression of the moisture front during testing. Breakthrough of the capillary barriers was identified visually.

The results of these tests confirmed the reliability of a capillary break. Breakthrough suctions were consistent with those predicted via K-function analysis,

independent of applied flow rate, and controlled by the water entry properties of the coarser soil layer. A coarser soil with more uniform pore size was shown to present the best option for capillary barrier performance. Similar conclusions have been made from other column testing on laboratory models of soil capillary barriers (Yang et al. 2004, McCartney et al. 2005). Stormont and Anderson (1999) also observed that the suction profile at breakthrough tends toward a unit slope given that the applied inflow is low enough relative to the soil saturated hydraulic conductivity. This behavior is in agreement with the proposed model of the suction profile at failure presented in Stormont and Morris (1998). Measured suction profiles at failure are shown in Figure 2.7, varying with applied inflow rate (Stormont and Morris 1998).

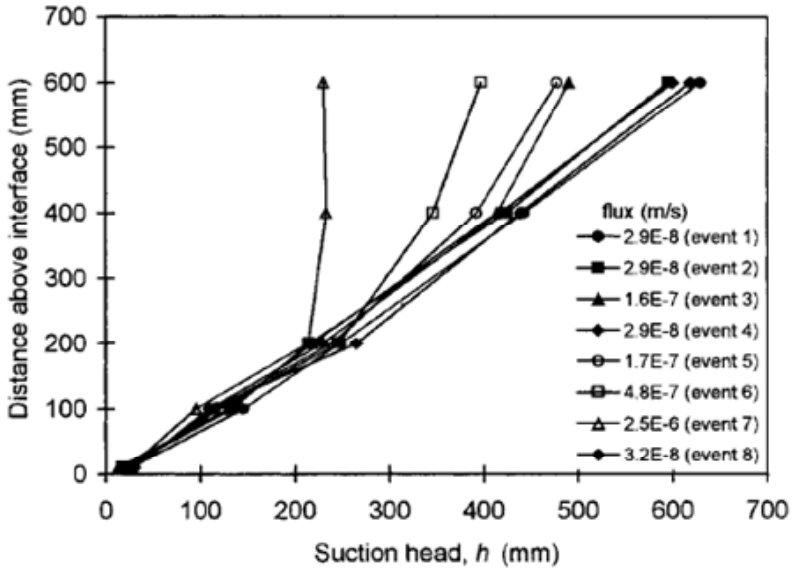

Figure 2.7: Suction profiles at failure from Stormont and Anderson (1999)

McCartney et al. (2005) used a column setup similar to that utilized in Stormont and Anderson (1999) to investigate the relative performance of two capillary barrier

systems, one created with a coarse layer of sand and the other with a geocomposite. The outer layers of the geocomposite consisted of a nonwoven geotextile, a material with retention properties similar to those of a coarse gravel of uniform pore size. Movement of the moisture front and creation of the capillary barrier was monitored with sensors measuring volumetric moisture content. Both materials created a temporary capillary barrier, but the nonwoven geotextile, with a more coarse, uniform pore structure, maintained the barrier to a lower breakthrough suction. Figures 2.8 and 2.9 show the change in volumetric moisture content with time obtained from the soil-geotextile capillary barrier test presented in McCartney et al. (2005).

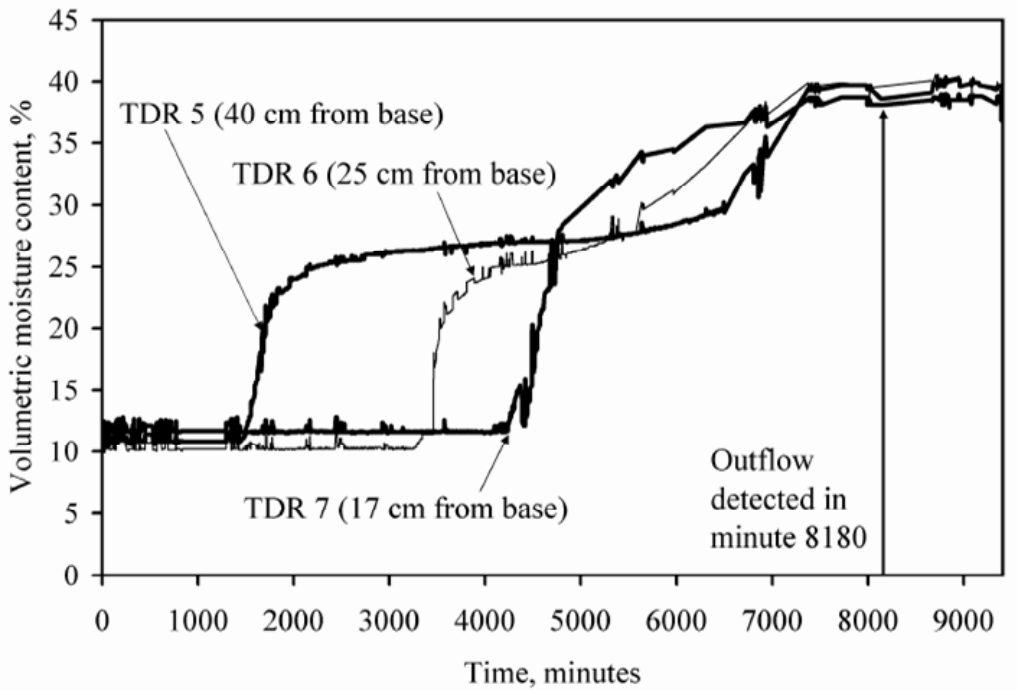

Figure 2.8: Change in volumetric moisture content with time from McCartney et al. (2005)

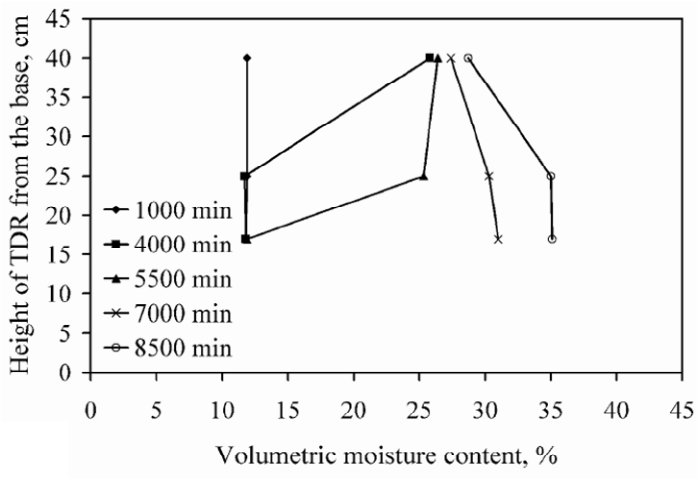

Figure 2.9: Volumetric moisture content profiles with time from McCartney et al. (2005)

Chapter 3: Materials, Methods and Instrumentation

Information pertaining to the materials, methods and instrumentation used as part of the experimental testing program is presented in this chapter. For some of the material covered, background information has been outlined in Chapter 2. This chapter focuses on the specific materials used and procedures followed in this study. Properties and characterization of the soil used are presented first. Next, an overview of relevant geotextile properties and unsaturated behavior is provided. Details on the design, construction, and use of the columns tested in this study complete the chapter.

3.1 Properties of Rocky Mountain Arsenal Soil

The soil used in this study was obtained from an evapotranspirative cover under construction at the Rocky Mountain Arsenal in Denver, CO. The soil was sampled from a borrow pit on site, packed into several 5-gallon buckets at field moisture content, and shipped to the University of Texas at Austin. Upon receiving the buckets, the soil was first homogenized by mixing to avoid any inconsistencies in soil properties during soil characterization as well as future testing. Next, a complete soil characterization was completed using ASTM-specified test methods.

3.1.1 Geotechnical Soil Classification

The granulametric curve shown in Figure 3.1 was obtained via sieve and hydrometer analyses, as specified in ASTM D 422 (ASTM 2007a). Sieve analysis was used for the portion of soil with particle size greater than a number 200 sieve (0.075mm). For the finer portion, particles less than 0.075 mm in diameter, a hydrometer analysis was completed. Approximately 50% of the soil passes the number 200 sieve.

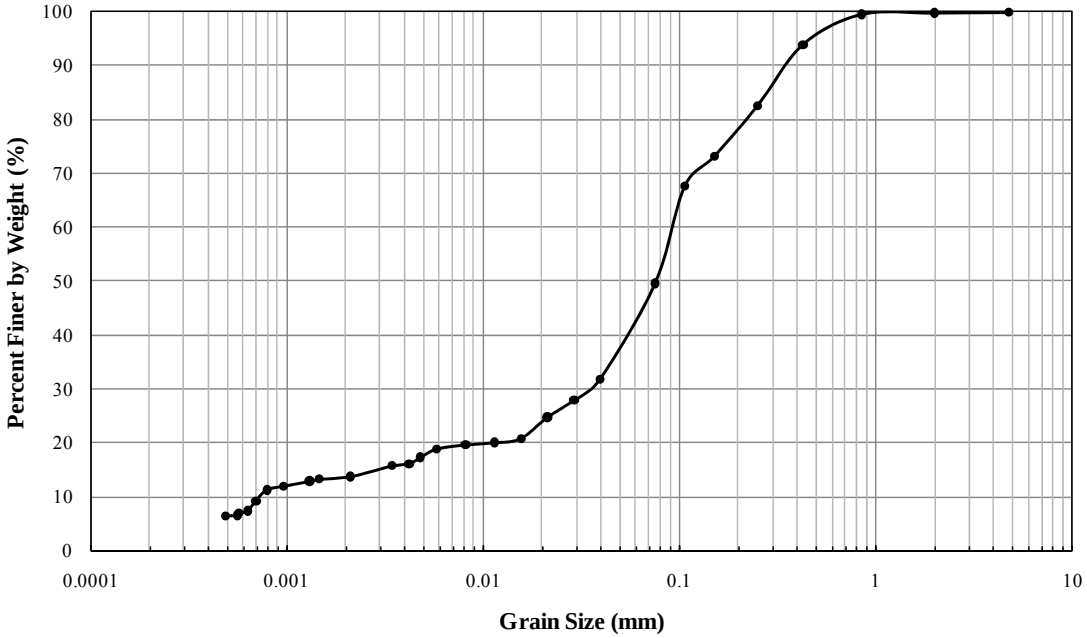

Figure 3.1: Granulametric curve for RMA soil

The Atterberg Limits were determined following procedures presented in ASTM D 4318 (ASTM 2005). Figure 3.2 shows the determination of the liquid limit based on the raw data presented in Table 3.1. Table 3.2 presents the laboratory data obtained for the plastic limit. The soil has a liquid limit (LL) of 32.3% and a plastic limit (PL) of 11.6%. After rounding these values to whole numbers, the calculated plasticity index (PI) is 20. A summary is given in Table 3.3.

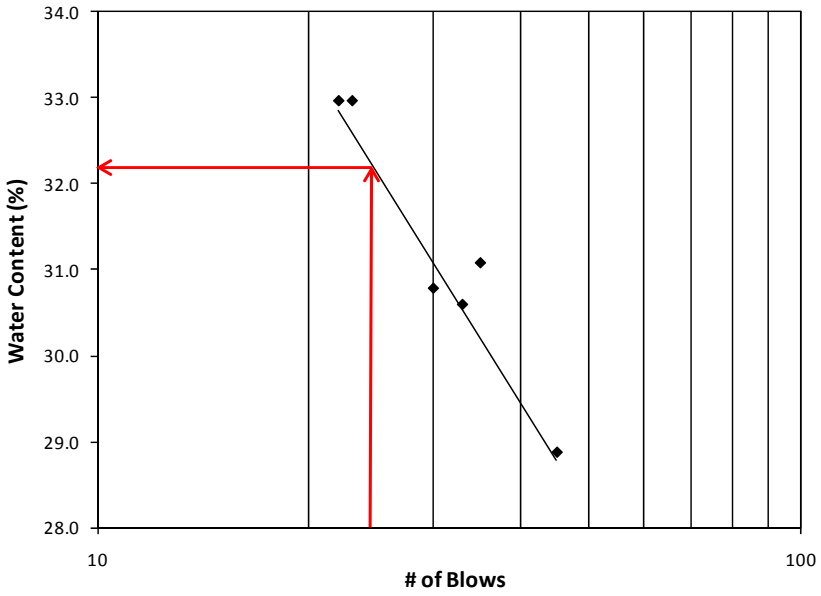

Figure 3.2: Determination of liquid limit

Table 3.1: Liquid limit raw data

Container mass (g)	Container with wet soil (g)	Container with dry soil (g)	Blow count	Water content (%)
19.89	28.20	26.14	23	33.0
19.90	32.93	29.70	22	33.0
19.51	30.73	28.07	35	31.1
19.78	29.85	27.48	30	30.8
19.84	30.00	27.62	33	30.6
19.47	32.28	29.41	45	28.9

Table 3.2: Plastic limit raw data

Container mass (g)	Container with wet soil (g)	Container with dry soil (g)	Water content (%)
2.34	5.1	4.83	10.8
2.33	5.01	4.71	12.6
2.26	4.92	4.65	11.3
		AVG:	11.6
		STDEV:	0.9

Table 3.3: Summary of Atterberg Limits

LL:	32
PL:	12
PI:	20

The specific gravity was determined to be 2.71 following the laboratory methods outlined in ASTM D 854 (ASTM 2006a). Knowing the particle size distribution and Atterberg Limits, the soil may be classified according to the United Soil Classification System (USCS). This soil classifies as "CL", a lean clay (ASTM 2006b).

3.1.2 Compaction Characteristics

Compaction characteristics of the RMA soil were obtained using standard proctor compaction effort, with procedures described in ASTM D 698 (ASTM 2007b). Seven soil samples, ranging in gravimetric water content from 11% to 19%, were tested. The dry densities of the samples ranged from 1.75 to 1.84 g/cc (17.2 to 18.1 kN/m^3). Optimum water content was determined to be 15%, corresponding to a dry density of 1.84 g/cc (18.1 kN/m^3). The standard proctor compaction curve is plotted in Figure 3.3, with corresponding data included in Table 3.4.

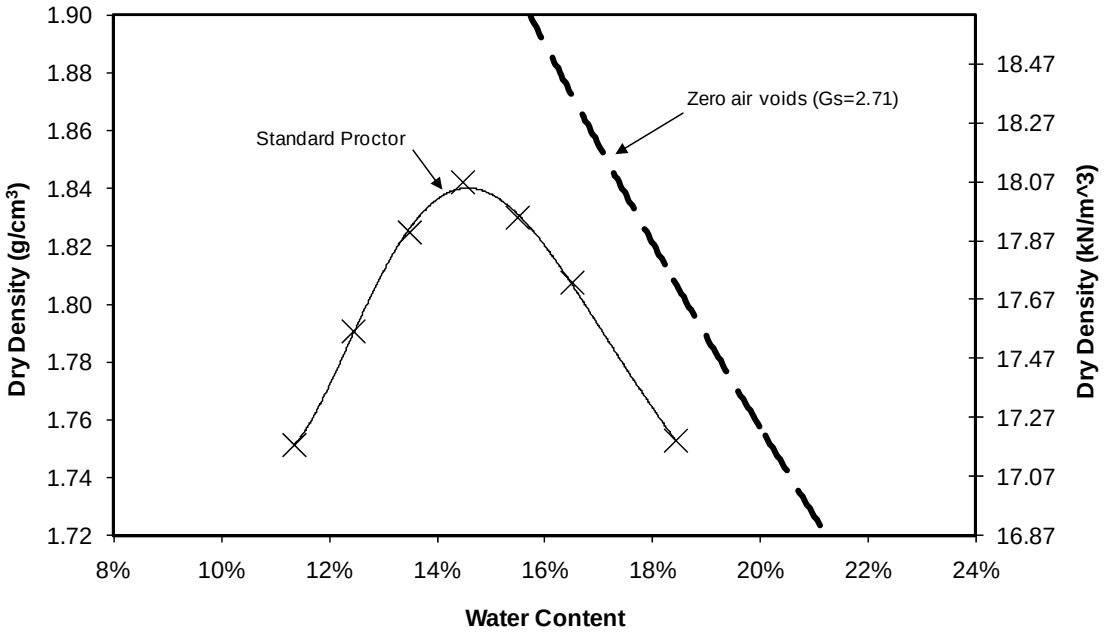

Figure 3.3: Standard proctor compaction curve for RMA soil

Table 3.4: Raw data for standard proctor compaction curve

Test #	Water Content	Soil + Water Mass (g)	Mass of Solids (g)	Volume Mold (cc)	Dry Density (g/cc)	Dry Density (kN/m^3)
1	11.36%	1829.40	1642.73	938.00	1.75	17.18
2	16.50%	1975.00	1695.28	938.00	1.81	17.73
3	14.48%	1978.00	1727.80	938.00	1.84	18.07
4	12.45%	1888.40	1679.33	938.00	1.79	17.56
5	18.43%	1947.00	1644.07	938.00	1.75	17.19
6	15.50%	1982.40	1716.36	938.00	1.83	17.95
7	13.50%	1942.80	1711.72	938.00	1.82	17.90

3.1.3 Saturated Hydraulic Conductivity

The saturated hydraulic conductivity of the soil was measured with a flexible wall permeameter test run in accordance with ASTM D 5084 (ASTM 2003). The sample tested, 7.1 cm in diameter and 5.1 cm in height, was prepared to an initial water content of 15% and compacted to 81.6% relative compaction (γ_d = 1.50 g/cc). After backpressure saturating the sample to a B coefficient of 0.97, the sample was consolidated to an effective stress of 69 kPa (10 psi). At the completion of consolidation, the pressure at the base of the sample was increased 2 psi, for an average applied hydraulic gradient of 27. Inflow and outflow measurements from the sample were taken via burettes on a pressure control panel. Measurements were taken until the ratio of inflow to outflow remained steady at one for an amount of flow equal to one full pore volume of the sample. Raw data is provided in Table 3.5. The saturated hydraulic conductivity of the RMA soil at 81.6% RC is $8.2*10^{-5}$ cm/s.

Table 3.5: Saturated hydraulic conductivity raw data

Elapsed Time (min)	Flow (mℓ)		Flow Ratio (out/in)	Incremental Flow Rate (cm/s)
	Bottom (Inflow)	Top (Outflow)		
94	18.2	18.1	0.99	8.12E-05
187	18.2	18.2	1.00	8.30E-05
225	7.9	7.9	1.00	9.21E-05
298	14.3	14.2	0.99	8.45E-05
379	15.7	15.7	1.00	8.23E-05
452	13.8	13.9	1.01	8.04E-05
547	17.2	17.3	1.01	7.68E-05
			Average (weighted):	8.20E-05

The specimen used to determine the saturated hydraulic conductivity was prepared to the optimum gravimetric water content of 15%. Soil compacted in the column tests is significantly dryer, as the target initial volumetric water content is 0.10. Accordingly, the saturated hydraulic conductivity of the column is expected to be higher as a result of its comparatively dry initial state, although this effect is not quantified. A very similar soil showed a significant range in saturated hydraulic conductivity over a similar range in compaction water content in previous work (McCartney 2007).

3.1.4 Water Retention Curve

The soil water retention curve (SWRC) for the RMA soil was obtained using three different test methods in order to cover the full suction range of interest. For low suctions, from 0 to approximately 10 kPa, the hanging column method was used. Pressure plate testing was used for suctions ranging from around 5 kPa to nearly 500 kPa. Suctions higher than 500 kPa were reached via thermodynamic methods. Raw data collected from the three methods is presented in Table 3.6.

A schematic of the hanging column setup is shown in Figure 3.4. The advantage of this system, with outflow measurements taken from the horizontal capillary tube, is the ability to take accurate readings of outflow with time while applying a constant suction head. The bubbling chamber is included to aid in saturating the entire system prior to starting the test and to provide a means for adding or draining water from the system while a test is in progress. After ensuring that the Büchner funnel and tubing are saturated and all air bubbles are removed from the system, the soil sample, prepared in a brass retaining ring, is seated atop the fritted glass disc contained in the Büchner funnel.

To ensure good hydraulic contact with the saturated fritted disc, the retaining ring is given a slight twist during placement.

Saturation of the sample may be obtained prior to placement in the hanging column setup, by inundation in a saturation tray or a saturation chamber (ASTM 2002), or directly in the hanging column itself. In this study, the latter approach was taken. The Büchner funnel was lowered so that the top of the sample was level with the horizontal capillary tube, and the two-way ball valves connecting the Büchner funnel to the bubbling chamber and the bubbling chamber to the capillary tube were opened. Measurements were taken periodically from the capillary tube to estimate the degree of saturation of the sample as inflow continued. Although the sample never reached 100 percent saturation as determined by the calculated porosity, saturation was deemed sufficient when water was visible both at the top of the sample and ponding atop the fritted disc around the edges of the retaining ring. The Büchner funnel was then raised so that the top of the fritted disc was even with the capillary tube, and the sample was allowed to equilibrate at zero suction.

Suction was applied in increments by raising the Büchner funnel to the desired suction head. For each increment, outflow measurements were taken with time until the system equilibrated. By closing the two-way ball valves between while the Büchner funnel is being raised to the next suction increment and opening only when the desired suction is applied, accurate outflow with time measurements may be obtained. The moisture content at the end of the test is obtained destructively, and outflow measurements from each suction interval are used to back-calculate the moisture content at each interval. Each calculated moisture content represents a point on the SWRC.

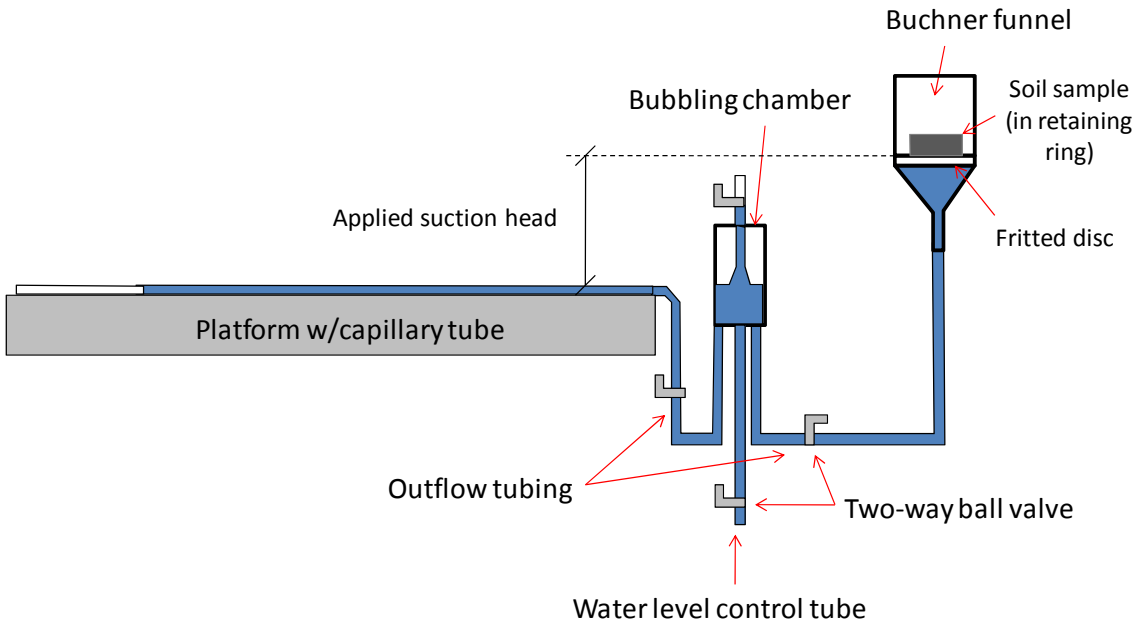

Figure 3.4: Schematic of hanging column setup

The pressure plate device used to characterize the RMA soil was developed at the University of Texas by Jeff Kuhn. Like other pressure plate devices, the axis translation technique is used to impose varying levels of suction. A soil specimen is placed atop a saturated ceramic disc inside a pressure vessel. Air pressure is increased inside the pressure vessel while water pressure connected to the ceramic disc remains constant. The applied suction is equal to the difference between air and water pressures. Applied air pressure forces outflow from the sample and into the ceramic disc—in order to ensure saturation for the duration of the test, the air entry pressure of the ceramic disc is higher than the maximum applied air pressure. A picture of the pressure vessel and a bubbling chamber used to maintain a constant pressure at the base and to aid in removal of air bubbles is presented in Figure 3.5. In the Kuhn setup but not pictured, saturated tubing runs from the ceramic disc to a horizontal capillary tube, allowing for accurate outflow measurement with time for a given suction increment. After outflow from the final

applied suction increment has leveled off, the sample is removed from the pressure vessel and a moisture content is obtained. Volumetric moisture contents for each suction increment are back-calculated using outflow data.

Thermodynamic methods were used to obtain points on the SWRC at suctions higher than around 500 kPa (70 psi). Four points were obtained, at suctions ranging from around 380 kPa (55 psi) to over 200,000 kPa (30,000 psi). These points were obtained by placing a soil sample in a thermally sealed desiccators chamber also containing a saturated salt solution. The salt solution brings the air in the chamber to equilibrium at a constant relative humidity, corresponding to a total suction present in the system. The soil sample is given time to equilibrate at this total suction and a water content is obtained at the end of this equilibration period.

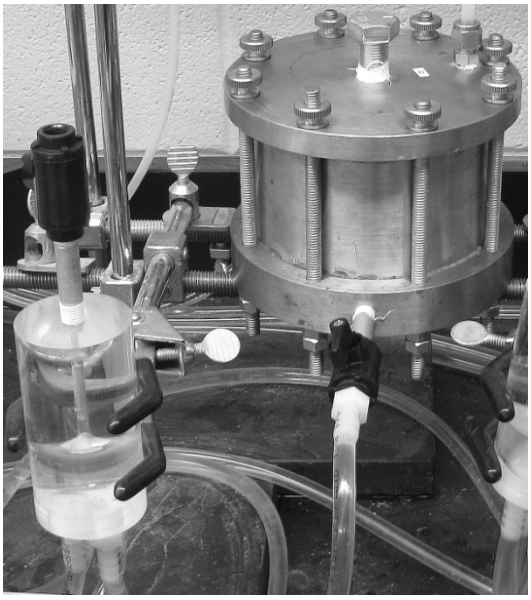

Figure 3.5: Pressure plate setup used in this study

Table 3.6: Raw data obtained for water retention curve

Hanging Column			Pressure Plate			Thermodynamic		
Suction (kPa)	w (%)	θ	Suction (kPa)	w (%)	θ	Suction (kPa)	w (%)	θ
8.8	22.1	0.32	483	13.7	0.20	207138	2.8	0.04
5.9	23.0	0.34	55	15.9	0.23	31188	4.1	0.06
2.9	25.0	0.37	55	16.0	0.24	13179	8.9	0.13
1.6	26.0	0.38	28	16.8	0.25	380	13.9	0.20
1.0	26.5	0.39	28	17.1	0.25			
0.6	27.1	0.40	14	18.1	0.27			
0.2	27.6	0.41	14	18.7	0.28			
0.1	27.6	0.41	3.5	22.8	0.34			
0.0	28.1	0.41	3.5	24.5	0.36			

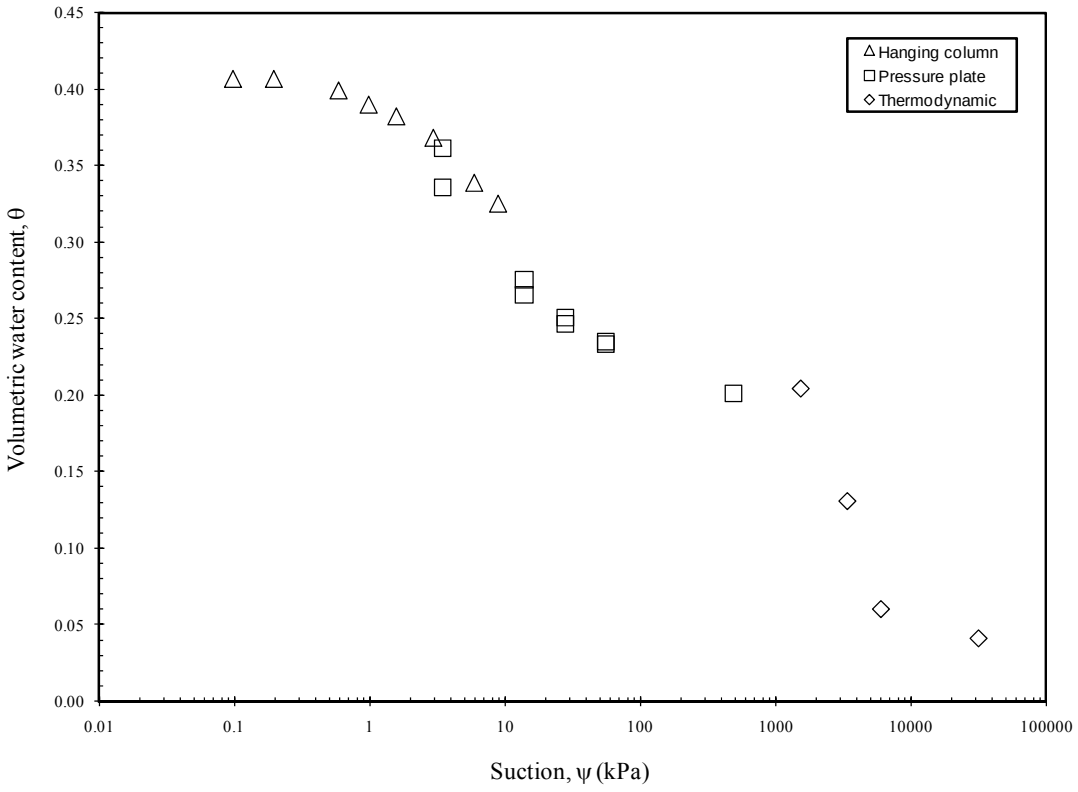

Figure 3.6: Water retention data for RMA soil—original

Figure 3.6 contains the SWRC data originally obtained from all three methods. Pressure plate results were obtained courtesy of tests run by Michael Plaisted, and thermodynamic test results are courtesy of Jeff Kuhn. A quick inspection of this plot reveals that the data obtained with the thermodynamic method does not follow the same log-linear trend seen from the other two physical methods. One possible explanation is the presence of an osmotic suction component in the soil. As the matric suction is the only component applied to the sample in both physical methods—hanging column and pressure plate—while the thermodynamic method equilibrates to a total suction, the presence of a significant osmotic component in the thermodynamic method would produce the type of curve shown in Figure 3.6.

A review of the soil properties from the borrow area in which our soil was originally obtained showed a calcium-carbonate equivalent of between 7.7% and 9.4% (Golder Associates 2008). Not enough information was reported to equate this calcium-carbonate equivalent to a percent salt by weight in the soil, which could then be used to estimate an osmotic potential present in the soil. However, if the assumption is made that the osmotic potential stays constant over the range in water content of interest, the osmotic potential may be estimated using the overlap in test results from the pressure plate and thermodynamic methods. This results in an osmotic potential of around 10,000 kPa (1,450 psi). Figure 3.7 shows the SWRC with the osmotic component removed from the thermodynamic data. This curve was used for subsequent fitting and calculations.

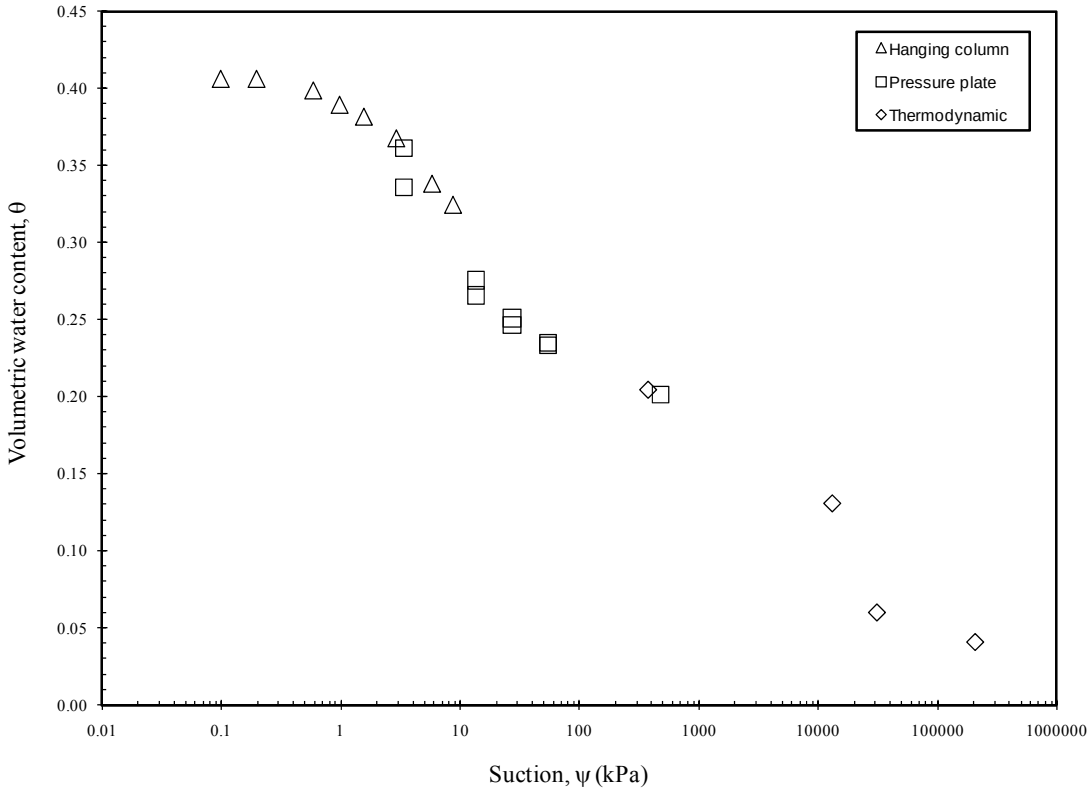

Figure 3.7: Water retention data for RMA soil—corrected for osmotic potential in thermodynamic testing

A fitted curve was applied to the water retention data using the van Genuchten fitting method. This curve is shown in Figure 3.8. At low suctions, the curve approaches a volumetric water content of 0.41. This is lower than the calculated porosity at 81.6% relative compaction, 0.446, as a result of the method used for saturation. A curve approaching some "effective saturation" due to the lack of back pressure during saturation is more representative of conditions in the columns used for subsequent testing. Along with a θ_{sat} value of 0.41, the residual water content, θ_r, was taken from the thermodynamic testing results as 0.04. Applying the van Genuchten model over the

entire range of laboratory data resulted in a best fit with parameter 'α' equal to 0.51 and 'N' equal to 1.19.

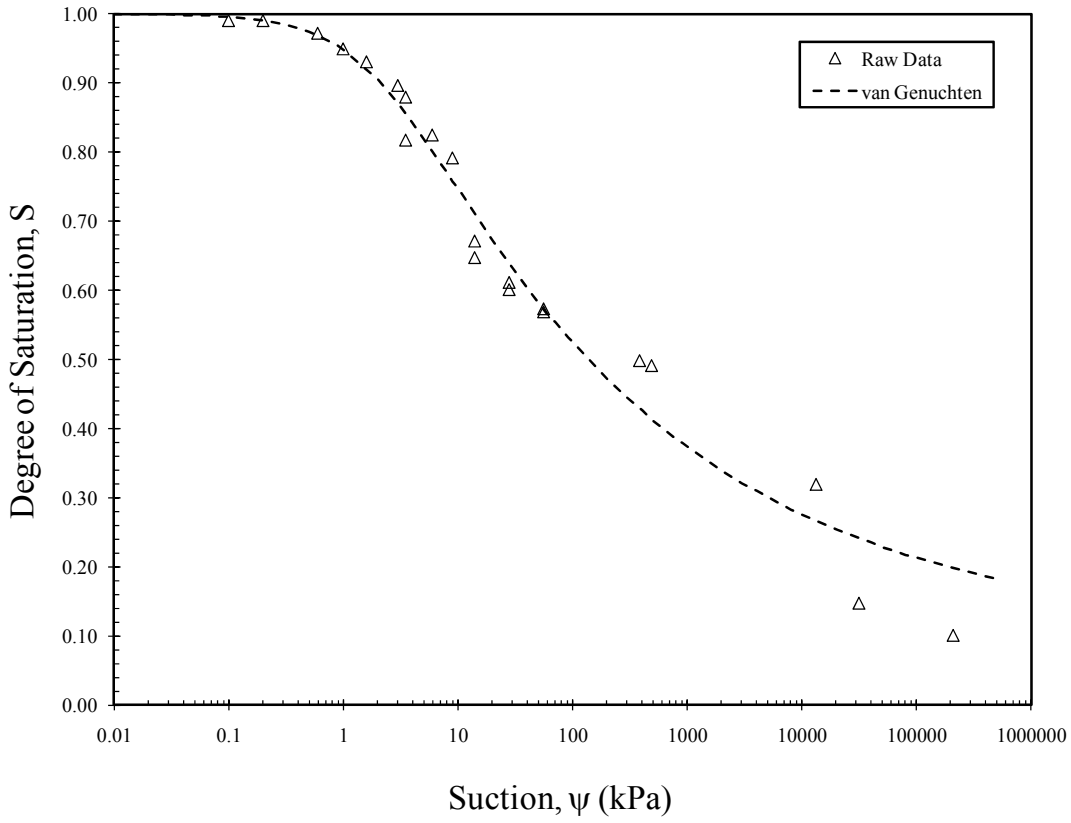

Figure 3.8: Fitted SWRC using van Genuchten model

Physical methods used to develop the water retention curve developed for the RMA soil used in this study—hanging column and pressure plate—were only performed on samples compacted to 80% relative compaction, equivalent to a γ_d of 1.47 g/cm^3 or a porosity, η, of 0.46. The most accurate analysis of test results on columns compacted to

different levels of relative compaction is obtained with water retention data specific to that relative compaction. Laboratory studies show that, for a similar soil, only the portion of the curve near saturation is affected, as shown in Figure 3.9 (McCartney 2005).

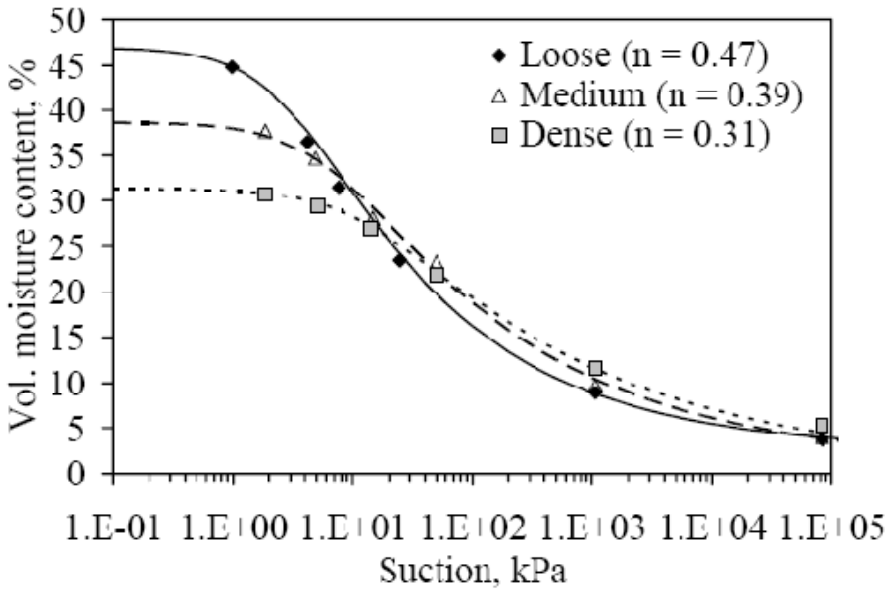

Figure 3.9: Effect of porosity on SWRC for similar soil (McCartney 2007)

3.1.5 Hydraulic Conductivity Function

The hydraulic conductivity function, or K-function, for the RMA soil was modeled using the van Genuchten–Mualem fitting method. Parameters used to fit the van Genuchten SWRC were used along with the laboratory-obtained saturated hydraulic conductivity to obtain the curve presented in Figure 3.10.

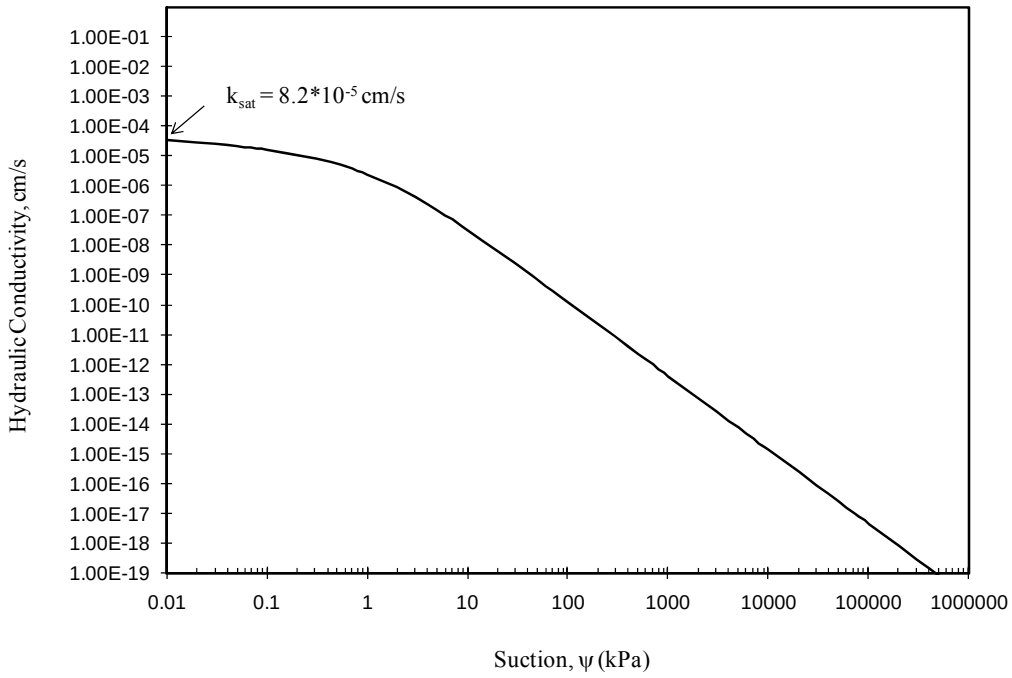

Figure 3.10: K-function for RMA soil

3.2 GEOTEXTILE PROPERTIES

The geotextile used in this study is the same product used in the field evapotranspirative cover after which the small soil columns are modeled. SKAPS Industries manufactures the geotextile, model GT-160. A portion of a roll was obtained directly from the manufacturer and used for testing. Laboratory characterization consisted of determining the unsaturated hydraulic behavior of the geotextile. Other parameters of interest were obtained from manufacturer literature.

3.2.1 Manufacturer-reported Values

The geotextile used in this study is a needle-punched nonwoven made of polypropylene staple fibers. Hydraulic parameters—permittivity, transmissivity, and AOS—are of primary concern when characterizing the unsaturated flow properties of a geotextile. Also of interest is the weight, an index property that gives a designer a general idea of the thickness and makeup of a geotextile. These properties, as reported in the most current manufacturer literature, are provided in Table 3.7.

Table 3.7: Manufacturer-reported geotextile property values

Property	Unit	Value
Weight	g/m^2	203
	oz/yd^2	6.0
Permittivity	sec^{-1}	1.6
Transmissivity	$l/min/m^2$	4480
	gpm/ft^2	110
AOS	mm	0.212
	U.S. Sieve #	70

3.2.2 Water Retention Curve

The water retention curve for the geotextile was developed with a simple laboratory setup designed to run capillary rise tests. While the most common method used to develop a geotextile water retention curve is the hanging column (Iryo and Rowe 2003, McCartney et al. 2005, McCartney et al. 2008), the capillary rise test is a simpler, much quicker alternative, and has been shown to provide similar results (Lafleur et al. 2000, Krisdani et al. 2006, Krisdani et al. 2008). Figure 3.11 shows a schematic of the laboratory testing setup used.

The basic premise of the capillary rise test is provided in section 2.3.1. In the tests performed as part of this study, a geotextile strip of 2 cm width and 30 cm height was suspended in a covered graduated cylinder with its base submerged in a reservoir of water. The system was allowed to equilibrate over a period of 48 hours. At the end of the equilibration period, the portion of the geotextile under suction (above the water reservoir) was cut into strips 2 cm in length and water contents were obtained from each strip. Each water content was plotted versus the average suction in the strip to form the water retention curve. The average suction for a given geotextile strip was calculated as follows:

$$\psi_{ave} = \rho_w g H_{ave} \tag{3.1}$$

where H_{ave} is the height above the water reservoir at the midpoint of the strip.

Hysteresis is expected between the wetting and drying behavior of the geotextile. Both wetting and drying curves may be obtained with the capillary rise test. The wetting curve is obtained by hanging a geotextile strip that is initially dry. In this study, the "dry" condition was achieved by allowing a geotextile in condition as received from the manufacturer to equilibrate at room temperature. Other studies have found that washing the geotextile, removing chemical coating present on the geotextile as a result of the manufacturing process, significantly changes the hydraulic behavior of the geotextile (Stormont et al. 1997). The drying curve was obtained by first boiling the geotextile strip to ensure saturation, then immediately hanging in the graduated cylinder used for the capillary rise test. Two tests were run for each curve, wetting and drying, with the results presented in Figure 3.12.

Results from the capillary rise test completed for the geotextile used in this study compare favorably with results from hanging column tests run on a similar nonwoven geotextile of the same polymer type and manufacturing method (McCartney et al. 2008). Figure 3.13 shows a comparison of the two sets of data. As seen in Figure 2.4, Iryo and Rowe (2003) present the most extensive database of water retention data for nonwoven geotextiles found in the literature, including data from earlier capillary rise tests completed by Lafleur et al. (2000). The data obtained via capillary rise tests in this study show behavior similar to results reported in both studies.

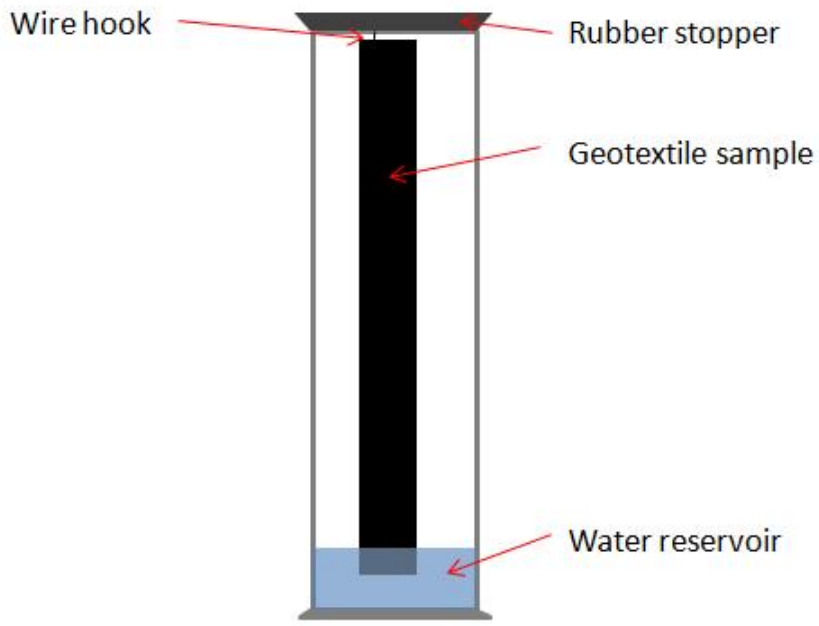

Figure 3.11: Schematic of capillary rise test

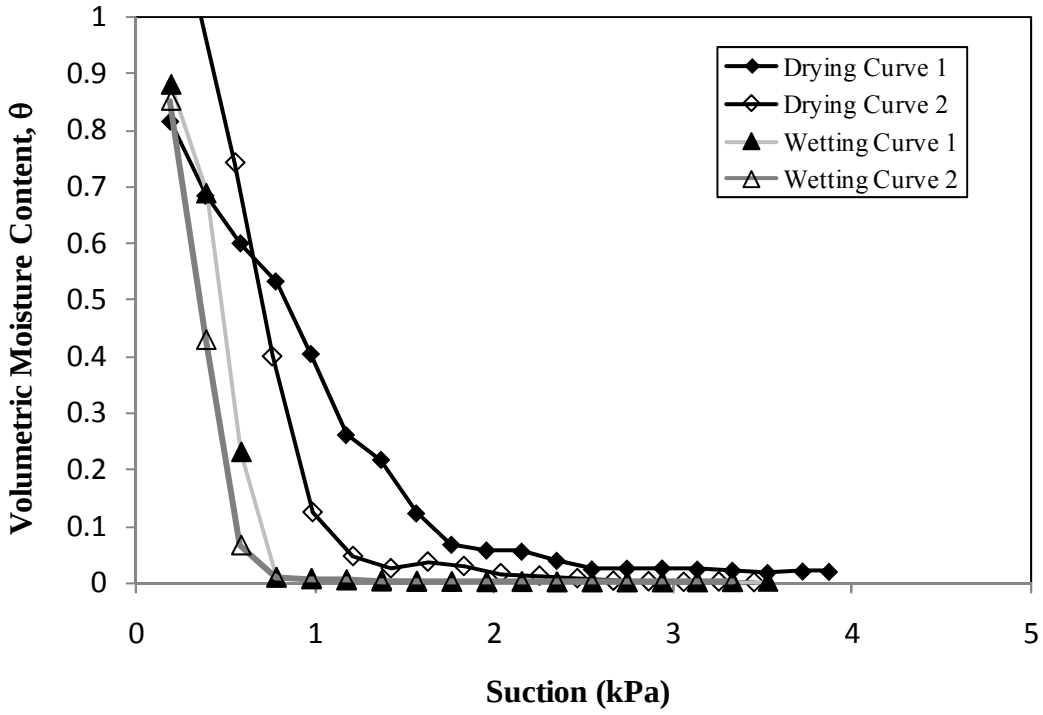

Figure 3.12: Capillary rise test results—wetting and drying curves

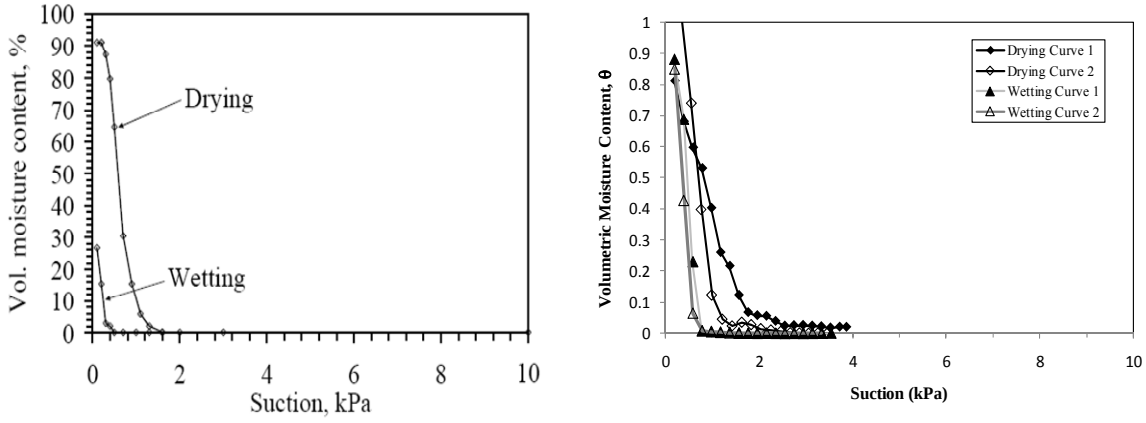

(a) (b)

Figure 3.13: Comparison of water retention data obtained in (a) McCartney et al. (2008) and (b) this study

Data from "Drying Curve 1" in Figures 3.12 and 3.13, obtained in this experimental study, contain volumetric moisture contents greater than 1.0 at the lowest end of the suction range tested. Obtaining accurate water contents from the strip of geotextile ending in the water reservoir presents problems due to the presence of free water not contained in the actual pore structure of the geotextile. This resulted in an overestimated θ at the lowest suction value for "Drying Curve 1"—however, due to lack of a standardized correction, the data point is included in retention data presented in Figures 3.12 and 3.13.

The van Genuchten fitting method provides a good fit for geotextile water retention data (Iryo and Rowe 2003). Figure 3.14 shows the curve constructed with the van Genuchten fitting method along with raw data obtained from "Wetting Curve 1" of the capillary rise tests. The van Genuchten fit requires the saturated volumetric water content as an input—this value is assumed equal to the calculated porosity, 0.865, determined as follows (Stormont et al. 1997):

$$n = 1 - \frac{\mu}{\rho_f t} \tag{3.2}$$

where μ = mass per unit area, ρ_f = fiber density (assumed to be 0.91 g/cm^3 for polypropylene), and t = specimen thickness at estimated appropriate confinement stress. The degree of saturation, useful for comparison of soil and geotextile behavior, is calculated from the obtained gravimetric water contents as follows:

$$S = \frac{w\mu}{t\rho_w \eta} \tag{3.3}$$

where w is the gravimetric water content and ρ_w is the density of water.

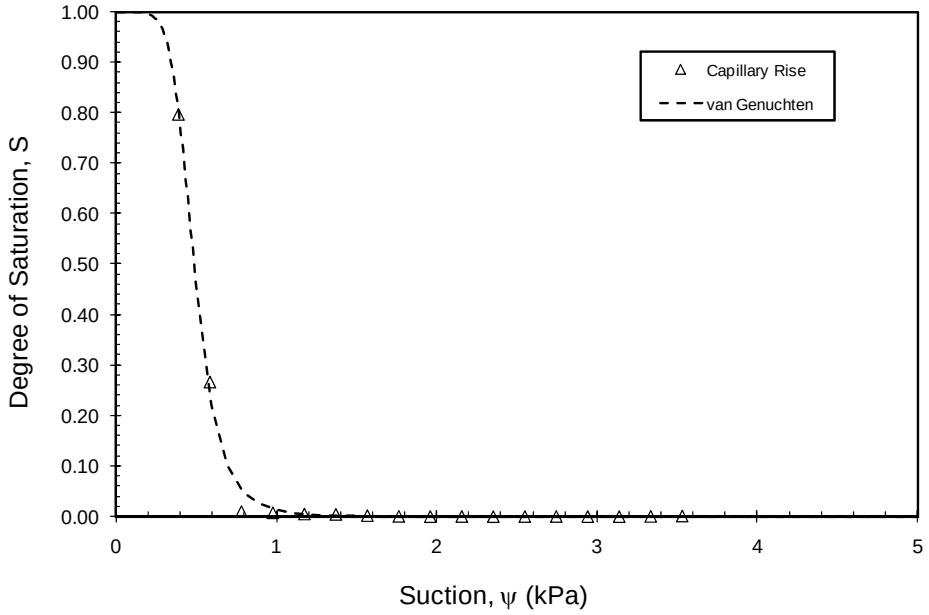

Figure 3.14: Geotextile water retention curve—van Genuchten fitting method

3.2.3 Hydraulic Conductivity Function

The hydraulic conductivity function for the geotextile used in this study, shown in Figure 3.15, was approximated with the van Genuchten-Mualem fitting method. In addition to the van Genuchten parameters, α and N, obtained from fitting the water retention curve, the cross-plane saturated hydraulic conductivity of the geotextile is a required input for the model. A reasonable approach for estimating cross-plane saturated hydraulic conductivity involves multiplying the geotextile permittivity by its thickness. Thickness will vary according to the overburden pressure placed on the geotextile, but a reasonable estimate may be made with confinement in the laboratory. In this study, a cross-plane saturated hydraulic conductivity of 0.264 cm/s was calculated from a manufacturer-reported permittivity of 1.6 sec^{-1} and a laboratory-measured thickness of

0.165 cm. This is similar to the value reported in McCartney et al. (2008) for a similar nonwoven geotextile—0.34 cm/s.

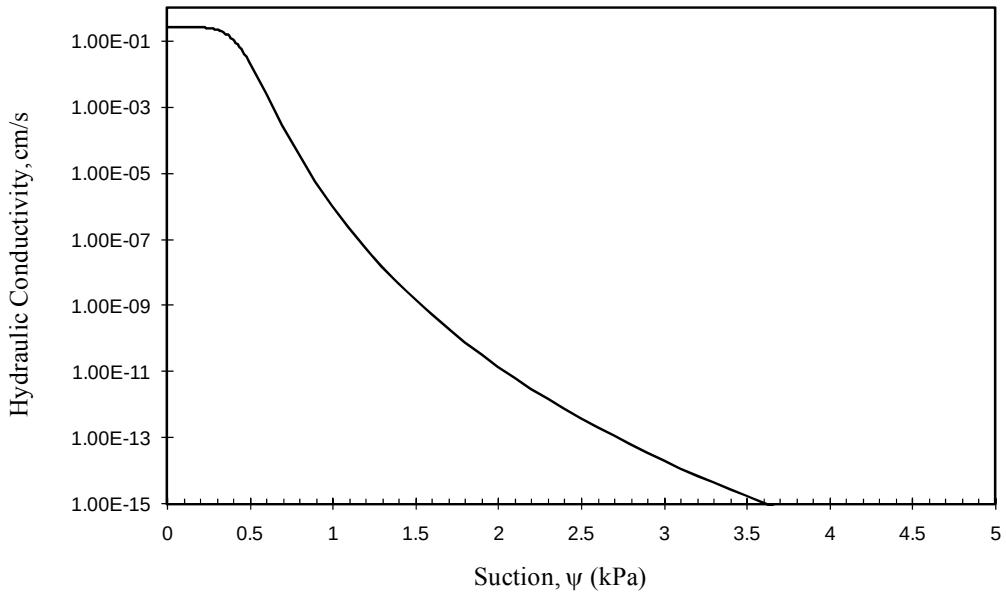

Figure 3.15: Geotextile K-function—van Genuchten-Mualem fitting method

3.3 DESIGN AND CONSTRUCTION OF SOIL COLUMNS

The column setup designed for this study allows observing the formation of a capillary break at the soil-geotextile interface, build-up of water above the geotextile, and eventual breakthrough as a critical suction is reached at the interface. The capillary barrier models tested include a section of cover soil atop a geotextile layer, which is in turn placed over a base gravel layer. In addition to fulfilling the primary objective of modeling an actual soil-geotextile capillary barrier system, a major focus during selection of column components and instrumentation was simplicity. The goal was to design small

columns that are able to provide information in a reasonably short amount of time given the low flow rates required, with minimal instrumentation.

Clear cast acrylic tubing with 19.7 cm diameter and 30.5 cm height was selected for the main column. This material allowed for visual monitoring of progression of the moisture front as well as formation and breakthrough of the capillary break. Columns were constructed atop a base plate of 0.64 cm thickness with holes drilled beneath the column cross-section to allow for drainage upon breakthrough of the capillary break. Drilled holes in the base plate had a diameter smaller than the relatively uniform particle size of the gravel layer placed beneath the geotextile. The base plate was mounted atop an opening sized to accommodate a 20 cm collar housing a rainfall collector funnel. The top plate extends behind the column to provide a platform for the pumps used to apply flow to the models. A table was constructed to provide simultaneous testing of four soil columns. The column setup is shown in Figure 3.16.

A small, pea-sized gravel layer was included at the base of the column to act as a transition layer from the geotextile to the hole-filled base plate, and to absorb some of the stress applied to the column due to compaction of the cover soil layer. The thickness of the gravel layer (2 cm) was minimized to decrease the lag time between actual breakthrough of the capillary barrier and the onset of flow, as measured with the tipping buckets. A minimum thickness was also desired to obtain a better estimate of the total storage provided by the cover soil layer, i.e., to minimize the amount of additional storage provided by the gravel layer at failure, which is difficult to estimate. It was determined that over 2 cm of gravel was not required to prevent harm to the cast acrylic base plate as a result of soil compaction.

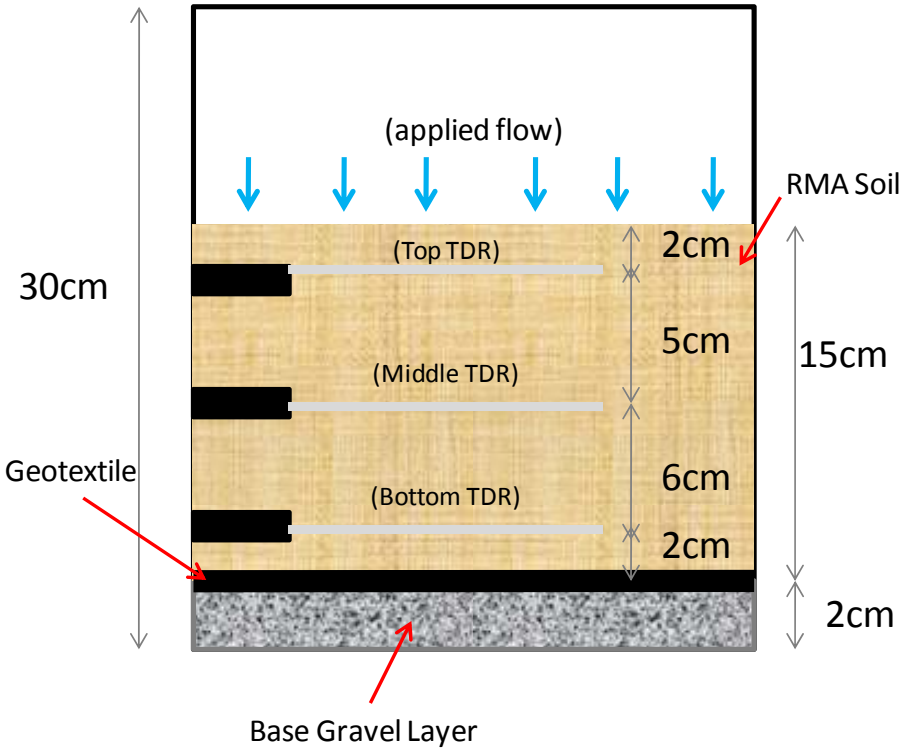

Figure 3.16: Soil column setup

For the initial tests, a thin layer of vacuum grease was applied to the inside of the soil column prior to compaction of the cover soil to minimize side wall leakage. This made visual inspection of moisture front progression impossible, which was one of the objectives for choosing a clear, cast acrylic material used for the columns. Column tests run without applying the vacuum grease provided similar results, and the added benefit of monitoring the moisture front visually. The remainder of the column tests were run without applying vacuum grease.

The first step in preparing each model for testing involved compacting the base gravel layer. As this layer was placed simply to act as a transition and is not involved in the analysis of the column results, it was not necessary to measure the relative density upon placement. Gravel was placed and compacted lightly with a compaction hammer

until a firm, level surface was obtained at an elevation 2 cm above the column's bottom plate.

Next, the geotextile was placed atop the gravel layer. The geotextile was cut to a diameter approximately 1 cm greater than the inner column diameter. This allowed for a slight overlap around the column wall, shown in Figure 3.17. This overlap ensured that no localized leaking would occur around the edge of the geotextile once the moisture front reached the soil-geotextile interface.

After placement of the geotextile, the soil cover layer was placed in five lifts of 3 cm each. TDR probes were placed in the bottom, middle, and top compaction layers. The probes were inserted through holes in the side of the column prior to compacting the corresponding layer. The coaxial cable leading to the TDR probe was threaded through a rubber stopper, which was then placed snugly into the hole cut for the TDR probe to prevent leakage.

A picture of a fully prepared column is shown in Figure 3.18.

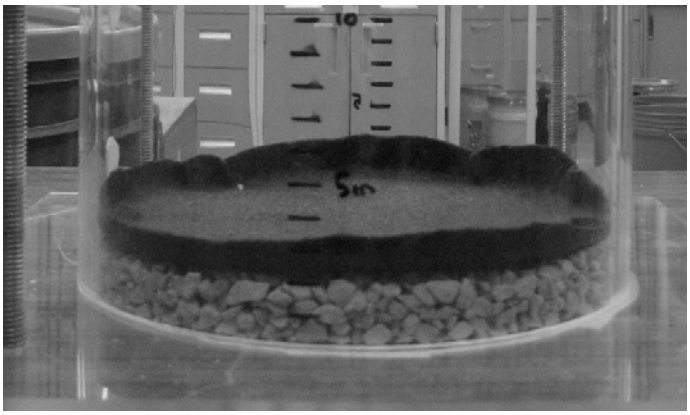

Figure 3.17: Geotextile placement with slight overlap at column sides

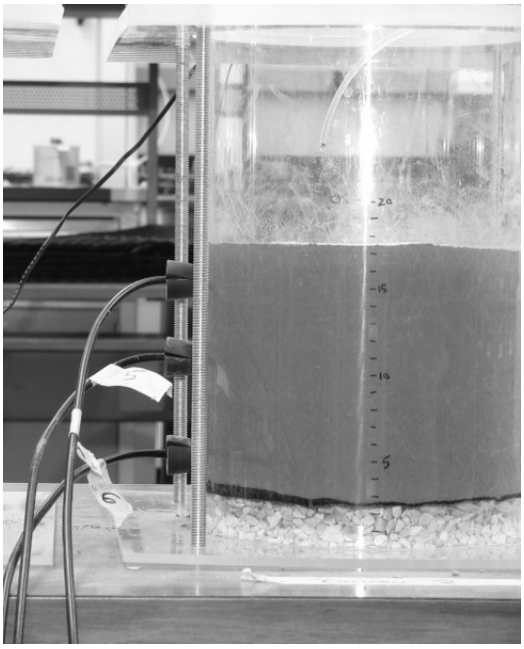

Figure 3.18: Prepared soil column

3.4 COLUMN PUMPS AND INSTRUMENTATION

Pumps and instrumentation were incorporated into the column setup to perform three objectives: apply flow to the top of the soil column, monitor progression of a moisture front down the column and creation of a capillary break at the soil-geotextile interface, and detect breakthrough of the capillary barrier.

3.4.1 Flow Pumps

Pumps capable of applying very low flow rates consistently for an extended period of time, from days to weeks, were required for this project. In order to maintain unsaturated conditions in the cover soil, the applied flow rate must be smaller than the soil's saturated hydraulic conductivity. The saturated hydraulic conductivity of the soil

used in this study, $8.2*10^{-5}$ cm/s, corresponds to an equivalent volumetric flow rate of 1.50 mℓ/min.

A peristaltic pump has been used in multiple studies in the literature to apply the low flow rates required for typical column tests (Stormont and Anderson 1999, McCartney et al. 2005). This system works well and is very accurate over long periods of time, with a digitally controlled flow rate regulator, but is expensive. Consistent with the objective of this project to create a more practical laboratory setup, this study used a simpler, cheaper alternative—a low flow peristaltic pump obtained from Fisher Scientific that maintains flows adequately over the testing periods of interest. The pumps, shown in Figure 3.19, use a mechanical dial regulator. A pump-specific calibration of flow rate with dial setting for a given tubing diameter is required.

Flow from the pumps was initially routed into a small Styrofoam cup and through synthetic wicks to be distributed evenly across the top of the column This approach was used in other, similar column testing (Stormont and Anderson 1999, McCartney et al. 2005). However, it was difficult to ensure that flow was distributed evenly amongst the wick ends after being pumped into the cup, resulting in uneven distribution. This was addressed routing the outflow from the peristaltic pump directly to a circular piece of filter paper placed atop the soil column. Both flow distribution methods are shown in Figure 3.20.

Figure 3.19: Low flow peristaltic pump

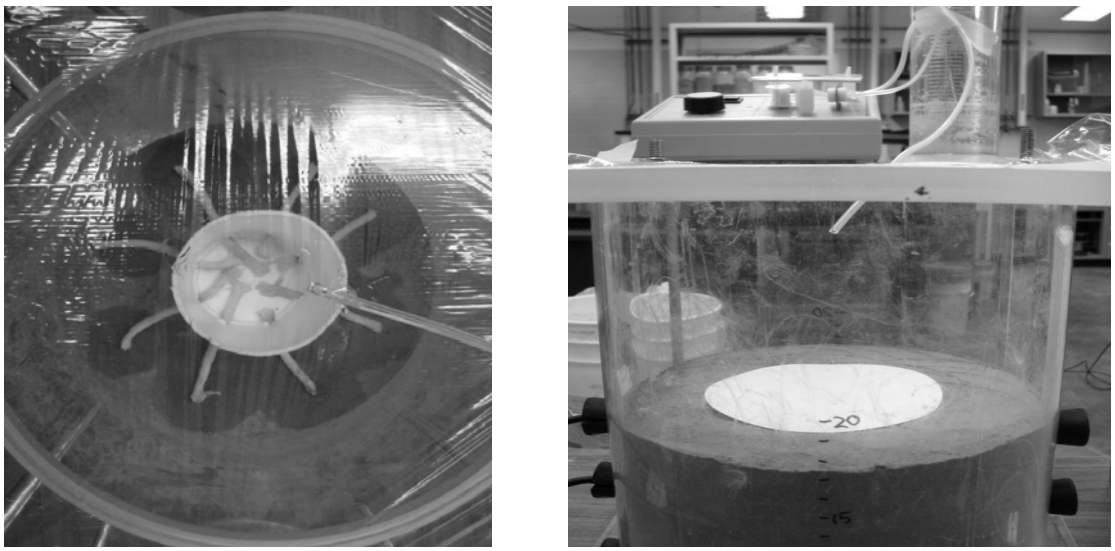

(a) (b)

Figure 3.20: Flow distribution methods—(a) synthetic wicks, (b) filter paper

3.4.2 Time Domain Reflectometry (TDR) Probes

Movement of the moisture front was monitored with a series of TDR probes installed horizontally at different column elevations. Since no suction readings were taken in this study, it was increasingly important to attain accurate, reliable volumetric water content readings. TDR probes were chosen because of an extensive record of reliable measurement of soil volumetric water content in the literature.

The TDR probes used, shown in Figure 3.21, contain three rods of 8.0 cm length and 0.32 cm diameter. The spacing between the center rod and each adjacent outer rod is 0.12 cm, giving the probes a radius of influence of 0.12 cm for the entire probe length. Three probes were installed in the columns, at 2 cm, 8 cm and 13 cm above the soil-geotextile interface. Both the top and bottom probes were 2 cm from the outer boundary, ensuring that the probes' full radius of influence was contained in the soil itself. Using an automated data acquisition system, volumetric water content readings were taken every 30 to 60 minutes for the duration of each test, producing a record of changes in the column's volumetric water content profile with time.

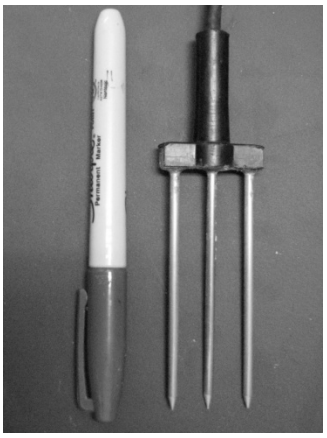

Figure 3.21: TDR probe

Obtaining a TDR probe reading involves transmitting an electrical pulse through a coaxial cable leading up to the probe through the probe head and steel rods, and measuring the reflected waveform with time. Analysis of the waveform is completed to obtain the apparent dielectric constant of the soil, which can be closely related to water content due to the large disparity between the dielectric constant of water and that of mineral soil particles or air. The initial reflection point chosen represents the time at which the applied electromagnetic pulse leaves the probe head and enters the portion of the metal rods in contact with the soil. The final reflection point represents re-entry of the pulse into the probe head after it has traveled down the length of the probe rods and back. The time taken to travel this length is related to the apparent dielectric constant of the soil as follows:

$$K_a = \left(\frac{c\Delta t}{2L}\right)^2 \tag{3.4}$$

where K_a is the apparent dielectric constant of the soil, c is the speed of light in a vacuum, and L is the actual probe length.

Location of the initial reflection point depends on the length of coaxial cable between the cable tester and the probe itself, as well as a small offset to account for the short length of metal rod contained in the probe head and not in direct contact with the soil. This value should remain constant for a given probe. A reliable method for obtaining the initial reflection point for a given probe is to use the reflection for a probe in air (Noborio 2001). However, it was observed in this testing program that the initial value is accurately obtained using a column test's initial reading, when the surrounding soil is still at a low placement volumetric water content. Once the initial value is

determined, analysis of the remaining waveforms for a given probe requires only determination of the final reflection point. Figure 3.22 presents a typical waveform and pair of reflection points.

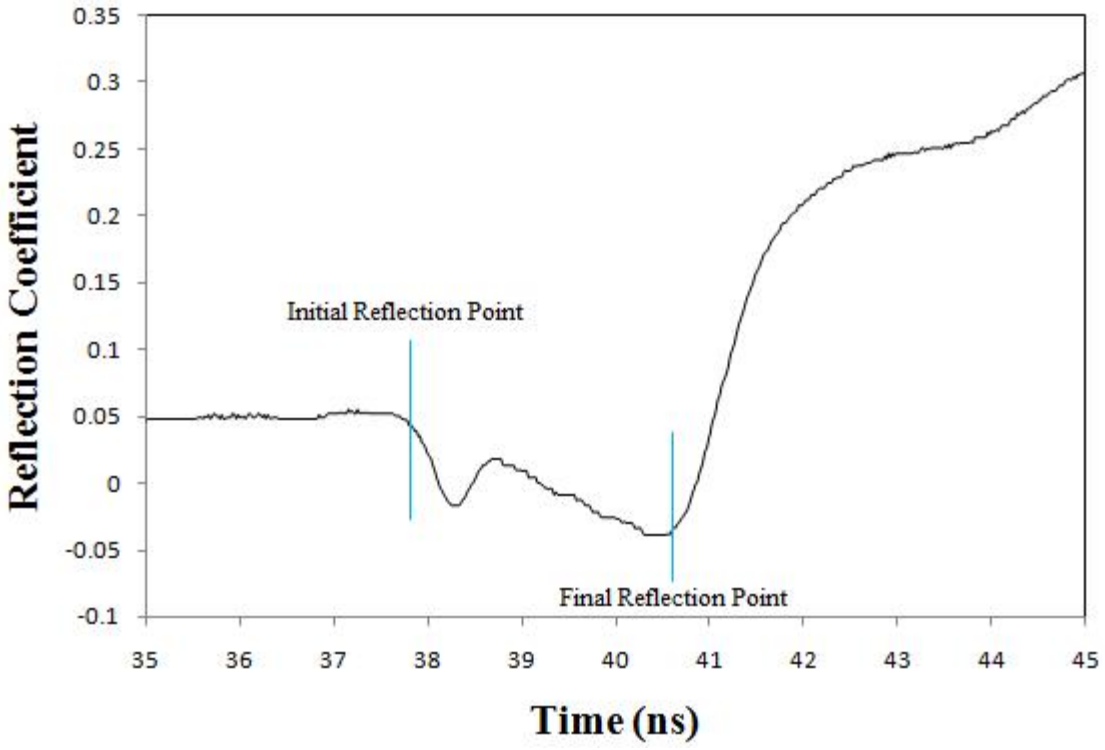

Figure 3.22: Typical reflected waveform from LabVIEW-controlled TDR100 system

A soil-specific calibration was performed with the RMA soil to obtain the most accurate TDR readings possible. This calibration was performed by a colleague, Yucao Tang, as part of a study primarily focused on closely related volumetric water content sensors, water content reflectometers (Tang 2009). Soil specimens of varying dry density and water content were compacted in a cylinder 8.9 cm in diameter and 32 cm in height. After compaction, a TDR probe was inserted into the top of the soil specimen and a

waveform was obtained with the PCTDR software accompanying the TDR100 system manufactured by Campbell Scientific (Campbell Scientific 2007). This commercial system automatically converts travel time to units of length and provides a waveform consisting of the reflection coefficient versus length traveled. In this case, selected reflection points provide an apparent length of the TDR probe, L_a. $\sqrt{K_a}$ is determined based the apparent and known lengths of the TDR probe:

$$\sqrt{K_a} = \frac{L_a}{L} \tag{3.5}$$

For mineral soils such as the lean clay used in this study, volumetric moisture content is a linear function of $\sqrt{K_a}$ over the range of practical interest—many commonly used empirical relationships are in the form of a linear relationship relating θ to $\sqrt{K_a}$ (Topp et al. 1998, Ledieu et al. 1986). To develop a soil-specific calibration for this project, a linear regression was used to determine the best fit for known volumetric water contents from each calibration specimen plotted against $\sqrt{K_a}$ calculated from waveform interpretation. Equation 3.6 gives the resulting calibration equation—the accompanying raw data is presented in Figure 3.23. Based on the data collected for this calibration, the accuracy of θ values obtained with the soil-specific calibration is around +/- 1%, or +/- 0.01 volumetric moisture content. This is consistent with reported values in the literature, generally +/- 2 to 3% for a generic calibration and +/- 1% if a soil-specific calibration is obtained (Noborio 2001).

$$\theta = 0.1003\sqrt{K_a} - 0.1921 \tag{3.6}$$

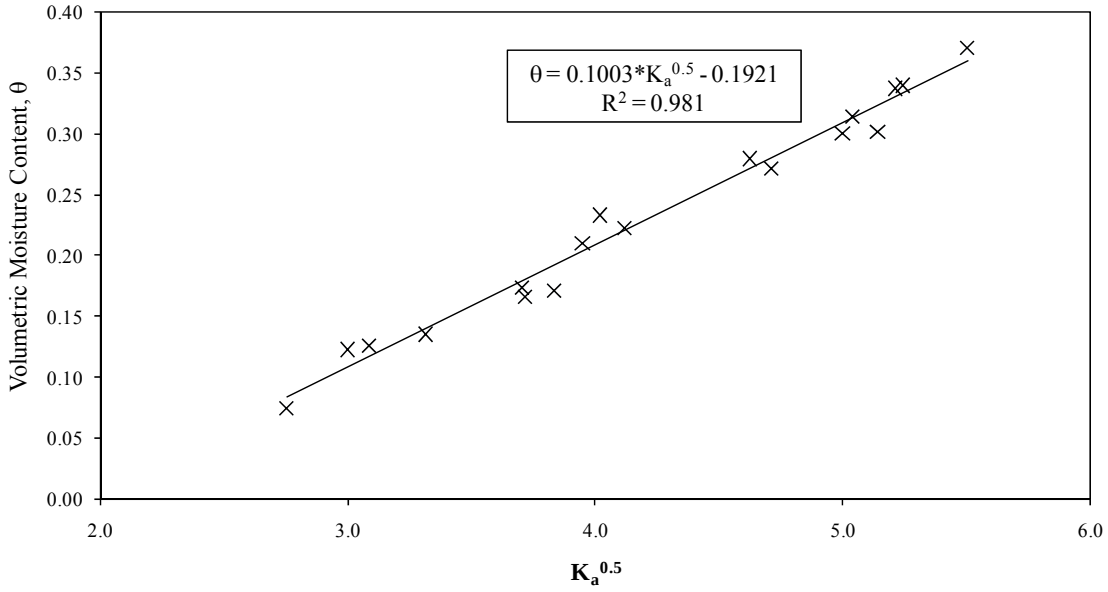

Figure 3.23: RMA-specific TDR calibration

In column tests, TDR readings were obtained with an automated data acquisition system set up with National Instruments LabVIEW software controlling a Campbell Scientific TDR100 system. The TDR100 system consists of a 12V power supply, a control module that generates a short rise time electromagnetic pulse and samples and digitizes the reflected waveform, and a multiplexer used to allow reading of multiple TDR probes in succession. Waveforms are in the form of reflection coefficient versus time. The LabVIEW program was set up to automate initiation of probe readings at a user-defined time interval and to store the collected waveforms in a convenient format. The LabVIEW program also allows for customization of waveform properties, such as start time and duration of the saved waveforms, number of points in the waveform, and number of measurements averaged at a given distance to create each respective waveform point.

3.4.3 Tipping Buckets

Breakthrough of the capillary barrier model results in a flux of water across the soil-geotextile interface. The time of breakthrough is measured with a tipping bucket, or rainfall gauge, placed beneath the column base plate. The specific model used in this study is a Texas Electronics model TR-525USW rain gauge, shown in Figure 3.24. A 20.3 cm (8 in) brass collector collar, attached to the top of the main gauge body, conveniently fits below and adequately collects all outflow from the 19.7 cm (7.75 in) diameter soil columns. Collected water is funneled into a tipping bucket, a mechanical device that tips when filled to its water capacity. When a tip occurs, an electric switch is momentarily closed, sending a voltage pulse to a data acquisition system set up with LabVIEW. The data acquisition system records the time of the initial tip, which signifies breakthrough of the capillary barrier.

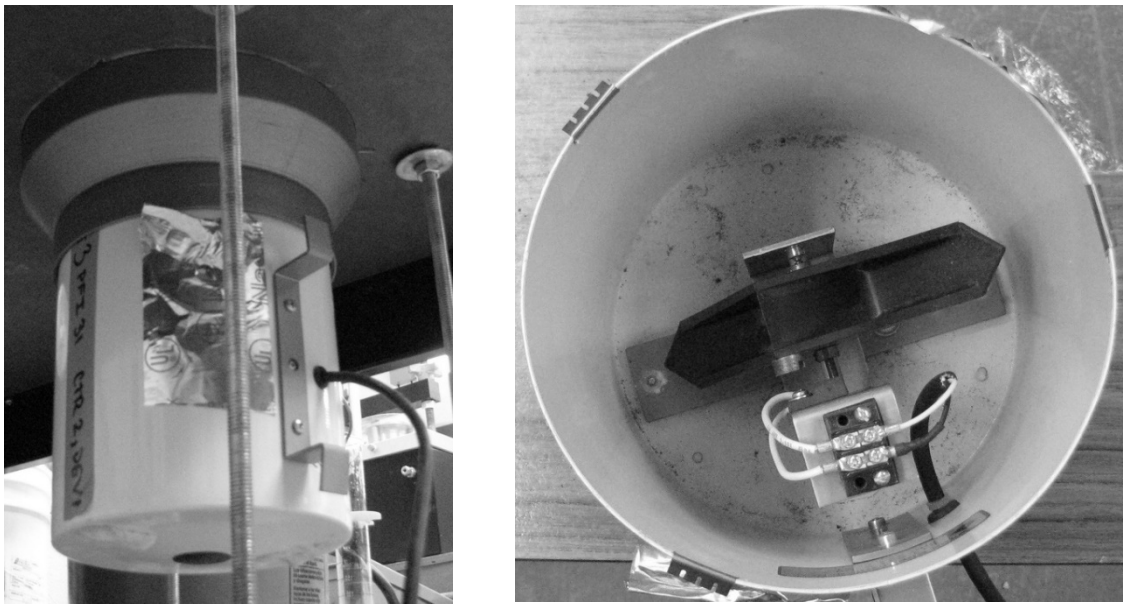

Figure 3.24: Tipping bucket

3.5 SCOPE OF THE TESTING PROGRAM

To address the objectives set forth in Chapter 1, a series of column tests were planned. A "baseline" case would be established, to which subsequent column tests would be compared. Preparation conditions for the baseline case, including initial volumetric water content and relative compaction, were chosen to represent conditions found in a cover soil actually constructed in the field. This study also included investigation of the effect of varying the soil relative compaction. The intent was to gain insight into the effect of this variation on the rate of flow down the column, the suction and corresponding moisture content at the soil-geotextile interface when breakthrough occurs, the complete moisture content profile at failure and associated storage capacity.

The actual capillary barrier system used as a basis for the small models constructed as part of this research project is located in a dry, arid environment in the western United States. As a result, a relatively low initial volumetric water content, θ_i of 0.10 was selected. This target initial water content was constant for all column tests. Initial plans called for testing columns at relative compaction levels of 70%, 80% and 90%. 80% relative compaction was chosen for the baseline case so that the effects of increasing or decreasing the compaction level could be investigated.

In addition to improving the current understanding of the behavior of a geotextile capillary barrier and the effectiveness of laboratory characterization in predicting this behavior, as well as investigating the effect of varying relative compaction on capillary barrier performance, another major objective was to work towards simplifying the testing setup required to understand the important parameters to capillary barrier performance. This resulted in several changes to the testing setup during implementation of the overall testing plan. For example, the first good data obtained from column testing was from a test performed on a soil column with only two TDR probes, at 2 cm and 8 cm above the

geotextile. After analyzing the data from this test, it was concluded that a much better representation of flow down the column and any moisture content profile would be obtained by adding another TDR probe near the top of the column. The remainder of the column tests were run with three installed TDR probes, at 2 cm, 8cm and 13 cm above the soil-geotextile interface.

Another example of a change in testing setup resulting from observations while implementing the overall testing plan is related to the applied flow rate. In order to select an appropriate flow rate, it was necessary to balance a desire to use a higher flow rate in order to speed up the required testing time with a need to keep the flow rate sufficiently below the saturated hydraulic conductivity of the soil. For the first two sets of tests, applied flow rates of 0.43 and 0.44 mℓ/min, respectively, were used, equivalent to Darcian velocities of $2.3*10^{-5}$ and $2.4*10^{-5}$ cm/s. This resulted in a total required testing time of around three days. However, considering the uncertainty inherently present in a saturated hydraulic conductivity value, the possibility of this applied flow rate being exceedingly close to the actual saturated hydraulic conductivity of the soil seemed viable. As a result, two column tests were run with an applied flow rate equivalent to a Darcian velocity of $8.1*10^{-7}$ cm/s and $7.6*10^{-7}$ cm/s, respectively. These tests took over 30 days to reach breakthrough, a much less practical testing setup. Additionally, analysis of the resulting data proved that similar test results were obtained with the higher flow rate.

Finally, it was found to be impossible to reach 90% compaction at the target initial water content without damaging column equipment. As a result, only columns with relative compaction levels 80% and below were tested.

The background information given in this section, on lessons learned and adjustments made during implementation of the testing program, is given to better

understand the progression of tests completed in this study. Table 3.8 summarizes relevant parameters for each column test completed.

Table 3.8: Summary of relevant properties for each column test

Test[1]	Column	Relative Compaction (%)	Applied Flow (cm/s)	Flow Distribution Method
2	1	78	$2.3*10^{-5}$	Synthetic Wicks
4	1	79	$2.4*10^{-5}$	"
	2	74	$2.4*10^{-5}$	"
5	1	73	$8.1*10^{-7}$	Filter Paper
	2	78	$7.6*10^{-7}$	"
6	1	60	$2.5*10^{-5}$	"
	2	70	$2.3*10^{-5}$	"
	3	80	$2.2*10^{-5}$	"
7	1	70	$2.7*10^{-5}$	"
	2	70	$2.7*10^{-5}$	"
8	1	80	N/A (ponded water test)	"

[1] Tests 1 and 3 were considered preliminary.

Chapter 4: Results of Small Column Capillary Barrier Testing

Results from each of the columns tested are presented in this chapter. Column parameters are presented in Table 3.8, but relevant setup information as well as any additional information helpful in understanding the results of each test are reviewed here. Processed raw data for each test gives a record of volumetric moisture content with time for each TDR probe. The data is presented in this chapter in chronological order. Detailed analysis of the data is provided in Chapter 5. The tests considered in this study are Tests 2, 5, 6, 7 and 8.

4.1 TEST 2

Test 2 consisted of a column prepared to 78% relative compaction, resulting in a dry density, γ_d, of 1.44 g/cm^3 and a porosity, η, of 0.47. An average flow rate of 0.43 mℓ/min, corresponding to a Darcian velocity of $2.3*10^{-5}$ cm/s, was applied to the top of the column using the synthetic wick distribution method illustrated in Figure 3.19. Only two TDR probes were placed in the column during compaction, at elevations of 2 cm and 8 cm above the soil-geotextile interface, respectively. A schematic of the column is illustrated in Figure 4.1. Readings from the two TDR probes were taken every 30 minutes—the volumetric moisture content versus time data is presented in Figure 4.2.

The moisture front reaches the TDR located 8 cm above the soil-geotextile interface approximately 1000 minutes after the applied flow started, after which the volumetric moisture content at that column elevation steadied at around 0.32. It should be noted that, in this chapter, "arrival" of the moisture front is loosely defined as the beginning of the sharp increase in moisture content for a given TDR probe—more detailed analysis is presented in Chapter 5. At approximately 2000 minutes, the moisture

front reached the bottom TDR, just 2 cm above the soil-geotextile interface. Consistent with the formation of a capillary break, the volumetric moisture contents measured at both TDR probe locations continue to rise (without breakthrough) for over 1500 minutes after the moisture front reaches the soil-geotextile interface. Breakthrough is indicated by outflow measured by the tipping bucket at an elapsed time of 4160 min. At the time of breakthrough, the volumetric moisture content measured by the TDR probe 2 cm above the geotextile was 0.41. TDR-measured moisture contents appear to level off around 200 minutes prior to the measured breakthrough, which is probably the actual time of breakthrough. This delay is attributed to storage in the base gravel layer.

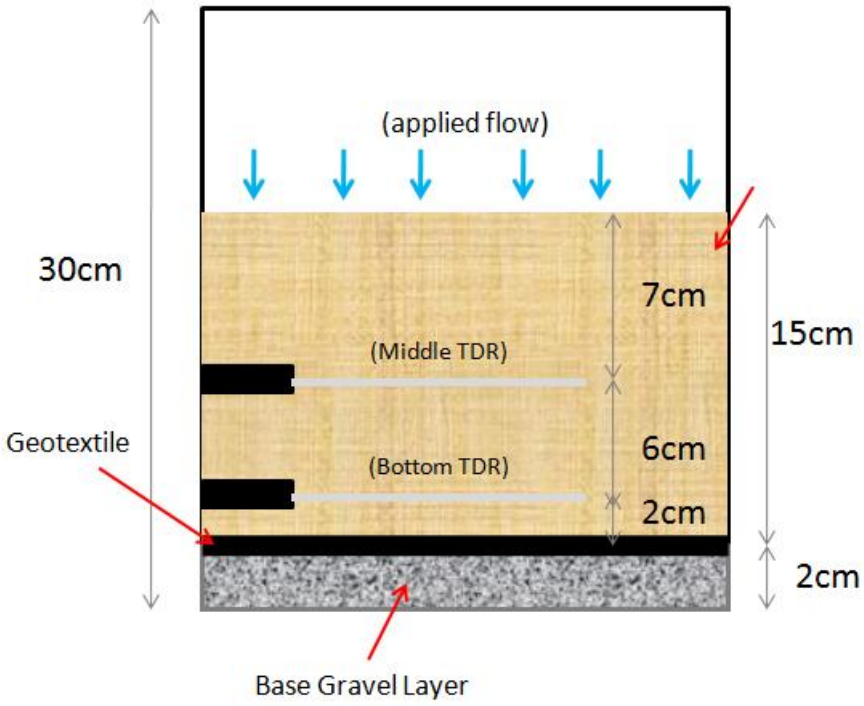

Figure 4.1: Test 2 column schematic

Analysis of the Test 2 data highlighted the need for an additional TDR probe to be placed closer to the top of the column. This probe would provide a better understanding of the movement of the moisture front down the soil column as well as the changing moisture content profile with time.

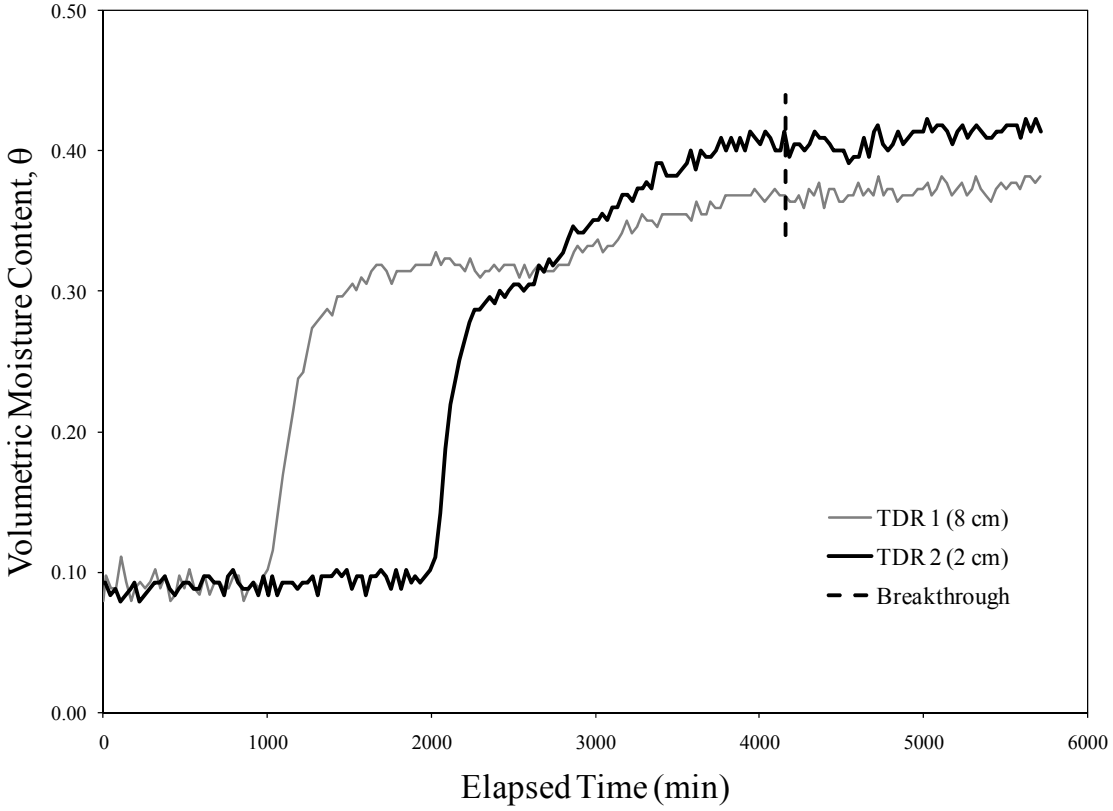

Figure 4.2: Volumetric moisture content versus time data for Test 2

4.2 TEST 4

Two columns were prepared for Test 4. The targeted relative compaction levels were 80% and 70% for Columns 1 and 2, respectively. Compaction levels actually

reached were 79% for Column 1 and 74% for Column 2, corresponding to dry densities of 1.45 and 1.36 g/cm^3 and porosities of 0.46 and 0.50, respectively. Both columns contained three TDR probes, at 2 cm, 8 cm and 13 cm above the soil-geotextile interface. The basic column layout, used by all remaining tests, is illustrated in Figure 3.16. A flow rate equivalent to a Darcian velocity of $2.4*10^{-5}$ cm/s was applied to the top of each column through the synthetic wick distribution system. TDR measurements, shown in Figures 4.3 and 4.4, were taken every 60 minutes.

A gap exists in the volumetric moisture content time series from around 1600 to 3000 minutes elapsed time. The multiplexer described in Section 3.4.2, part of the Campbell Scientific TDR100 system, provides the ability to switch between multiple probe channels via electrical switches. The gap in the data for Test 4 was caused by a hardware malfunction in the multiplexer, which in turn failed to switch probe channels with each reading. Two columns were being tested simultaneously, so the only TDR measurements obtained from around 1600 to 3000 minutes elapsed time came from the bottom TDR in column 2, the probe on which the multiplexer was "frozen." The data still provides a chance for meaningful analysis, as shown in Chapter 5, so it is included in the presented results.

An increase in moisture content begins immediately at the location of the top TDR, only 2 cm from the surface of the column. This TDR measures a rise in moisture content up to around 0.20, where θ levels off. The middle TDR, 8 cm from the surface of the geotextile and 5 cm below the top TDR, detects a sharp rise in moisture content, signifying arrival of the moisture front, at around 800 minutes elapsed time. Volumetric moisture content continues to increase at this location to around 0.30 before steadying just before the gap in the data. This is well above the θ value at which the top TDR probe levels out. An increase in the bottom TDR's moisture content begins at around 1500

minutes, just at the beginning of the gap in moisture content data. Assuming the moisture front velocity stays nearly constant, it is reasonable to estimate that the moisture front reaches the geotextile interface at around 2000 minutes. Formation of a capillary break results in a continued rise in moisture content for the bottom TDR probe. This rise is also reflected in measurements at the middle of the column, and after a slight delay the top TDR probe registers a steady rise in θ. At breakthrough, the bottom TDR indicates a volumetric moisture content of approximately 0.38 near the soil-geotextile interface.

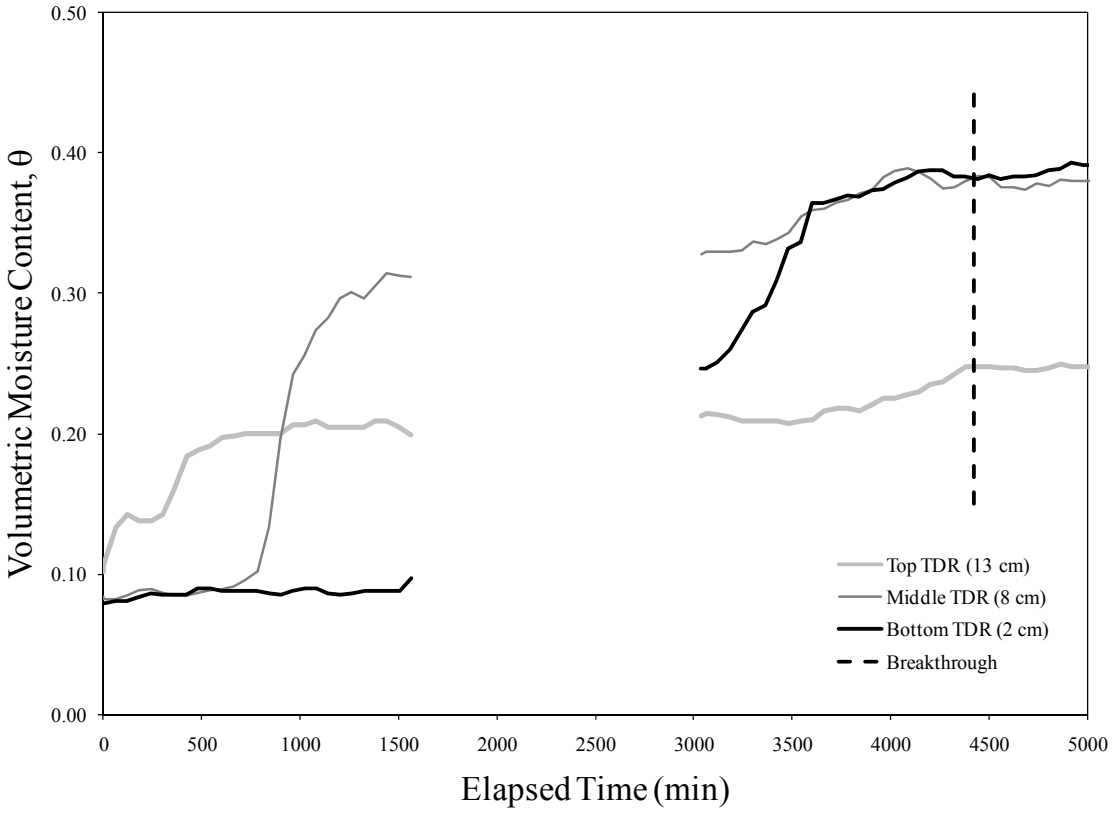

Figure 4.3: Volumetric moisture content versus time data for Test 4, Column 1

The bottom TDR probe in Column 2 was not affected by the multiplexer malfunction, as the electric switch was "stuck" on its channel. The behavior of Column 2 is similar to that of Column 1. A rise in moisture content is measured immediately by the top TDR probe. The moisture front reaches the middle probe slightly sooner than seen in Column 1, at around 500 minutes as opposed to 800. Measured θ at the middle probe increases rapidly to around 0.23, before rising steadily at a lower rate. Presumably, θ continues to rise at this rate until breakthrough occurs, although the exact behavior is unknown, as this portion of the curve is lacking. At breakthrough, the volumetric moisture content 2 cm above the soil-geotextile interface is 0.39.

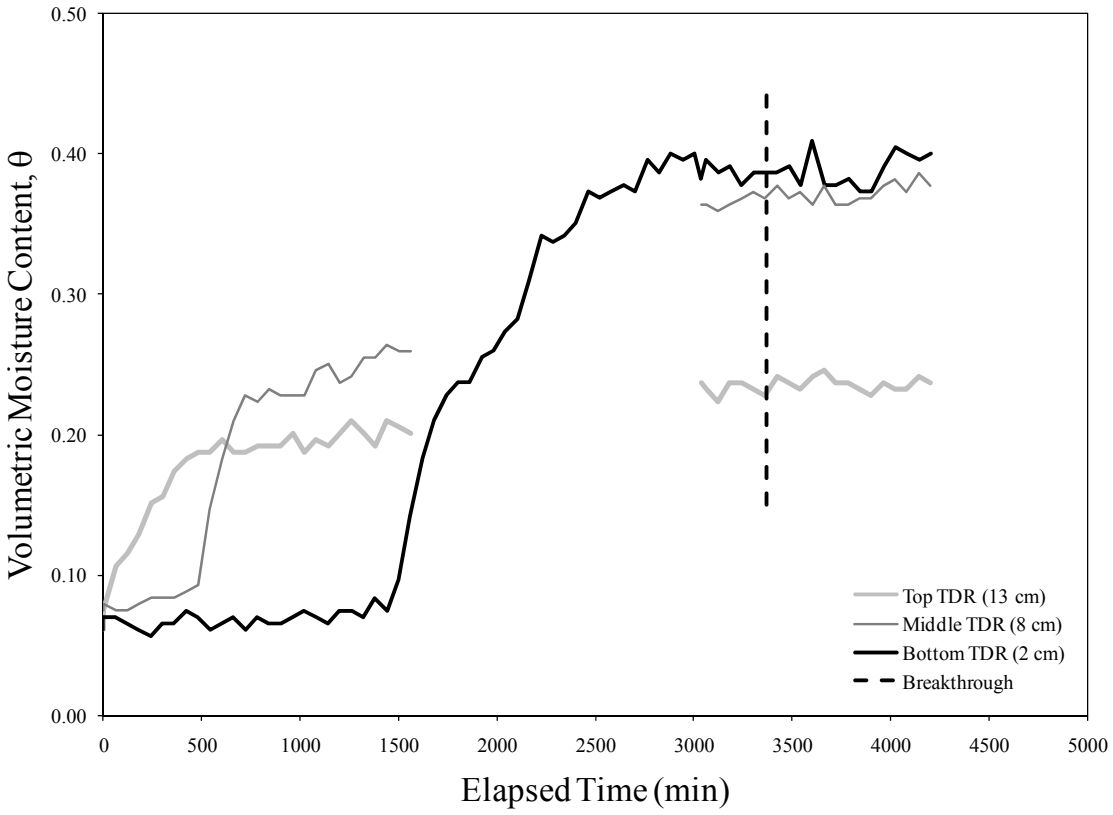

Figure 4.4: Volumetric moisture content versus time data for Test 4, Column 2

4.3 TEST 5

As mentioned in Section 3.5, two columns were tested to investigate the effect of applying a lower flow rate. These two columns make up Test 5. Column 1 was prepared to 73% relative compaction (γ_d = 1.34 g/cm^3; η = 0.50) and subjected to an applied flow rate equivalent to a Darcian velocity of $8.1*10^{-7}$ cm/s. An equivalent flow rate of $7.6*10^{-7}$ cm/s was applied to Column 2, prepared to 78% relative compaction (γ_d = 1.44 g/cm^3; η = 0.47). Results from the two tests are shown in Figures 4.5 and 4.6. TDR readings were taken once every 60 minutes. In addition to the lower applied flow rate, the major change in Test 5 was the method for distributing the flow to the top of the column. It became obvious from visual observation of previous tests that travel of the moisture front was not uniform down the soil column—this was attributed to the distribution system. Therefore, instead of a cup and synthetic wick system, used in Tests 2 and 4, the flow in Test 5 was applied directly to a circular piece of filter paper, 10 cm in diameter, sitting atop the column. This distribution system is shown in Figure 3.20.

Lowering the applied flow rate resulted in a testing duration approximately ten times that required for previous tests. In Column 1, the top TDR indicates arrival of the moisture front at approximately 1000 minutes, while the moisture front reaches the middle TDR after 3000 minutes elapsed time. Volumetric moisture content at both the top and middle TDR probes rises sharply to approximately 0.22 before leveling off. A significantly longer time is observed for the moisture front to travel from the middle TDR to the bottom TDR. While the distance between these probes, 6 cm, is close to the distance between the top two probes, 5 cm, over 7000 minutes in elapsed time passes before the bottom probe indicates arrival of the moisture front. As the moisture front

arrives at the bottom TDR, the volumetric moisture content rises sharply to around 0.21 before beginning a slower rise after formation of the capillary break occurs at the soil-geotextile interface. The top two TDR probes start this "secondary rise" in moisture content approximately 3000 minutes after the bottom probe, after which all three probes rise steadily until the breakthrough suction is reached at the soil-geotextile interface and breakthrough occurs. Volumetric moisture content at the bottom TDR was approximately 0.40 at breakthrough.

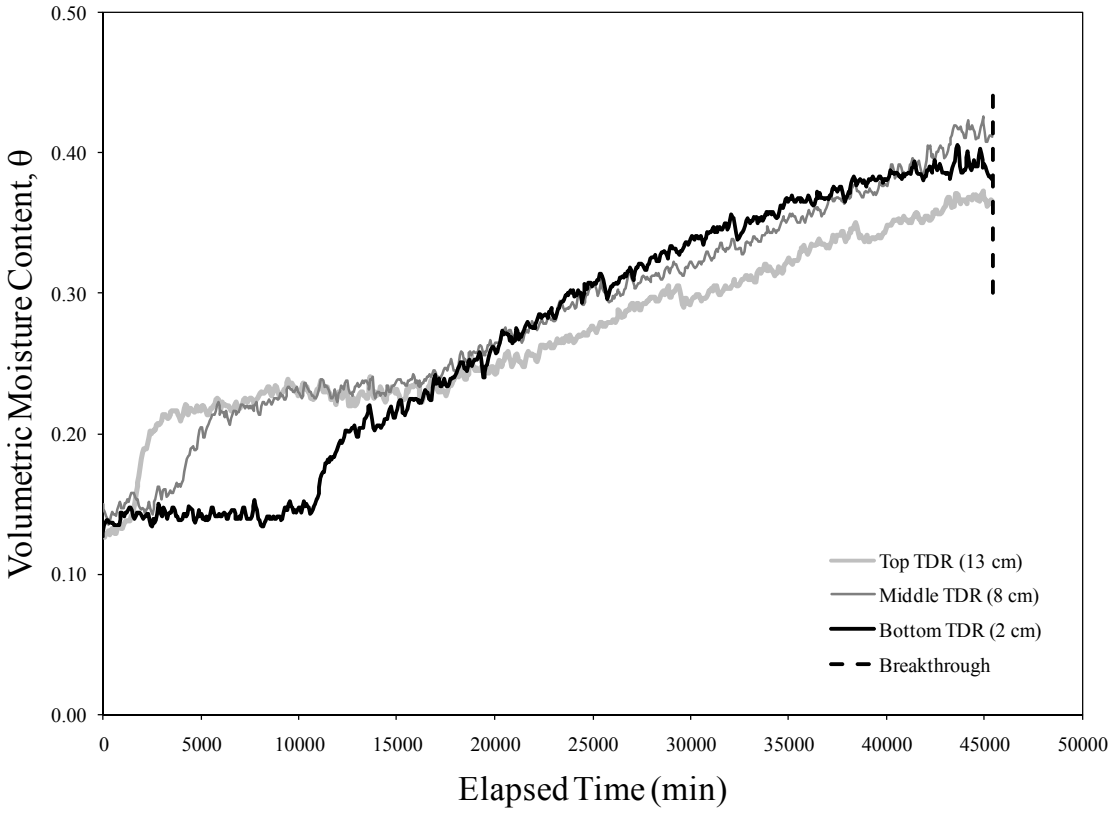

Figure 4.5: Volumetric moisture content versus time data for Test 5, Column 1

Column 2 behaves similarly to Column 1. A similar lag in travel time for the moisture front occurs between the middle and bottom TDR probes—approximately 2000 minutes pass while the moisture front passes from top to middle probes, after which about 4500 minutes pass before the moisture front reaches the bottom probe. In this column, the rise in volumetric moisture content with passage of the moisture front changes behavior after θ reaches approximately 0.20. Using the initiation of a "secondary slope" in the rise in volumetric water content for the top and middle TDR probes as an indicator, the capillary barrier looks to form at approximately 13000 minutes elapsed time. This is consistent with Column 1. However, there seems to be a slightly longer delay until the top TDR indicates a significant rise in moisture content from buildup due to the capillary barrier. Moisture content at the bottom probe increases to around 0.39 at breakthrough.

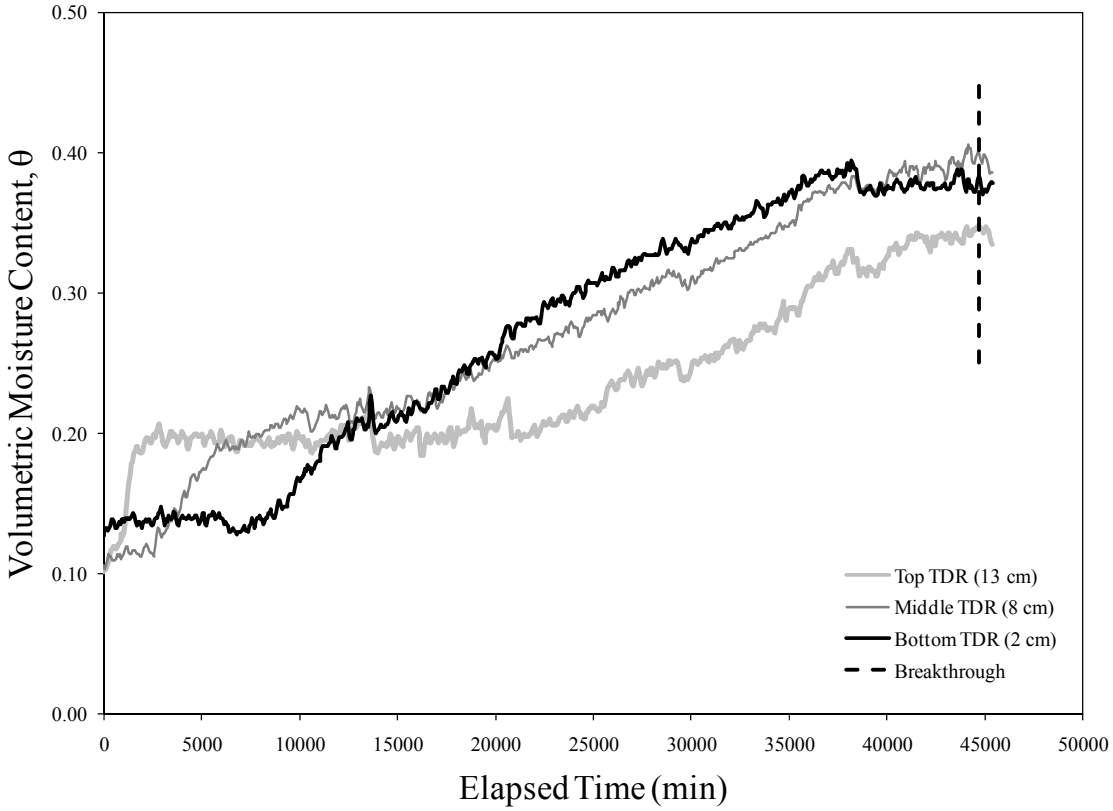

Figure 4.6: Volumetric moisture content versus time data for Test 5, Column 2

4.4 TEST 6

Three columns were prepared for Test 6, at 60%, 70% and 80% relative compaction, corresponding to dry densities of 1.10, 1.29 and 1.47 g/cm^3 and porosities of 0.59, 0.52 and 0.46, respectively. Analysis of the data from Test 5 does not justify use of a lower flow rate, which results in a required testing time of over a month. As with Tests 2 and 4, higher flow rates were applied to Test 5 to achieve more practical testing times—an equivalent flow rate of $2.5*10^{-5}$ cm/s was applied to Column 1, $2.3*10^{-5}$ cm/s to Column 2 and $2.2*10^{-5}$ cm/s to Column 3. TDR readings were taken every 60 minutes. Data from Columns 1, 2 and 3 are presented in Figure 4.7, 4.8 and 4.9.

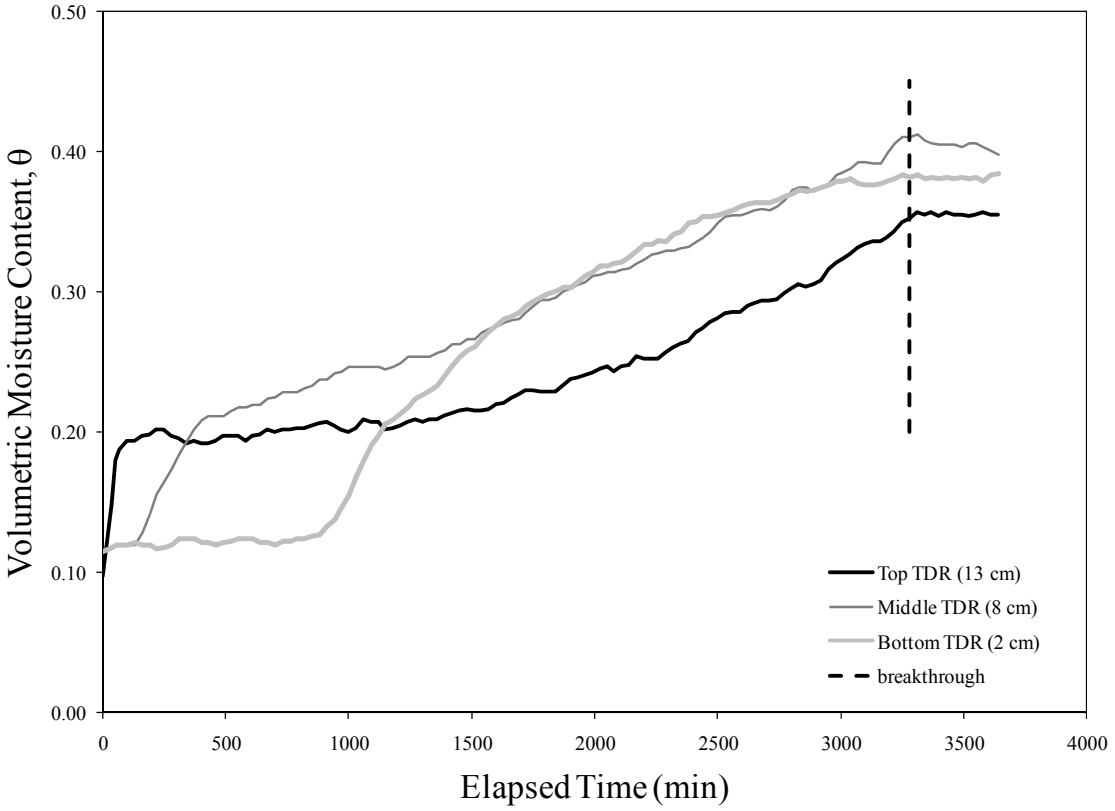

Figure 4.7: Volumetric moisture content versus time data for Test 6, Column 1

Trends seen in the behavior of Column 1 are similar to those seen in previous tests. The top TDR indicates presence of the moisture front immediately, and the front's movement to the middle TDR probe is much quicker than its subsequent movement down to the bottom TDR probe. After a sharp rise in moisture content as the moisture front arrives, each TDR probe indicates a significant change in behavior around a θ of 0.20. The top TDR levels off at this moisture content until after formation of the capillary break, while the middle and bottom TDR probes continue to indicate a rise in moisture content, but at a much slower rate. At breakthrough, the moisture content 2 cm above the soil-geotextile interface is approximately 0.38. It is important to note that the middle TDR actually indicates a higher θ, around 0.40, at the column's mid-height. However,

this difference is within the range of expected accuracy for the TDR probes—these values are probably the same. All three probes indicate a stabilization in moisture content after breakthrough occurs at around 3300 minutes elapsed time.

The top and middle probes in Column 2 behave similarly to those in Column 1. Arrival of the moisture front at both locations is signified by a sharp rise in θ up to a value of approximately 0.22, where the volumetric moisture content temporarily level off until increased moisture due to formation of the capillary barrier. The bottom TDR probe rises to a significantly higher θ value before showing the decrease in slope synonymous with passage of the moisture front and creation of the capillary break. In previous tests this break occurs at θ values between 0.20 and 0.23, while in Column 2 this break occurs at a volumetric moisture content around 0.34. Volumetric moisture contents at all three probe locations increase until breakthrough, at which time θ at the bottom TDR probe is approximately 0.40. Breakthrough occurred after approximately 3600 minutes elapsed time.

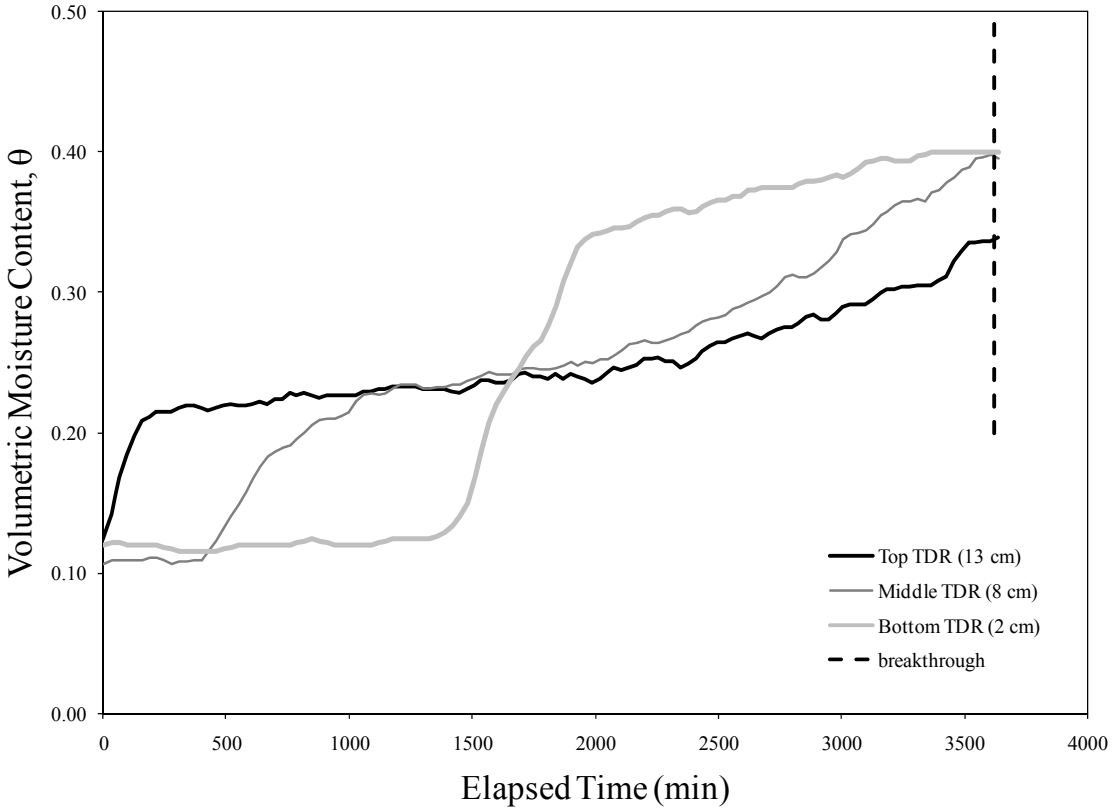

Figure 4.8: Volumetric moisture content versus time data for Test 6, Column 2

The familiar lag in moisture front velocity between the first two and last two TDR probes is present in Column 3, as approximately 1200 minutes pass for the latter interval versus approximately 400 for the former. The break in rise in volumetric moisture content occurs at around a θ of 0.23 in this column. Breakthrough occurs at approximately 3300 minutes elapsed time, with θ equal to 0.38 at the bottom TDR.

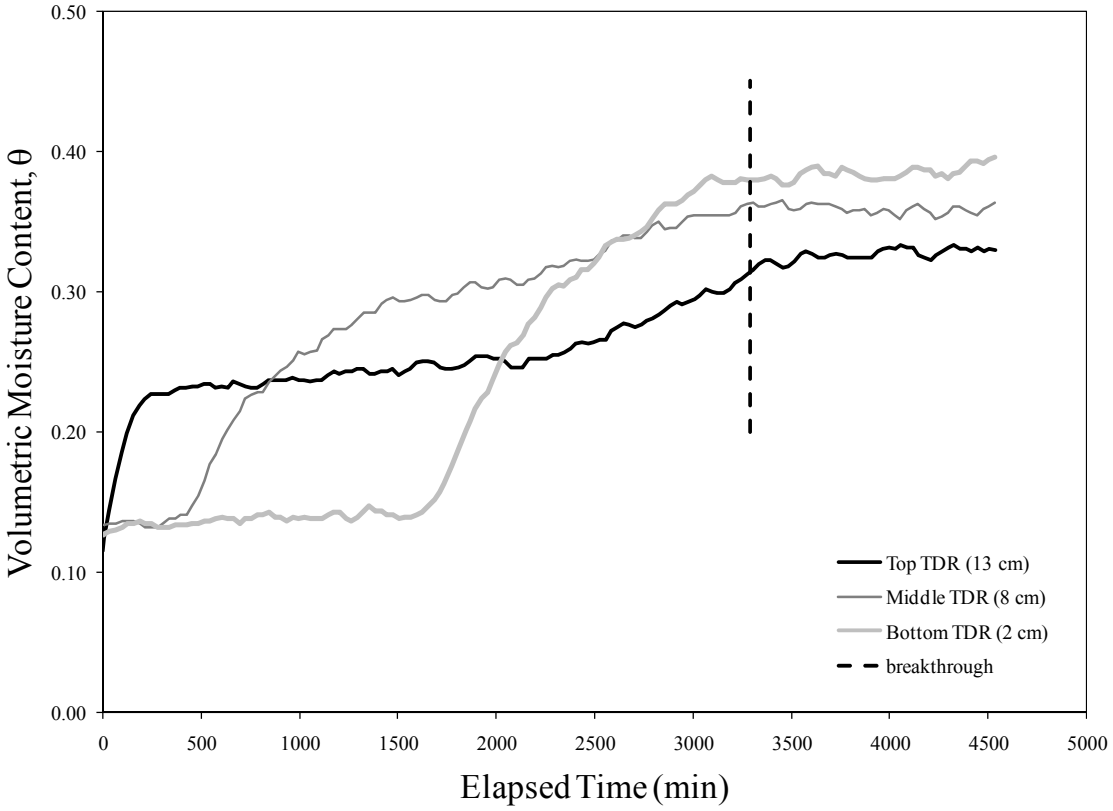

Figure 4.9: Volumetric moisture content versus time data for Test 6, Column 3

4.5 TEST 7

After analyzing the results of tests run up to this point in the experimental testing program, questions arose regarding some unexpected behavior observed in the columns. First, prior to any effects due to formation of a capillary barrier, movement of the moisture front down the column is expected to a relatively constant volumetric moisture content profile throughout the column. This behavior is observed in the column tests run by McCartney et al. (2005), shown in Figure 2.7. However, several of the columns tested up to this point in the experimental program showed a continued increase in measured θ

at the middle TDR probe after the initial sharp rise signifying arrival of the moisture front, and prior to any increase in θ at the bottom TDR probe. Also, there appears to be a significant slowing down of the moisture front after passing the mid-height of the column, as discussed in previous sections. A relatively constant rate of flow is expected.

A proposed explanation for this behavior was a layering effect—some resistance to flow soon after the moisture front passes the mid-height of the column, perhaps due to discontinuity between compaction layers beneath the middle TDR probe. In order to investigate this, two columns were prepared for Test 7 with different compaction methods. Column 1 was prepared with only two compaction layers. The first layer, containing both the bottom and middle TDR probes, was compacted to an elevation of 10 cm above the geotextile. The second layer was compacted to 5 cm and contains the top TDR probe. Column 2 was prepared with five layers, similar to other tests conducted up to this point. There was some concern as to what relative compaction level could be reached with only two layers in Column 1, so the two columns were prepared to 70% relative compaction (γ_d = 1.29 g/cm^3; η = 0.52). Software allowing time lapse photography at a specified time increment was acquired and a camera was set up to provide visual evidence of movement of the moisture front with time. TDR data from Columns 1 and 2 are presented in Figures 4.10 and 4.11, respectively. Results from the time lapse photography are illustrated in Figure 4.12.

Results from Column 1 effectively rule out the layering effect explanation for the unexpected column behavior. The middle and bottom TDR probes were compacted in the same soil layer, yet the major lag in moisture profile velocity is still present. If the layering effect were to blame, there would be no lag between the middle and bottom TDR probes. If anything, the lag would be present between the top and middle probes, as the layer boundary lies between the two. Additionally, the middle TDR shows a steady

increase in moisture content after the initial sharp rise and well before the bottom TDR indicates arrival of the moisture front. It is interesting to note that the top TDR levels off at a significantly higher θ value, around 0.27, than seen in previous tests. Volumetric moisture content at the bottom TDR is approximately 0.40 at breakthrough, which occurs at just over 3100 minutes elapsed time.

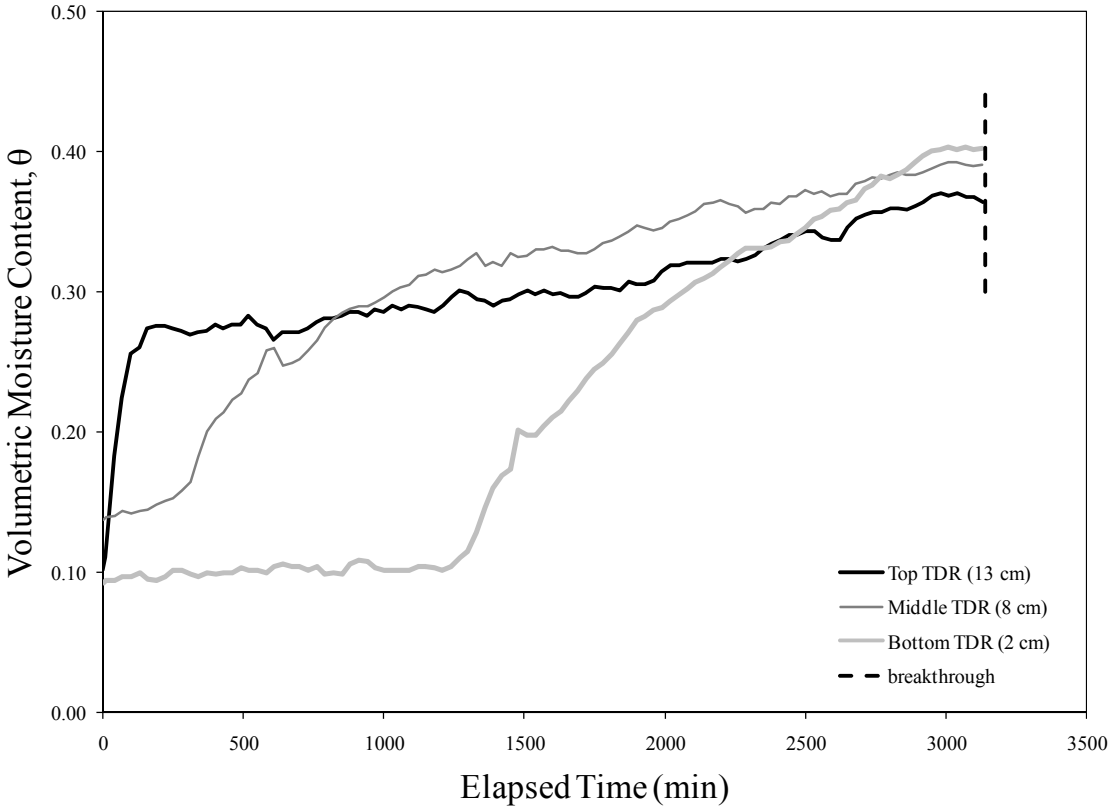

Figure 4.10: Volumetric moisture content versus time data for Test 7, Column 1

The top TDR probe in Column 2 levels off at a slightly lower θ value, around 0.24. Behavior as the moisture front flows down the column and the capillary break is created is similar to that seen in previous tests. Breakthrough occurs slightly earlier than

previously seen, at around 2900 minutes elapsed time. Volumetric moisture content measured by the bottom TDR probe at failure is 0.41.

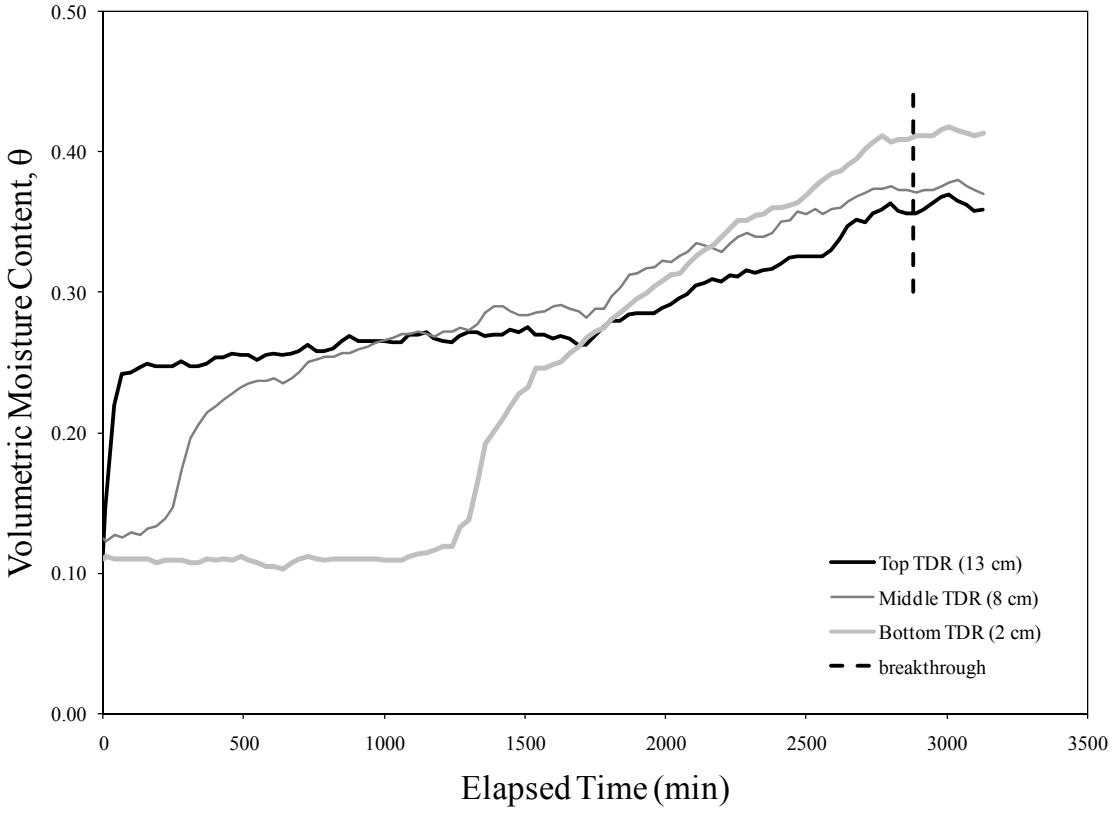

Figure 4.11: Volumetric moisture content versus time data for Test 7, Column 2

Figure 4.12 shows six pictures selected from a time lapse sequence set to photograph Test 7 every 30 minutes. The pictures are selected to provide a basic sense of the flow path down the column. The first aspect noted from these pictures is that, even with the exact same flow distribution method and applied flow rate, the wetting front created in the two columns is different. Column 1, on the left in Figure 4.12 photos, is characterized by a nearly uniform moisture front, while the moisture front for column 2 is

drastically different near the top of the column. However, by the time the moisture front reaches approximately ¾ of the way down the soil column, both moisture fronts have nearly evened out.

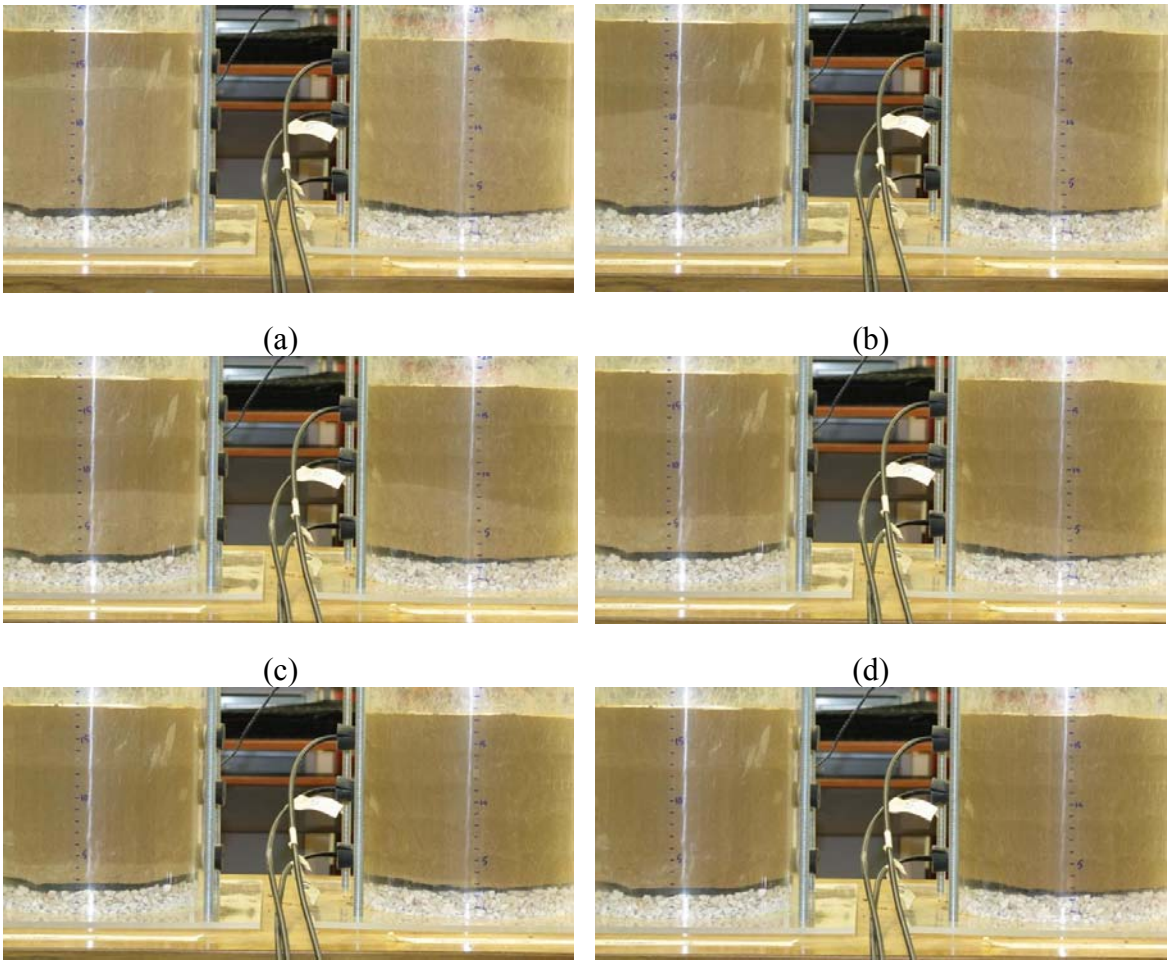

(a) (b)

(c) (d)

(e) (f)

Figure 4.12: Photograph of Test 7 columns at (a) 562 min, (b) 789 min, (c) 1005 min, (d) 1215 min, (e) 1395 min, (f) 1640 min

Also of note from Figure 4.12 is that there is a significant delay between the time when a TDR probe at a given elevation signifies arrival of the moisture front and the time when it visually reaches that point. For example, Figure 4.10 shows that the TDR signals arrival of the moisture front to the middle TDR at around 400 minutes. However, the moisture front does not arrive at the middle TDR location in Figure 4.12 until approximately 800 minutes (just after Figure 4.12b). However, note that arrival times at the bottom TDR probe, after the wetting front has had a chance to even out, are nearly synchronous between TDR and visual indications. Both signify an arrival time of around 1200 to 1300 minutes for either column.

4.5 TEST 8

Test 8 consisted of one column run to determine a "maximum saturation" value possible. The saturated volumetric water content equals the porosity of the compacted soil—the only way this water content could truly be reached is through backpressure saturation. As flow in the columns is gravity-driven, full saturation is not expected. However, a test run at a limiting maximum flow rate would provide an estimate as to the maximum saturation reachable by strictly gravity-driven flow. This would provide additional insight into analysis of data from the experimental testing program.

Test 8, prepared to 80% relative compaction (γ_d = 1.47 g/cm^3; η = 0.46), was run with water continuously ponded at the top of the column to a height of approximately 1 cm. Water was periodically added to the top by pouring from a graduated cylinder, and a record of total applied flow was kept with time. Considering the method for applying flow, the height of ponded water was not constant, but ponding was consistent for the duration of the test. The higher flow rate required much more frequent TDR readings,

every four minutes, and time lapse photography was set up so that a picture of the column was taken once a minute. TDR measurements with time are shown in Figure 4.13, while Figure 4.14 presents selected results from the time lapse photography.

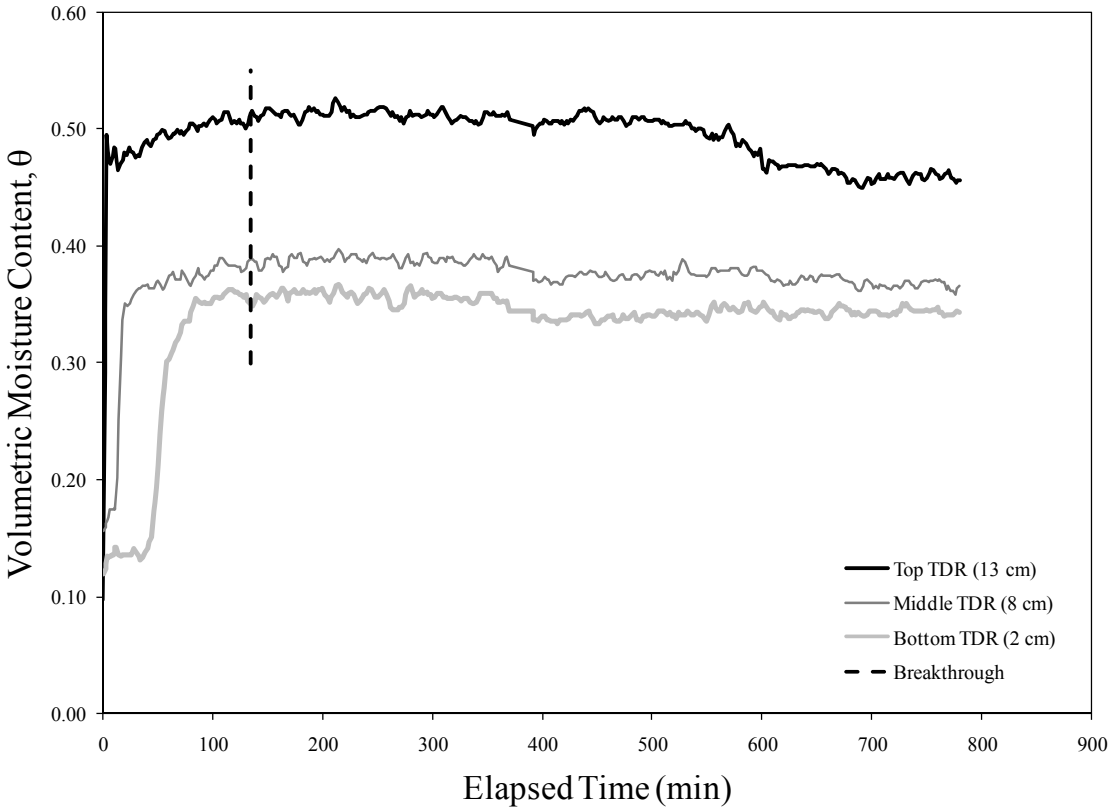

Figure 4.13: Volumetric moisture content versus time data for Test 8

The higher θ value reached at the top TDR is believed to be a result of the influence of ponded water close to the top TDR probe, as localized areas of scour occurred during to application of flow. This is visible in Figure 4.14. The "maximum saturation" value appears to be between 0.36 and 0.38, as seen in Figure 4.13. Ponded water results in the progression of a relatively uniform wetting front.

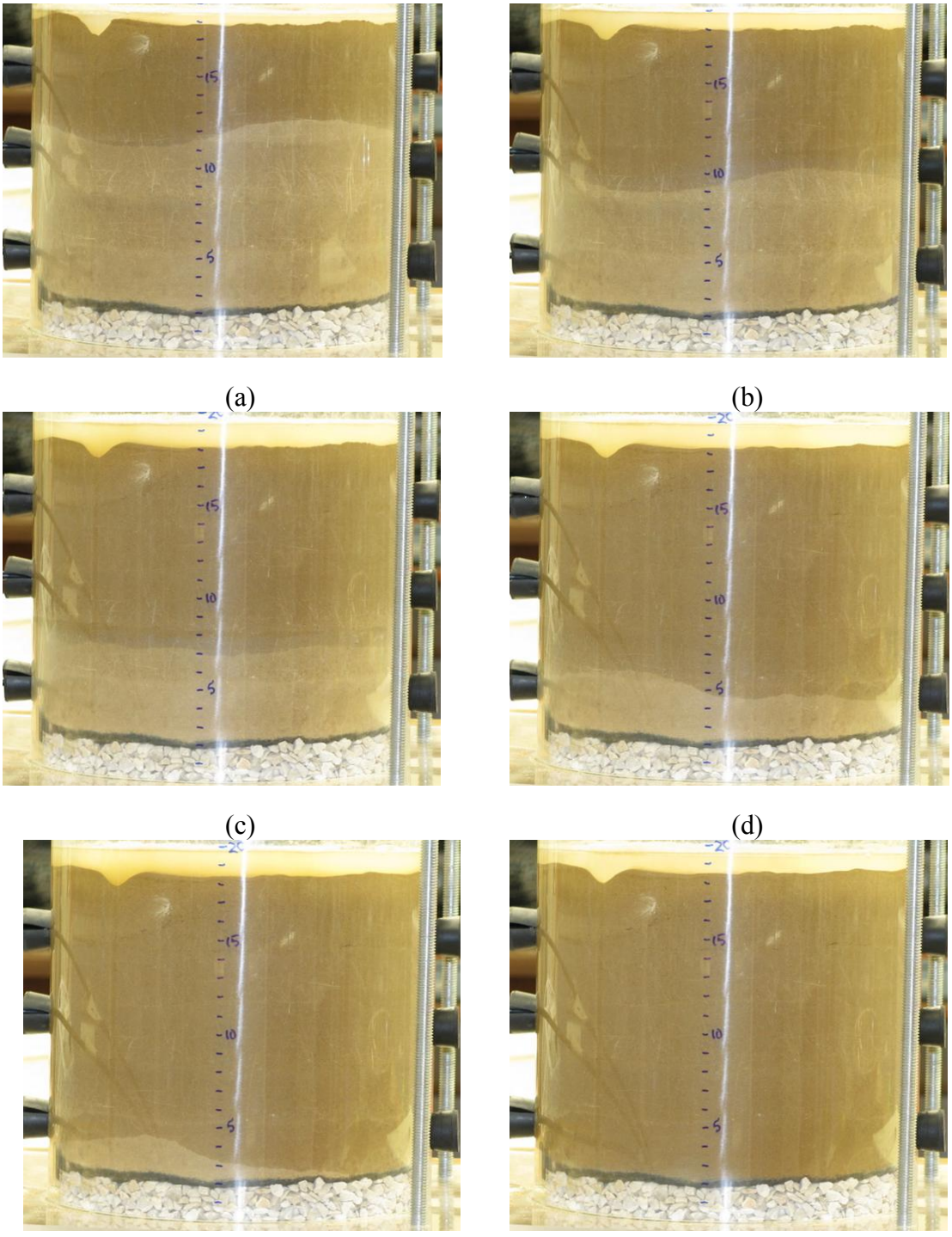

(a) (b)

(c) (d)

(e) (f)

Figure 4.14: Photograph of Test 8 at (a) 10 min, (b) 18 min, (c) 30 min, (d) 49 min, (e) 69 min, (f) 89 min

Chapter 5: Analysis of Experimental Results

Analysis of the data presented in Chapter 4 is the focus of this chapter. Analysis is presented within the framework of a model encompassing each aspect of capillary barrier performance—movement of water vertically down a soil column, creation of a capillary break, storage of moisture above the soil-geotextile interface and eventual breakthrough. Experimental results from this testing program are compared to expected results based on the literature whenever possible. Additionally, the expected and observed effect of relative compaction of the overlying soil layer are investigated.

5.1 Inflow Volumetric Moisture Content

The first step in modeling the behavior of a capillary barrier system should address the movement of applied flow down the soil profile. Ignoring any potential bottom boundary effects, i.e., assuming an infinitely long column, a constant applied flow rate leads to downward progression of a uniform wetting front that results in a constant volumetric water content. This volumetric moisture content is a function of the initial soil compaction and water content, the rate of applied flow, and the soil retention properties. For simplicity, we will refer to the moisture content as θ_{inflow}.

Dell'Avanzi et al. (2004) present an analytical solution used to predict the suction profile in a soil section with steady-state infiltration:

$$\psi(z) = -\frac{1}{a}\ln\left(e^{\left(\ln\left|\left(\frac{v}{k_{sat}}\right)+e^{-a\psi_0}\right|-a\rho_w g z\right)} - \frac{v}{k_{sat}}\right) \quad \text{if } \left(\frac{v}{k_{sat}} + e^{-a\psi_0}\right) > 0$$
$$\psi(z) = -\frac{1}{a}\ln\left(-e^{\left(\ln\left|\left(\frac{v}{k_{sat}}\right)+e^{-a\psi_0}\right|-a\rho_w g z\right)} - \frac{v}{k_{sat}}\right) \text{ if } \left(\frac{v}{k_{sat}} + e^{-a\psi_0}\right) < 0 \qquad (5.1)$$

where v is the discharge velocity, ψ_0 is a suction value imposed at the base of the soil profile, and α is the fitting parameter from the Gardner K-function model presented in Equation 2.6. Dell'Avanzi et al. (2004) impose a zero suction bottom boundary for provided examples of suction profiles with varying applied discharge velocities. This bottom boundary condition is potentially applicable for predicting the suction profile in the columns used in this experimental program at breakthrough, as the soil near the soil-geotextile interface will be very near saturation, i.e., zero suction, when breakthrough occurs.

Figure 5.1 shows a number of suction profiles calculated at steady-state for varying imposed discharge velocities on a 1.5 m soil column with an imposed zero suction bottom boundary (McCartney 2007). Away from the imposed suction of 0 kPa at the bottom of the soil column, the suction profile approaches a limiting value at a certain elevation, with both the limiting suction and the elevation at which the suction is approached dependent upon the imposed discharge velocity. As the discharge velocity increases, the limiting suction value and the elevation at which this value is reached both decrease, and vice versa for a decreasing discharge velocity. The limiting suction is not affected by the imposed bottom boundary condition—varying the boundary only changes the elevation at which the limiting suction is reached (Dell'Avanzi et al. 2004).

Knowing the limiting suction that would develop in our soil columns without the presence of a capillary barrier along with the water retention properties of the soil allows for an estimation of θ_{inflow}. From Dell'Avanzi et al. (2004), the limiting suction is calculated as follows:

$$\lim_{z_p \to \infty} \psi = \psi_{lim} = -\frac{1}{a} \ln\left(-\frac{v}{k_{sat}}\right) \tag{5.2}$$

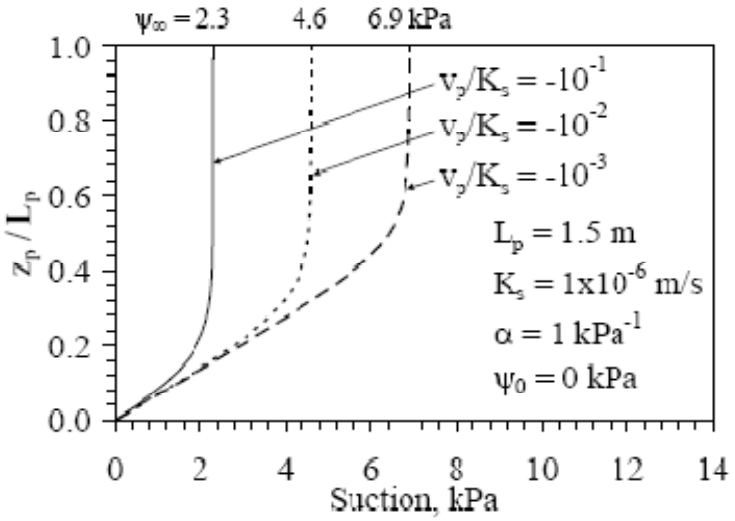

Figure 5.1: Steady-state suction profiles calculated for varying infiltration rates (McCartney 2007)

Knowledge of the hydraulic conductivity function of the soil is required to reasonably estimate the α fitting parameter. Our K-function is developed only through a model—no laboratory data was obtained. However, with an observed θ_{inflow} value and the water retention curve, it is possible to estimate ψ_{lim} for certain tests with data that look to best fit the expected flow behavior and, subsequently, back-calculate a Gardner α to use for this experimental study:

$$a = -\frac{1}{\psi_{lim}} \ln\left(-\frac{v}{k_{sat}}\right) \tag{5.3}$$

From the test results presented in Chapter 4, Column 2 from Test 6 and Column 2 from Test 7 both have well-defined θ_{inflow} values. Figure 4.8 shows that Column 2 from Test 6 approaches a θ_{inflow} of 0.22. This is equivalent to a degree of saturation of 0.54, as defined in the water retention curve presented in Figure 3.8. The limiting suction,

therefore, corresponding to a degree of saturation of 0.54, is around 85 kPa. The discharge velocity imposed on Test 6, Column 2 was $2.3*10^{-5}$ cm/s (see Table 3.8), and the saturated hydraulic conductivity of the soil is $8.2*10^{-5}$ cm/s. Using Equation 5.3, the back-calculated Gardner α parameter in this case is equal to 0.015. Similarly, for Test 7, Column 2, the back-calculated α value is 0.022. Data presented for a column test with a similar soil over a nonwoven geotextile and an applied discharge velocity of $2*10^{-5}$ cm/s, presented in McCartney et al. (2005), results in a calculated α parameter of 0.016. The analytical solution presented in Dell'Avanzi et al. (2004) appears to adequately model θ_{inflow} for the experimental results using a Gardner α value of 0.02.

As discussed in Chapter 4, not all of the test results show such a clearly defined θ_{inflow} value. Several of the tests show a leveling off of the top TDR probe at a presumed θ_{inflow} value and a significant change in behavior, i.e., lowering of the rate of change in θ with time, of the middle TDR. However, the middle TDR continues to indicate a rise in moisture content after the initial sharp increase to θ_{inflow}. This appears to be a result of 2D flow effects stemming from an uneven distribution of flow across the top of the soil column. This uneven distribution results in a non-uniform wetting front that lags behind in some portions of the column cross-section. As the θ measurement obtained represents an average θ over the length of the TDR probe, this lag behind the initial pulse from the wetting front could result in the behavior seen in the middle TDR probe of several columns.

Having acknowledged this deviation from expected behavior, it is still possible to estimate an observed θ_{inflow} using the end of the sharp increase signifying arrival of the moisture front. For cases in which observed behavior between different TDR probes in a single column suggests different θ_{inflow} values, a representative value is assumed for the sake of this comparison. Table 5.1 includes a comparison of observed values with θ_{inflow}

values obtained from ψ_{lim} calculated using Equation 5.3 and a Gardner α parameter of 0.02. The observed θ_{inflow} is also converted to an observed ψ_{lim} value using the soil WRC and reported to the nearest 5 kPa.

Table 5.1: Comparison of observed and calculated θ_{inflow} values

Test	2	4		5		6			7	
Column	1	1	2	1	2	1	2	3	1	2
$\theta_{inflow,obs}$	.32	.25	.22	.22	.20	.21	.22	.23	.26	.24
$\psi_{lim,obs}$ **(kPa)**	10	40	85	85	160	115	85	65	30	50
$\psi_{lim,calc}$ **(kPa)**	64	61	61	231	234	59	64	66	56	56
$\theta_{inflow,calc}$	.23	.23	.23	.19	.19	.23	.23	.23	.24	.24

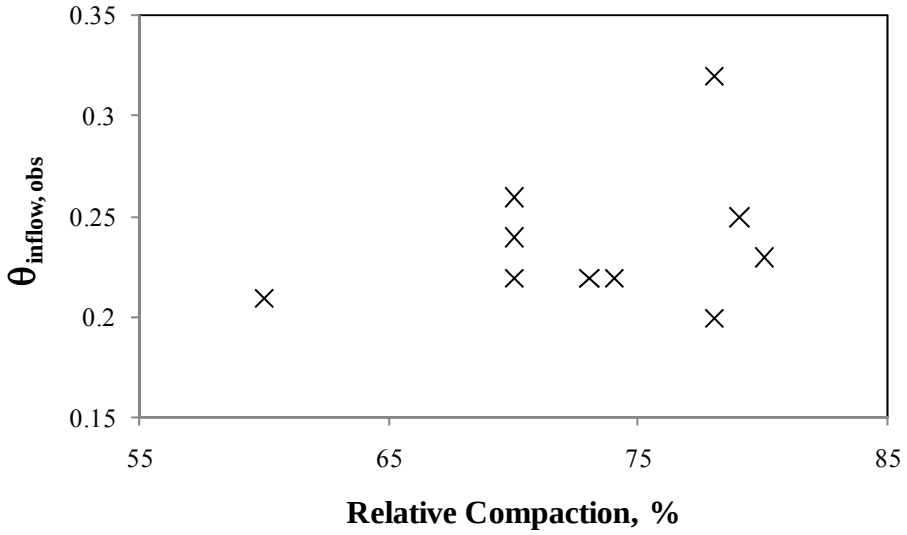

Figure 5.2: $\theta_{inflow,\ obs}$ versus relative compaction

There is no clear relationship between relative compaction and soil water retention characteristics for specimens compacted dry of optimum (Tinjum et al. 1997). Any potential relationship would be reflected either in the Gardner α parameter, if it were calibrated to match laboratory data, or directly from the use of the soil WRC to convert ψ_{lim} calculated with Equation 5.2 to a corresponding $\theta_{inflow,\ calc}$ value. There is no clear relationship between relative compaction and θ_{inflow} values observed from the experimental program, as presented in Figure 5.2.

5.2 MOISTURE FRONT VELOCITY

The ability to predict θ_{inflow} for a soil capillary barrier system leads directly to prediction of the moisture front velocity, v_{mf}, given knowledge of the initial soil conditions and the applied discharge velocity. Assuming an idealized unsaturated "plug flow" behavior of a soil column, where the applied inflow is distributed evenly across the surface, results in the progression of a uniform moisture front that takes soil from its initial moisture content, θ_i, to θ_{inflow}. Assuming θ_i is constant throughout the column, the following simple volumetric continuity relationship applies:

$$Applied\ flow\ \left(\frac{mL}{s}\right) = A_{col} v_{mf} \left(\theta_{inflow} - \theta_i\right) \tag{5.4}$$

where A_{col} is the column cross-sectional area. The total applied flow divided by the area over which it is applied, A_{col}, is the discharge velocity, v. Using this simplification and solving for the moisture front velocity:

$$v_{mf} = \frac{v}{\left(\theta_{inflow} - \theta_i\right)} \tag{5.5}$$

This equation is applicable to results from the experimental testing program in multiple ways. Two θ_{inflow} values are available for use—one observed from TDR measurements and one predicted based on the limiting suction calculated with Equation 5.2. Calculated v_{mf} values may be compared to observed values from TDR measurements. For this comparison, observed v_{mf} values are obtained by considering the time it takes for the wetting front to travel the known distance between two TDR probes. As the TDR probe measures the water content over its entire range of influence, the point at which the wetting front truly arrives at the level of the TDR probe is in the middle of the sharp rise in water content. However, the most consistent results are obtained by using the point of initial rise in water content for each probe. Sample volumetric moisture content data with time is shown in Figure 5.3, with arrival times used for calculation of v_{mf} identified.

Table 5.2 contains moisture front velocity data from each column test. Two calculated v_{mf} values are included—one using θ_{inflow} calculated using the limiting suction obtained with Equation 5.2, i.e., the theoretical θ_{inflow}, and another using θ_{inflow} observed from experimental data. Also included are two observed v_{mf} values, one from the travel time between the top and middle TDR probes and another from the travel time between the middle and bottom probes. It is clear from Table 5.2 that the θ_{inflow} value used to calculate v_{mf} has a relatively minor effect. Also, there is a clear difference between moisture front velocities observed in the upper and lower halves of the soil column. The basic assumption for the model presented to calculate v_{mf} is a uniform wetting front of constant velocity. Observed v_{mf} data presented in Table 5.2 show that the moisture front velocity in the upper half of the column is consistently higher than that observed in the lower half.

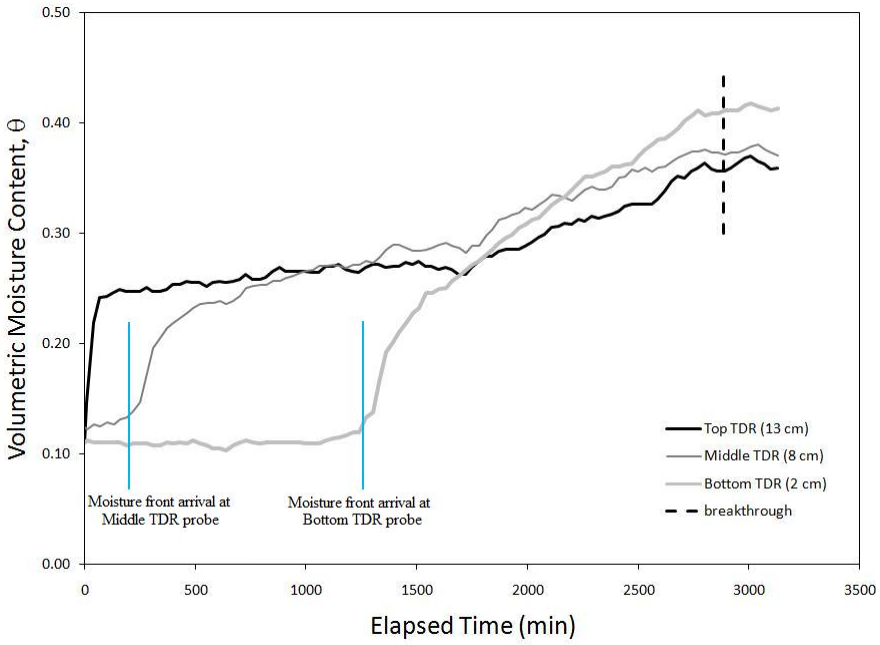

Figure 5.3: Example TDR data with identification of moisture front arrival times

Figures 5.4 and 5.5, where "TDR 1" refers to the top TDR probe and "TDR 2" to the bottom probe, are presented to further examine the relationship between calculated and observed v_{mf} values. Figure 5.4 contains observed v_{mf} values plotted against v_{mf} calculated using theoretical θ_{inflow}, while Figure 5.5 contains observed values plotted against v_{mf} calculated using observed θ_{inflow}. The dashed line in each plot is included to show a 1:1 slope. Both figures show that the calculated v_{mf} values generally fall in between observed moisture front velocities—lower than those observed in the upper half of the soil column and higher than those observed in the lower half.

As seen in Equation 5.5, any predictable trend in v_{mf} with respect to relative compaction of the capillary barrier soil layer would be an extension of the relationship seen between θ_{inflow} and relative compaction. Figure 5.2 shows no clear trends with respect to θ_{inflow}. Observed v_{mf} values from the top portion of the column, presented in Figure 5.6a, appear to show a slightly negative trend with increasing relative compaction.

Figure 5.6b presents observed v_{mf} values for the bottom portion of the column plotted versus relative compaction. Values in the bottom portion of the column are fairly constant, regardless of relative compaction.

Table 5.2: Calculated and observed v_{mf} values

Test	Column	θ_i	$\theta_{inflow,\ calc}$	$\theta_{inflow,\ obs}$	v (cm/s)	$v_{mf,calc}$ (cm/s) (using θ_{calc})	$v_{mf,calc}$ (cm/s) (using θ_{obs})	$v_{mf,\ obs}$ (cm/s) (Top to Middle)	$v_{mf,\ obs}$ (cm/s) (Middle to Bottom)
2	1	0.09	0.23	0.32	2.3E-05	1.6E-04	1.0E-04	8.8E-05	1.0E-04
4	1	0.08	0.23	0.25	2.4E-05	1.6E-04	1.4E-04	1.0E-04	1.4E-04
	2	0.07	0.23	0.22	2.4E-05	1.5E-04	1.6E-04	1.9E-04	1.0E-04
5	1	0.13	0.19	0.22	8.1E-07	1.4E-05	9.0E-06	4.2E-05	1.3E-05
	2	0.12	0.19	0.20	7.6E-07	1.1E-05	9.5E-06	4.2E-05	2.2E-05
6	1	0.11	0.23	0.21	2.5E-05	2.1E-04	2.5E-04	5.6E-04	1.3E-04
	2	0.11	0.23	0.22	2.3E-05	1.9E-04	2.1E-04	2.1E-04	1.0E-04
	3	0.12	0.23	0.23	2.2E-05	2.0E-04	2.0E-04	2.1E-04	8.3E-05
7	1	0.11	0.24	0.26	2.7E-05	2.1E-04	1.8E-04	3.3E-04	9.5E-05
	2	0.12	0.24	0.24	2.7E-05	2.3E-04	2.3E-04	4.2E-04	1.0E-04

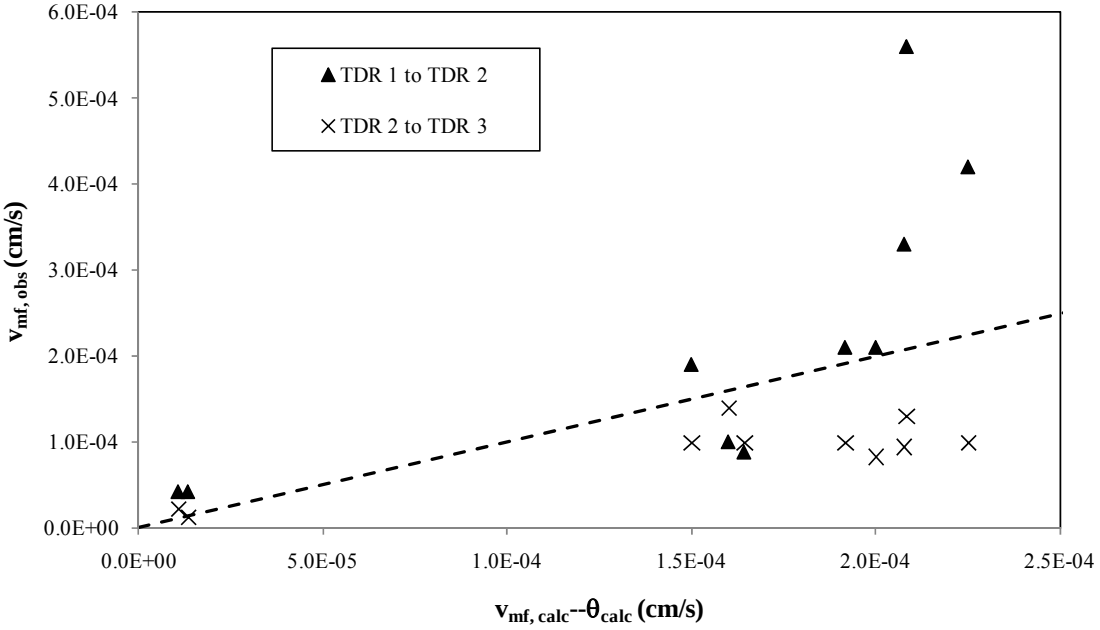

Figure 5.4: Observed v_{mf} versus v_{mf} calculated with theoretical θ_{inflow}

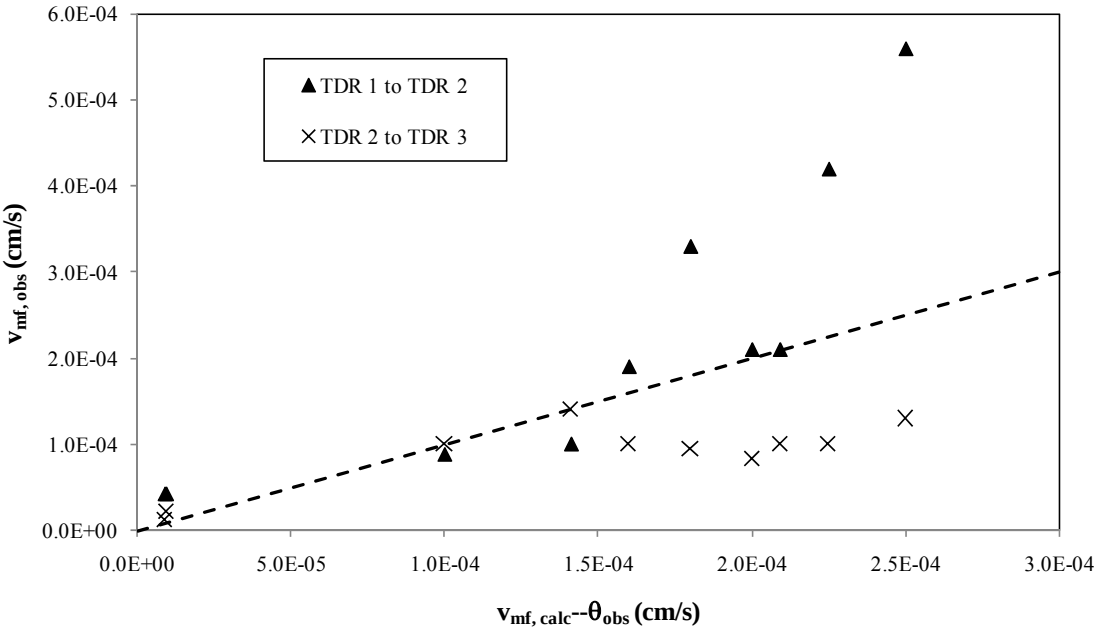

Figure 5.5: Observed v_{mf} versus v_{mf} calculated with observed θ_{inflow}

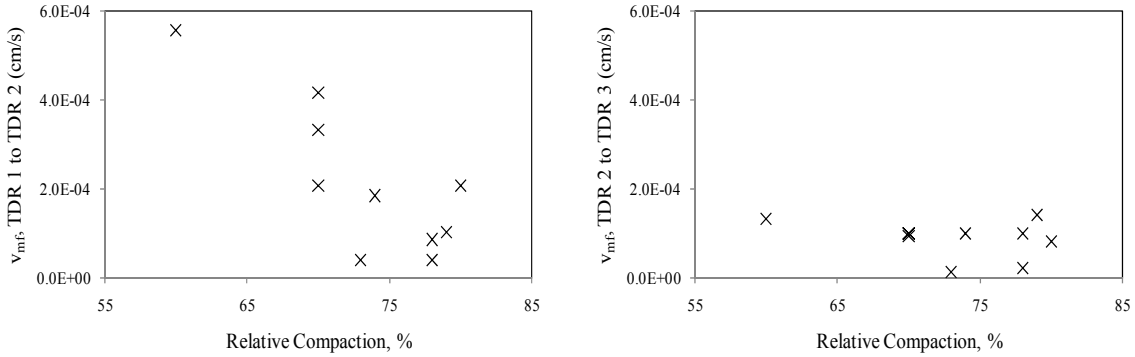

(a) (b)

Figure 5.6: Observed v_{mf} values in (a) top portion of column and (b) bottom portion of column, plotted versus relative compaction

5.3 FORMATION OF CAPILLARY BREAK

If no capillary break were to form at the soil-geotextile interface, the moisture front would continue down the soil column and through the geotextile after passing the bottom TDR, and breakthrough would be detected soon after with the tipping bucket. However, as discussed and seen in plots of volumetric moisture content with time presented in Chapter 4, the front stops at the soil-geotextile interface and moisture from the applied inflow builds up above the interface. The build-up is marked by a continued, although slowed, increase in moisture content at all three TDR locations. The rate of rise in moisture content is significantly slower than that associated with arrival of the initial moisture front, and continues until breakthrough occurs.

Another approach to show the effects of the capillary break is to display the progression of moisture content profiles with time. Moisture content profiles with time for Test 6, Column 2 are presented in Figure 5.7. At time zero, the column is at a relatively constant θ, around 0.11. Progression of the top two TDR probes to a θ_{inflow}

around 0.22 is shown through an elapsed time of 1100 minutes. The bottom TDR reaches a value consistent with the top two TDR probes, 0.24, after 1600 minutes. In the absence of a capillary break effect, the moisture content profile would remain relatively constant while the moisture front progresses through the geotextile layer and exits the column. However, a significant increase is shown in moisture content measured by the bottom TDR for the next 400 minutes, followed by a continued rise in all three TDR probes up until breakthrough occurs at around 3600 minutes elapsed time.

Similar behavior is seen in the progression of moisture content profiles in other columns. Profiles from each column are provided in Appendix A.

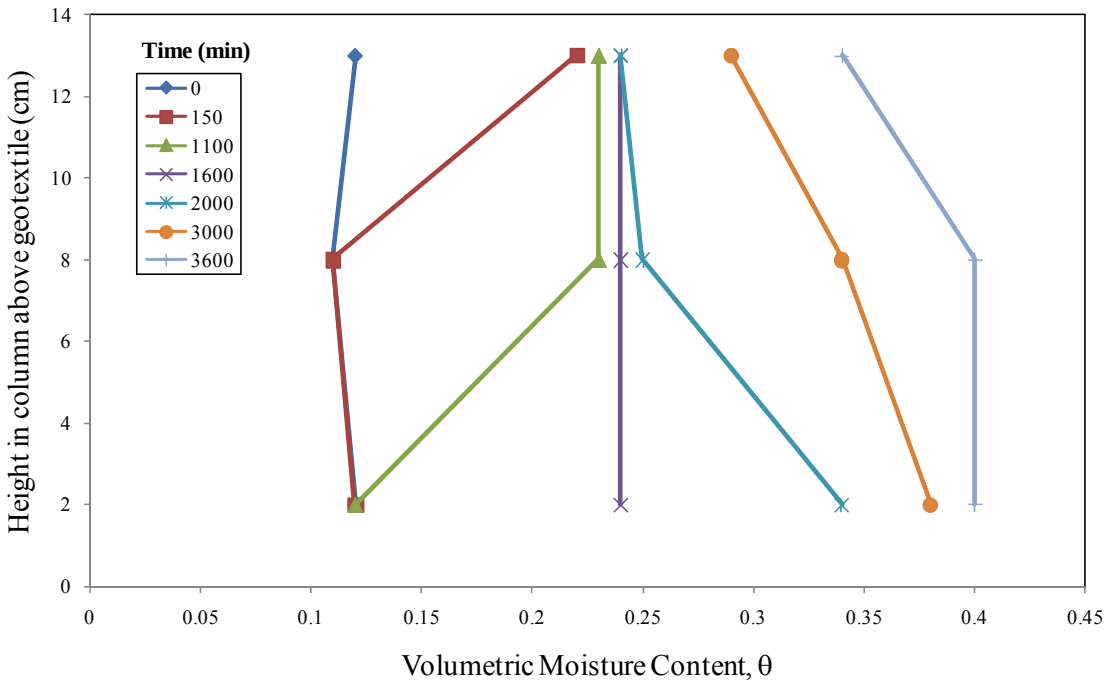

Figure 5.7: Test 6, Column 2—θ profile with time

5.4 BREAKTHROUGH SUCTION

As discussed in Section 2.4, the breakthrough suction is estimated at the intersection of the K-functions for the soil and geotextile. Figure 5.8 contains a plot of the two K-functions, with the breakthrough suction at intersection, ψ_{bkt}, identified as approximately 1.0 kPa. No suction measurements are taken in the column tests from this experimental testing program, so it is more useful to convert the breakthrough suction to a volumetric moisture content, θ_{bkt}, using the water retention properties of the RMA soil. This correlation is presented in Figure 5.9, where θ_{bkt} is identified as approximately 0.39.

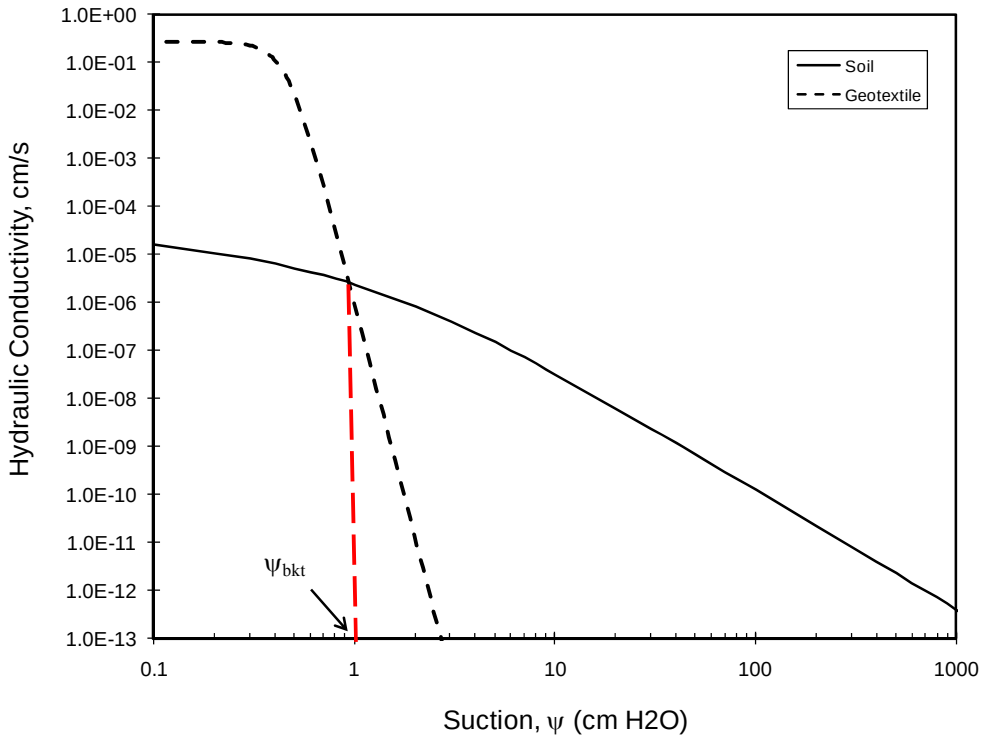

Figure 5.8: Intersection of soil and geotextile K-functions

The actual θ_{bkt} for each of the column tests is estimated via examination of the volumetric moisture content with time series obtained from TDR measurements. Time of breakthrough for each column test is identified along with its volumetric moisture content data displayed in Chapter 4. Measured volumetric moisture content for the bottom TDR at the time of breakthrough is accepted as θ_{bkt}. This is only an approximation, as the bottom TDR is actually 2 cm above the soil-geotextile interface. θ_{bkt} values for each column test performed are displayed in Table 5.3. These values show good agreement with θ_{bkt} predicted from intersection of the soil and geotextile K-functions, 0.39, considering the approximate +/- 0.01 accuracy of volumetric moisture content readings obtained with these TDR measurements.

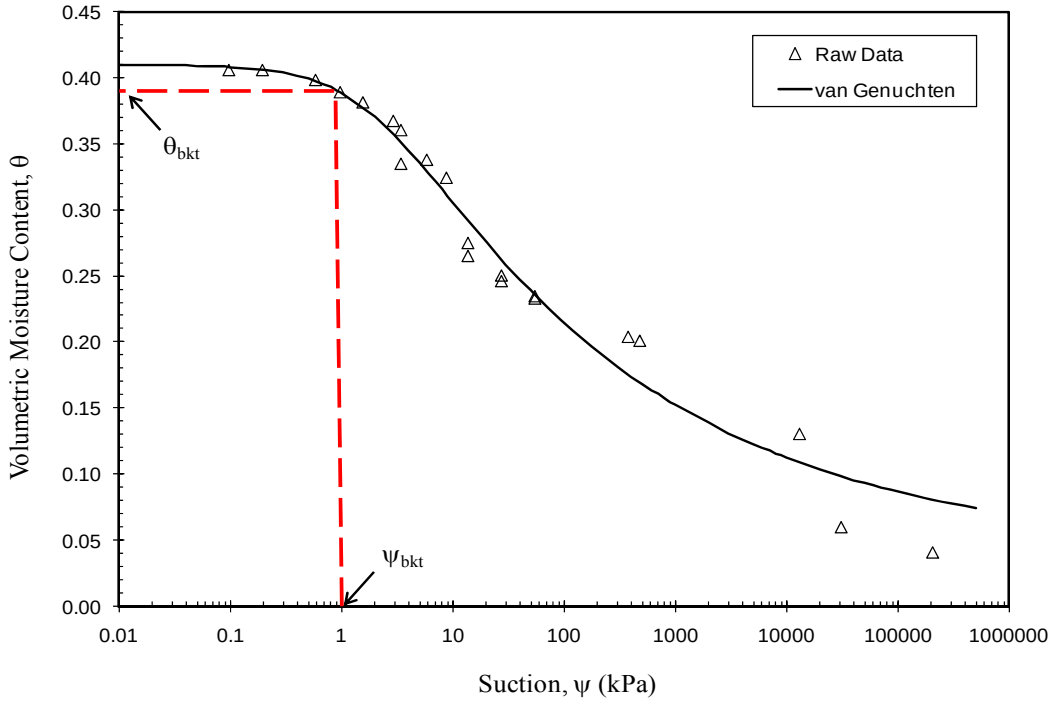

Figure 5.9: Identification of θ_{bkt} from ψ_{bkt} and soil WRC

A plot of θ_{bkt} versus relative compaction is presented in Figure 5.10. It appears that relative compaction of the overlying soil layer has little effect on the moisture content at breakthrough. This implies that the retention behavior of the soil at various relative compaction levels, from 60% to 80%, would be similar, at least within approximately +/- 0.01 volumetric moisture content, at suctions around ψ_{bkt}.

Table 5.3: Observed θ_{bkt} values

Test	Column	RC (%)	θ_{bkt}
2	1	78	0.41
4	1	79	0.38
	2	74	0.39
5	1	73	0.40
	2	78	0.39
6	1	60	0.40
	2	70	0.40
	3	80	0.38
7	1	70	0.40
	2	70	0.41

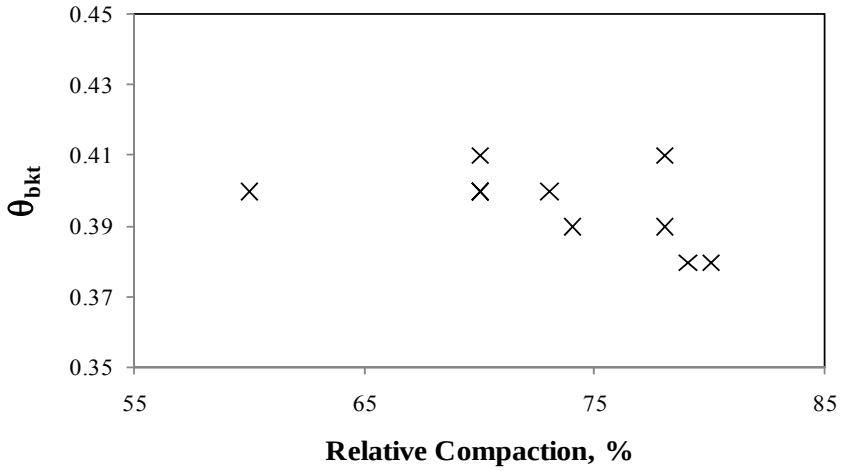

Figure 5.10: θ_{bkt} versus relative compaction

5.5 MOISTURE PROFILE AT BREAKTHROUGH

After reviewing a method for predicting conditions at the soil-geotextile interface that result in breakthrough of the capillary barrier, and investigating the effectiveness of this method by comparing it with observed results, the next logical step is to address the conditions at breakthrough present in the rest of the column. Stormont and Morris (1998) estimate the suction profile above a capillary barrier at breakthrough as follows:

$$h = z + h_w^* \tag{5.6}$$

where z is the height above the capillary barrier interface and h_w^* is the water entry head of the coarse layer, in this case the geotextile. This is based on an assumption of a unit slope in total head with depth:

$$\frac{dh}{dz} = 1 \tag{5.7}$$

The unit slope will be approached but not fully achieved, as flow down the column requires a nonzero total head gradient. Accordingly, the lower the applied inflow, the closer the column will come to a unit slope condition. Approximation of the suction profile using Equation 5.6 is a conservative approach for capillary barrier analysis, as it underestimates the total amount of water stored above the barrier interface at breakthrough.

In Equation 5.6, the water entry head is used to approximate the suction head at the soil-geotextile interface at breakthrough. As discussed in section 5.4, the breakthrough suction estimated for this soil-geotextile capillary barrier system is around 1.0 kPa. This is equivalent to a h_w^* value of 10 cm. Application of Equation 5.6 results

in an estimated suction profile at failure shown in Figure 5.11a. The soil WRC displayed in Figure 3.8 is used to convert the estimated suction profile to a profile of volumetric moisture content with depth in the column, shown in Figure 5.11b.

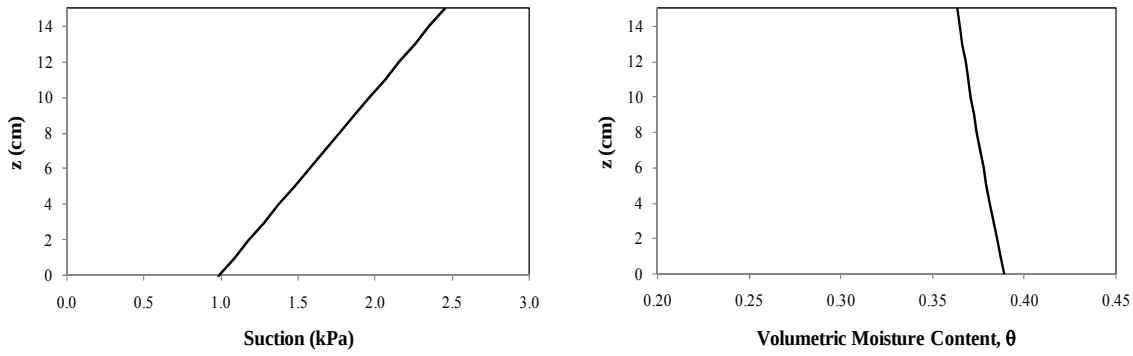

(a) (b)

Figure 5.11: Estimated profiles of (a) suction and (b) volumetric moisture content with depth in column

An estimation of the moisture profile at breakthrough may be made for each of the columns in this experimental program using TDR measurements at the time of breakthrough. Figure 5.12 contains an illustrated summary of the moisture content profiles at breakthrough for each column. Variability exists within the data. Most notably, results from the top TDR measurement for both columns in Test 4 are much lower at breakthrough than in any other test completed in this study. The major difference between this and the other tested columns was in the method used to distribute flow. Test 4 used synthetic wicks, while other tests that included a TDR at an elevation of 13 cm above the soil-geotextile interface—synthetic wicks were also used in Test 2, but only the lower two TDR probes were installed—used the filter paper approach.

There is significant variation between the experimentally observed moisture profiles at failure and that predicted with an assumption of a linear suction profile. Most notably, the observed middle TDR reading is consistently higher than that predicted in Figure 5.11b. In some cases, the moisture content near the column mid-height is equal to or slightly higher than that measured near the interface. In addition, the observed top TDR reading is consistently lower than the predicted θ value. These observations were consistent throughout the tests, as shown in Figure 5.13, a comparison of predicted and observed moisture profiles.

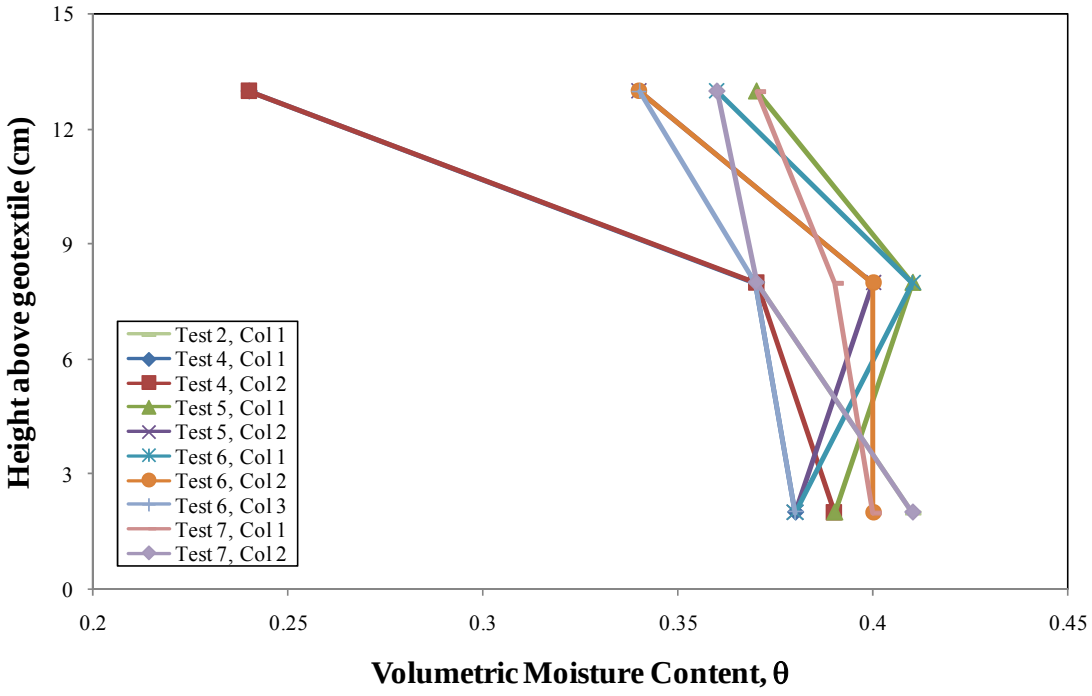

Figure 5.12: Moisture content profiles at breakthrough

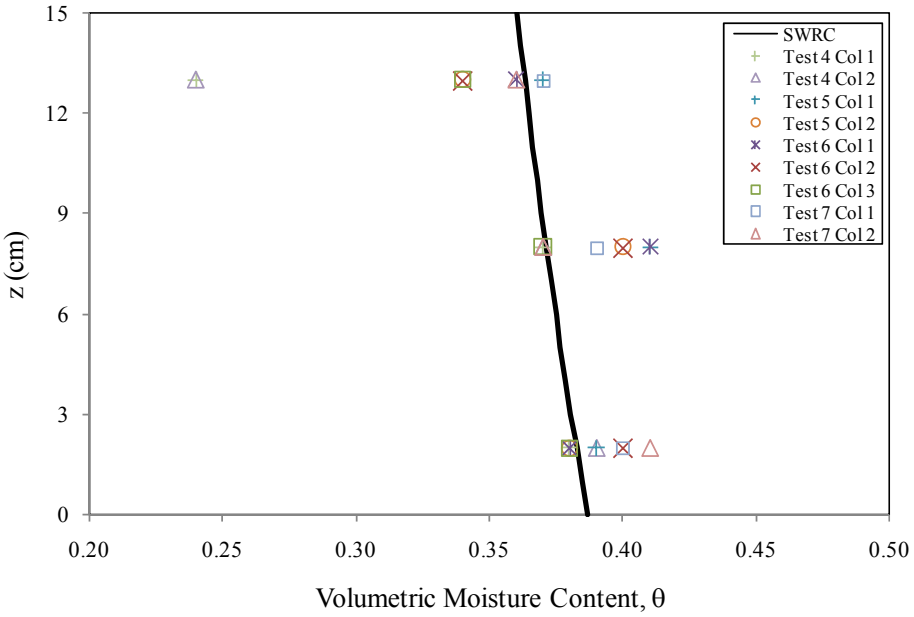

Figure 5.13: Comparison of moisture profiles predicted with a linear suction profile and observed at breakthrough

The variation shown in Figure 5.13 may be partially explained by the behavior described in Figure 3.9, where variations in porosity affect the water retention parameters of a similar soil at low suctions (McCartney 2007). The water retention characteristics used to convert the linear suction profile to a moisture profile, shown in Figure 5.11, were obtained at a relative compaction of 80%. Using data obtained at a lower density, and corresponding higher porosity, would shift the predicted moisture profile to the right if the behavior described in Figure 3.9 applied. This may result in a slightly better fit, but the same trends described in the preceding paragraph would still be seen in the experimental data obtained in this study. Accordingly, other fitting methods were explored in an effort to better model the moisture profile at breakthrough.

Fitting the data with an elliptical function was investigated in an effort to adequately model the fairly constant moisture content present in the bottom half of several column tests at breakthrough. This fit requires the vertical axis, or elevation above the geotextile interface, to be the major axis of the ellipse. Volumetric moisture content is the minor axis. The origin is located at an elevation of 0 cm, the geotextile interface, and a θ equal to θ_{inflow}. The following equation defines the ellipse of interest:

$$\frac{\left(\theta - \theta_{inflow}\right)^2}{\left(\theta_{bkt} - \theta_{inflow}\right)^2} + \frac{z^2}{a^2} = 1 \tag{5.8}$$

where *a* is equal to the elevation at which θ modeled with the ellipse equals θ_{inflow}, or z($\theta = \theta_{inflow}$).

Conceptually, *a* refers to the elevation in a soil profile at which the effects of a capillary break are no longer evident, i.e., there is no increase in water content resulting from formation of the capillary barrier. Volumetric moisture with time series, shown in Chapter 4, consistently show a rise in moisture content at all three TDR probe locations soon after formation of the capillary barrier. As a result, it is impossible to declare an appropriate *a* value based solely on the test results presented in this study.

Another option is to use the results of a single representative test to calibrate the model. In this study, an *a* value is obtained based on a least squares squares optimization from the results of Test 6, Column 2. Figure 5.14a contains an elliptical function plotted alongside the data used for calibration, from Test 6, Column 2. This test was characterized by a θ_{inflow} of 0.22 and θ_{bkt} of 0.40. An *a* value of 18.1 cm resulted in the best fit. The resulting elliptical function is plotted alongside all experimental TDR readings at breakthrough in Figure 5.14b.

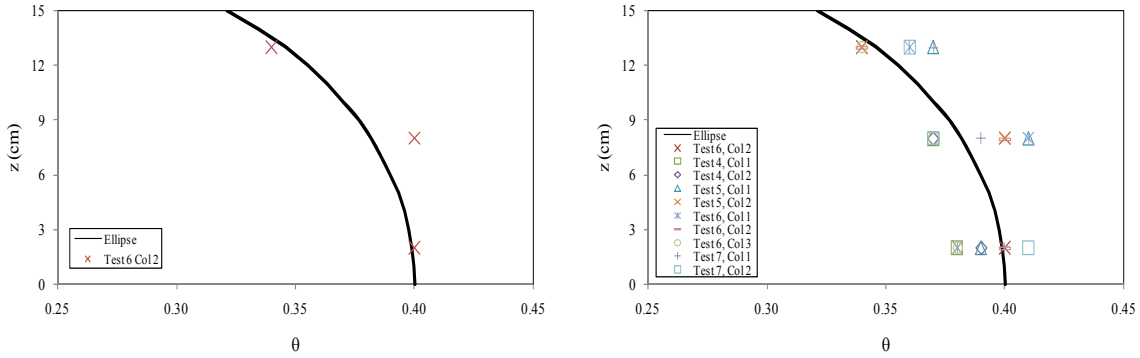

(a) (b)

Figure 5.14: Elliptical function used to fit moisture profile data at breakthrough plotted with (a) calibration data, and (b) all experimental data

5.6 STORAGE CAPACITY

Capillary barrier storage capacity, defined in this study as the total moisture storage in the soil layer above the soil-geotextile interface, may be estimated by integrating the volumetric moisture content with depth at breakthrough, as follows:

$$SC = A_{col}\left[z_n\theta_n + \sum_{i=1}^{n}(z_i - z_{i+1})\left(\frac{\theta_i + \theta_{i+1}}{2}\right) + (H_{col} - z_1)\theta_1\right] \tag{5.9}$$

where SC is the capillary barrier storage capacity, A_{col} is the column cross-sectional area, z and θ refer to the elevation above interface and volumetric moisture content of a TDR probe, and subscripts 1 and n refer to the top and bottom probes, respectively. The columns tested in this study contain three TDR probes, so n is equal to three. Estimated

storage capacities based on Equation 5.9 are plotted versus soil relative compaction in Figure 5.15. A storage capacity is not available for Test 2 because only two TDR probes were installed. A slightly negative trend in total storage capacity is seen with increasing relative compaction. The two columns from Test 4 are plotted separately from the other tests as a result of the anomalous behavior seen in the top TDR probe of these columns, discussed previously.

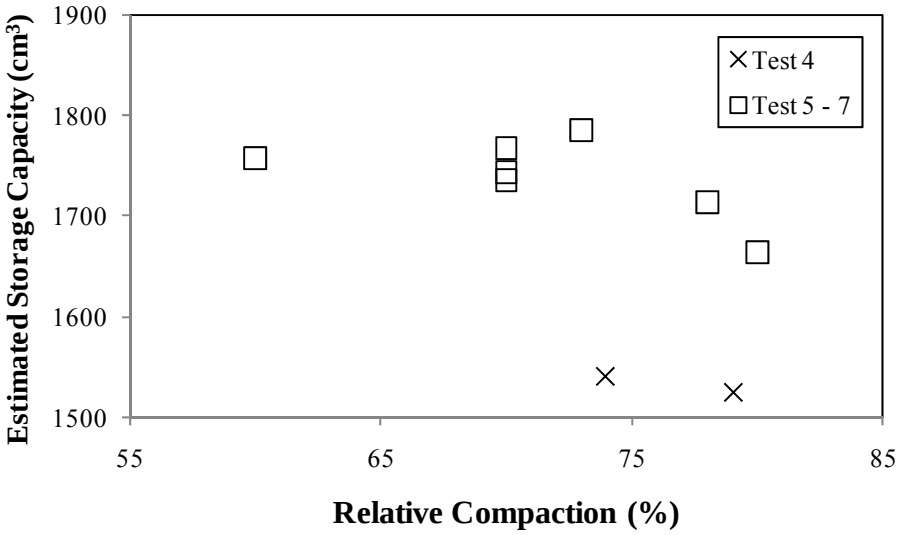

Figure 5.15: Estimated storage capacity versus relative compaction

A general comparison may be made between the estimated experimental storage capacities, presented in Table 5.4, and a theoretical storage capacity calculated using the Stormont and Morris (1998) moisture content profile shown in Figure 5.11b. The average storage capacity calculated via Equation 5.9 is 1691 cm^3, with a standard deviation of 91 cm^3, while the storage capacity estimated by the moisture content profile presented in Figure 5.11b is 1680 cm^3. Assumption of a linear suction profile results in an estimation of storage capacity that fits well with experimental data. However, this

may be an overly simplified comparison if the behavior described in Figure 3.9 and discussed in Section 5.5 holds true.

For the 15 cm tall soil columns tested in this study, with a continuous function used to model the moisture content profile at breakthrough, storage capacity is estimated as follows:

$$SC = A_{col} \int_0^{15} \theta \, dz \tag{5.10}$$

Applying this relationship to the elliptical model, a combination of Equations 5.8 and 5.10, results in the following estimation of storage capacity:

$$SC = A_{col} \int_0^{15} \left(\sqrt{\left(1 - \frac{z^2}{a^2}\right)\left(\theta_{bkt} - \theta_{inflow}\right)^2} + \theta_{inflow} \right) dz \tag{5.11}$$

Table 5.4: Storage capacities

Test	Column	RC (%)	SC—Eq. 5.9 (cm^3)	SC—Eq. 5.11 (cm^3)
2	1	78	N/A	N/A
4	1	79	1526	1657
	2	74	1541	1679
5	1	73	1786	1719
	2	78	1713	1667
6	1	60	1758	1713
	2	70	1744	1719
	3	80	1663	1645
7	1	70	1768	1742
	2	70	1736	1770

Storage capacities estimated with Equation 5.11 for each column are compared to experimentally observed storage capacities, calculated with Equation 5.9, in Table 5.4 and Figure 5.16. As in Figure 5.15, results from Test 4 are clearly identified.

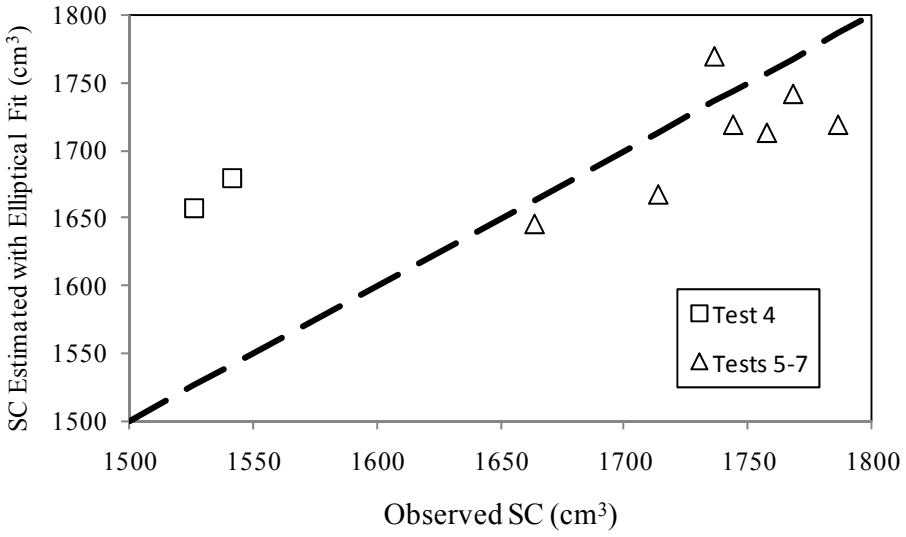

Figure 5.16: Storage capacity estimated via elliptical fit versus experimental observations

5.7 SUMMARY OF PROPOSED MODEL

Analysis in this chapter is presented in the form of a model that covers each stage of a geotextile capillary barrier's life cycle. Figure 5.17 presents a qualitative schematic of this model, showing changes in the volumetric moisture content profile with each stage: unsaturated flow down a soil profile (Figure 5.17a), arrival at soil-geotextile interface and creation of a capillary break (Figure 5.17b), build-up of moisture above the interface (Figure 5.17c), and breakthrough (Figure 5.17d).

Movement of the moisture front through the soil profile, shown in Figure 5.17a, is characterized by θ_{inflow}, determined from the limiting suction calculated with Equation 5.2, and v_{mf}, calculated with Equation 5.5. The time required for the moisture front to reach the geotextile interface, shown in Figure 5.17b, may be calculated with v_{mf}.

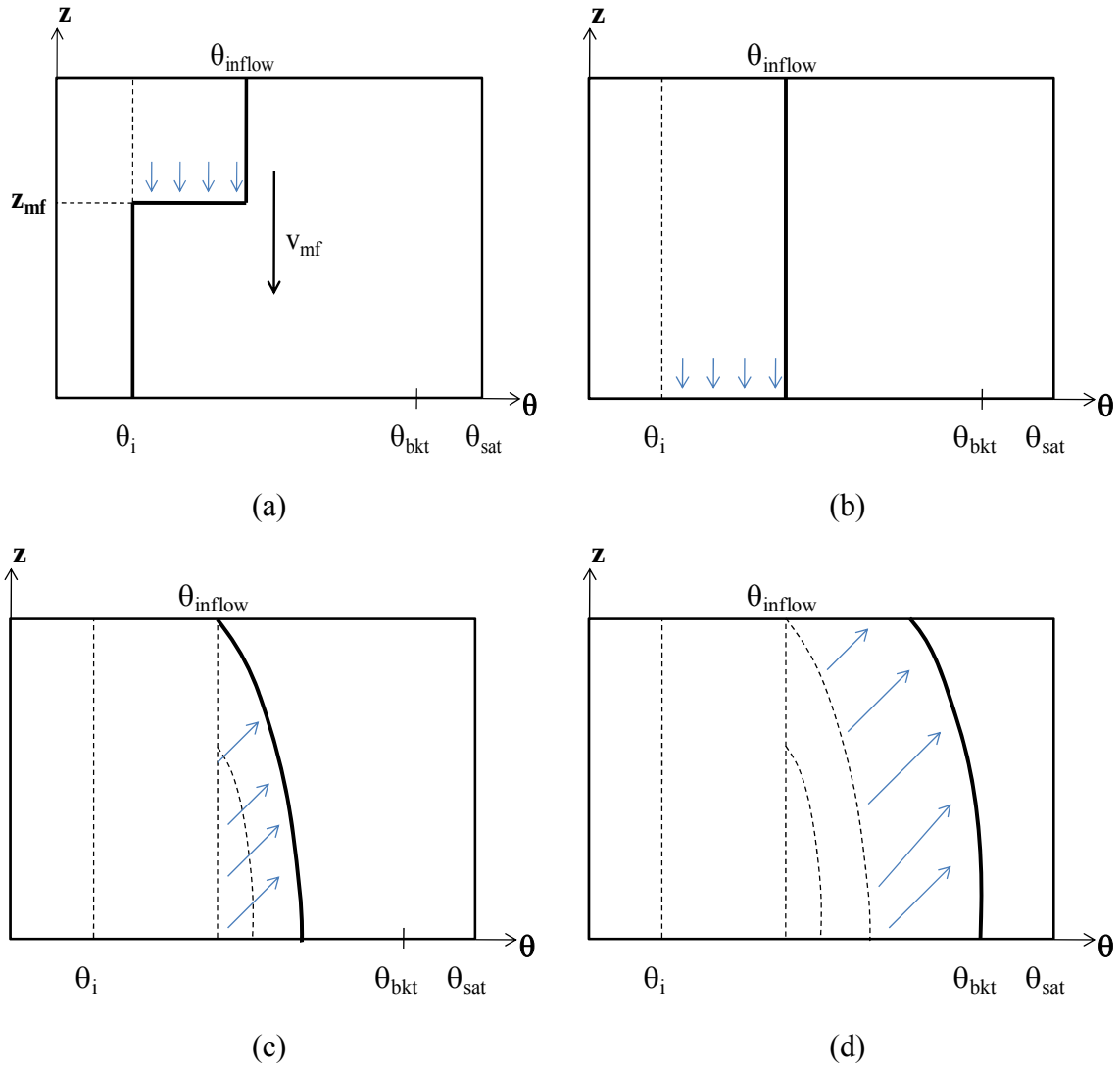

Figure 5.17: Qualitative schematic of capillary barrier model

Figure 5.17c is presented as a general estimate of the build-up of water above the geotextile interface, after creation of the capillary barrier and leading up to breakthrough. This behavior is chosen to resemble the general trend seen in columns tested in this study. For reference, moisture content profiles at breakthrough for each column are presented in Appendix A. From a review of the changes in moisture content profile with time, it appears that build-up above the capillary break is not characterized by a linear suction profile. The elliptical function better models the moisture content profile at breakthrough. While the moisture content profile appears to shift in an elliptical fashion, as shown in Figure 5.17c, it is not possible to model this shift more precisely given the experimental data.

Another major need for validation lies in the predicted θ_{inflow} value. As discussed in Chapter 4 and Section 5.1, many tests in this experimental study are not characterized by a clearly defined θ_{inflow}. More consistency between predicted and observed θ_{inflow} values is needed.

While some of the weaknesses in the model are noted, the overall goal in developing the model is still relevant. The model is presented to provide a framework for predicting an entire capillary barrier life cycle, given several site- and material-specific inputs. Required inputs include:

- soil water retention properties: WRC and θ_{sat}
- height of soil profile: H
- initial compaction conditions: θ_i (relative compaction is addressed by the soil WRC)
- applied flow rate: v

With these inputs, the model can conceptually predict each stage of the capillary barrier life cycle.

As an example application of the model, Figure 5.18 contains a comparison between predicted and observed behavior for Test 6, Column 1. Given the applied flow rate, $2.5*10^{-5}$ cm/s, a ψ_{lim} of 59 kPa is calculated with Equation 5.2. Using the soil WRC presented in Figure 3.8, θ_{inflow}, corresponding to a ψ_{lim} value of 59 kPa, is 0.23. The predicted v_{mf}, calculated with Equation 5.5, is $2.1*10^{-4}$ cm/s. Given this moisture front velocity, the top TDR probe is predicted to indicate a rise in moisture content from θ_i, approximately 0.11, to θ_{inflow}, 0.23, after 160 minutes. This is shown at time (*a*) in Figure 5.18. Similarly, the moisture front is modeled to reach the middle TDR at 560 minutes, shown as time (*b*), the bottom TDR at 1040 minutes, time (*c*), and the geotextile interface at 1200 minutes, time (*d*).

The volumetric moisture contents at breakthrough, shown as time (*e*) in Figure 5.18, were calculated with the elliptical function described in Section 5.5. An *a* value of 18.1 was used, as calibrated per the discussion in Section 5.5. The change in volumetric moisture content between times (d) and (e) is shown with dashed lines in Figure 5.18 because only an approximation may be made with the current state of the proposed model. However, this behavior was chosen to resemble results from the experimental testing, presented in Chapter 4.

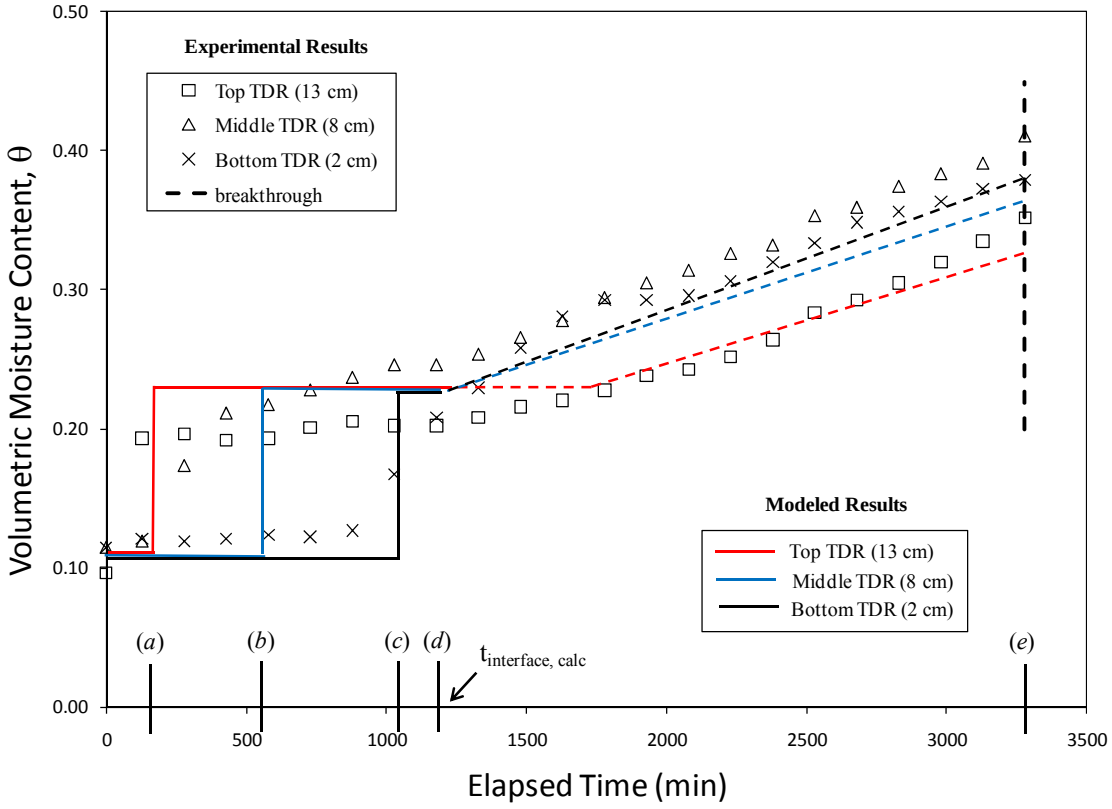

Figure 5.18: Modeled versus experimental results for Test 6, Column 1

Chapter 6: Conclusions and Recommendations

Understanding the capillary barrier phenomenon, specifically with regard to installation of nonwoven geotextiles in common engineered soil structures, is important in light of detrimental, often counter-intuitive behavior that may arise if unsaturated conditions are not appropriately accounted for during design (Bouazza 2006a, Richardson 1997). Recently, as the level of understanding has increased, more opportunities for the application of designed capillary barrier systems are being realized for common engineering structures such as landfills and roadways (Gabr et al. 2006, Bouazza 2006a, McCartney et al. 2005). However, while confidence in the formation and reliability of capillary barrier systems has increased, design information is lagging behind.

Identification of the soil and geotextile parameters critical for capillary barrier performance is imperative for effective design. So, too, are development of a standardized framework from which to assess capillary barrier behavior, and a laboratory characterization approach that is both widely accepted and commercially feasible. Accordingly, an experimental testing program was designed and completed in an effort to investigate geotextile capillary barrier performance in a laboratory setting.

6.1 SUMMARY

The testing approach centered on application of a known constant inflow to a model of a soil-geotextile capillary barrier system and monitoring the resultant moisture front progression and capillary barrier life cycle. Small soil columns were designed and constructed to facilitate observance of the moisture front progression. Tested columns consisted of soil and geotextile layers from an evapotranspirative landfill cover, containing a soil-geotextile capillary barrier, currently under construction at the Rocky

Mountain Arsenal close to Denver, Colorado. Time domain reflectometry (TDR) probes were included at three column elevations during compaction. The probes were used to monitor progression of the wetting front down the column, formation of a capillary barrier, and breakthrough as the critical suction was reached at the soil-geotextile interface.

The base testing setup was designed to make progress toward a more practical, economical laboratory setup for investigation of capillary barrier performance from what is currently found in the literature. Instrumentation was minimized—inexpensive mechanical pumps were used for application of low flow rates, no suction measurements were taken, only three volumetric moisture content probes were installed in each column, and a simple rain gauge was used for indication of breakthrough. Column height was minimized and applied flow rate maximized in an effort to achieve short testing times. In addition to measures taken with the column itself, a simple, economic laboratory test was used for unsaturated characterization of the geotextile used in this study.

A framework for predicting and analyzing the performance of capillary barrier laboratory models was developed from the literature and applied to the results of this testing program. Each stage of the life cycle of a capillary barrier is addressed within this framework—initial unsaturated flow of water down a soil profile, formation of a capillary break at the soil-geotextile interface, accumulation of water above the capillary break, and breakthrough.

Relative compaction of the soil layer was varied to investigate its influence on capillary barrier performance.

6.2 CONCLUSIONS

The following conclusions are drawn from this study:

1. Placement of a nonwoven geotextile beneath the lean clay used in this study consistently created a temporary capillary barrier when subjected to an applied inflow rate less than the soil's saturated hydraulic conductivity.
2. Breakthrough of the capillary barrier occurred at a suction close to that predicted by analysis of the hydraulic conductivity functions of both system components—soil and geotextile.
3. The breakthrough suction is also closely predicted by the water entry suction of the nonwoven geotextile.
4. Consistent with the results from this study as well as reported values in the literature, the water entry suction for a nonwoven geotextiles can reasonably be estimated as between 1 and 2 kPa.
5. The water content near the soil-geotextile interface at breakthrough remained relatively constant, regardless of variations in relative compaction and/or applied flow rate.
6. Characterization of the nonwoven geotextile water retention properties obtained via the capillary rise test compares well with results obtained for similar materials using other established laboratory methods.
7. The method of applying flow to the columns tested in this experimental program did not evenly distribute flow across the entire column surface area, leading to creation of a non-uniform wetting front and inconsistent flow patterns through a majority of the column height. This made it difficult to ascertain the effectiveness of methods used to predict θ_{inflow} and v_{mf}.

8. Observed moisture content profiles at failure varied significantly, but generally approached a constant volumetric moisture content in the bottom half of the column, higher than that observed near the top, as a result of the build-up of moisture from the capillary barrier.
9. An elliptical function may be used to reasonably model the moisture profile at breakthrough.
10. Capillary barrier storage capacity decreases with increasing relative compaction.

6.3 PRACTICAL IMPLICATIONS

Using the framework presented, a preliminary understanding of the performance of a particular soil-geotextile capillary barrier system may be obtained. The only laboratory characterization required involves obtaining the soil WRC. Providing a constant applied flow rate and initial soil conditions as inputs, a simplified model of unsaturated flow down the soil profile provides an estimate of the volumetric moisture content approached by the progressing wetting front, as well as the wetting front's average velocity.

Water retention characteristics of nonwoven geotextiles are very consistent in the literature, with water and air entry suctions typically lying within a range of 1 to 2 kPa. Accordingly, an estimate of a water entry head around 1 to 2 kPa may be confidently made for a nonwoven geotextile. For a coarse material of highly uniform pore size, such as a nonwoven geotextile, this narrow range also serves as an accurate estimate of the breakthrough suction. Such a narrow range in suction corresponds to a similarly narrow range in water contents in the WRC of fine soil generally used in soil-geotextile capillary

barrier systems. As a result, the volumetric water content of a cover soil near the soil-geotextile interface at the time of breakthrough may be accurately estimated.

Two options are presented for developing an estimate of the total moisture storage available as a result of the soil-geotextile capillary barrier system. The unit slope suction profile presented in Stormont and Morris (1998) may be converted to an equivalent moisture profile using the soil WRC. This study showed better performance with the use of an elliptical function.

The framework for analysis of a potential soil-geotextile capillary barrier design presented in this study, albeit overly simplified and certainly in need of further validation, is an attempt at combining observations on the various stages of a capillary barrier's life cycle into a complete model. Each aspect presents ample opportunity for future research.

6.4 Recommendations for Future Research

Many experimental difficulties were encountered during this study. Most notably, it was difficult to achieve a uniform wetting front near the top of the column. This was mainly attributed to a lack of even flow distribution across the top of the column. Future column tests should ensure that applied flow is evenly distributed, whether through a rainfall simulator or another approach.

Only one soil-geotextile parameter was investigated in this study—relative compaction of the soil layer. The most obvious parameter to vary in future tests is the geotextile itself. It would be interesting to continue the investigation of how water retention properties for various geotextiles compare and whether the capillary rise method for determining those retention properties continues to adequately predict the water entry value important for the proposed analysis.

The TDR probes used in this study were a bit problematic and cumbersome due to the complex data acquisition system used, as well as the need for analysis of each individual waveform. In order to achieve the goal of a quick, economical test that could potentially be utilized in a commercial setting, simpler instrumentation is needed. One alternative is the use of frequency domain reflectometry, or capacitance probes. These are similar to TDR probes in build and dimensions, but are typically characterized by a simple voltage output, easily collected and quickly analyzed with a simple calibration. In addition to greater ease of use, these probes and the accompanying acquisition equipment are significantly cheaper than the TDR approach. Capacitance probes are less established in the literature, but could potentially be very beneficial to a laboratory capillary barrier model approach to commercial characterization.

There are many gaps in the proposed model, covered in detail in Chapter 5. Prediction of θ_{inflow} needs further validation in future column tests. A more detailed picture of changes in the moisture profile with time should be obtained with more numerous moisture content sensors placed along a column height. The build-up of moisture content with time, between formation and breakthrough of the capillary barrier, needs to be more well-defined.

Various other objectives could be addressed with the column setup constructed as part of this experimental study. The effect of cycling capillary barrier events by repeated wetting and drying of the soil layer is very applicable to the real-world setting. Also applicable is a study into the effects of soil intrusion into the nonwoven geotextile. Pulsing rainfall and drying events is certainly more realistic than a constant applied flow rate for several days, and would provide interesting insight into expectations of a soil-geotextile capillary barrier in the field.

Appendix A: Moisture Content Profiles with Time

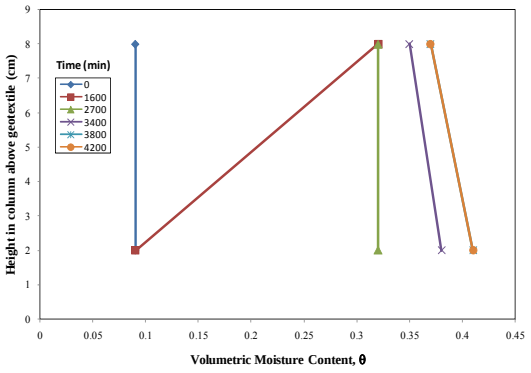

(a)

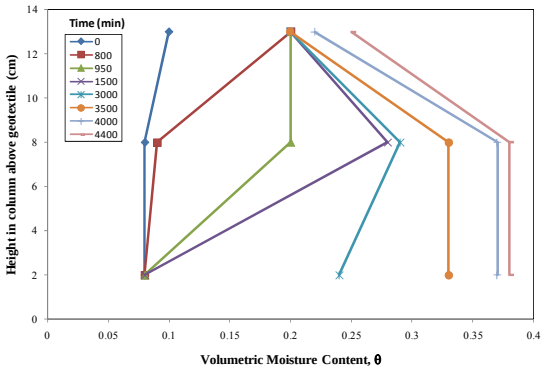

(b)

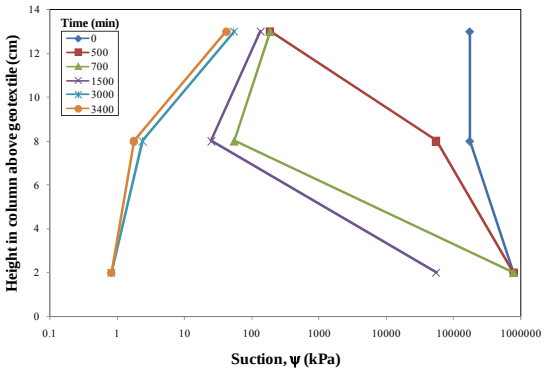

(c)

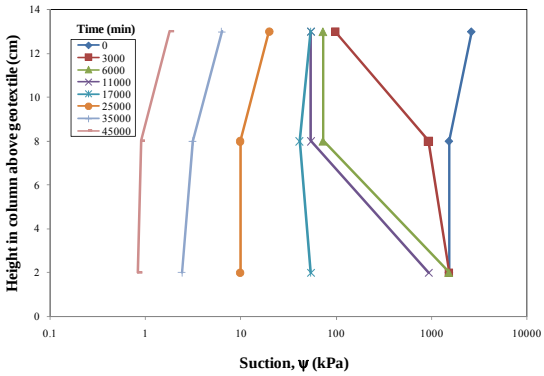

(d)

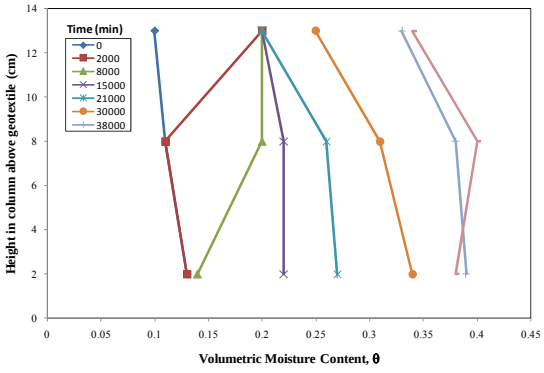

(e)

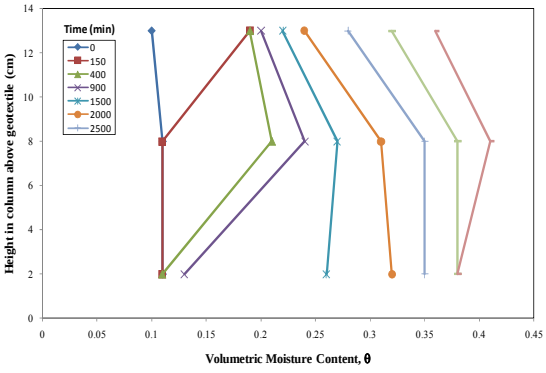

(f)

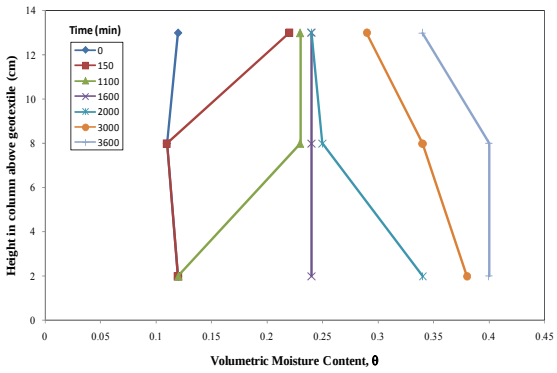

(g)

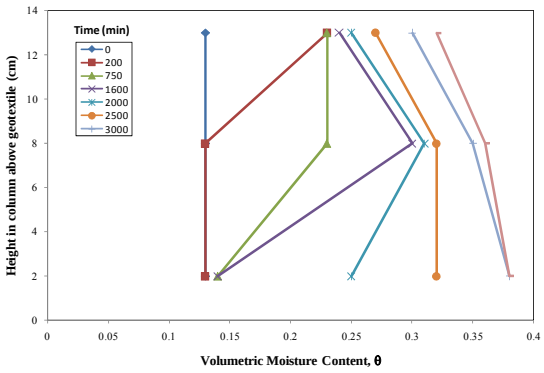

(h)

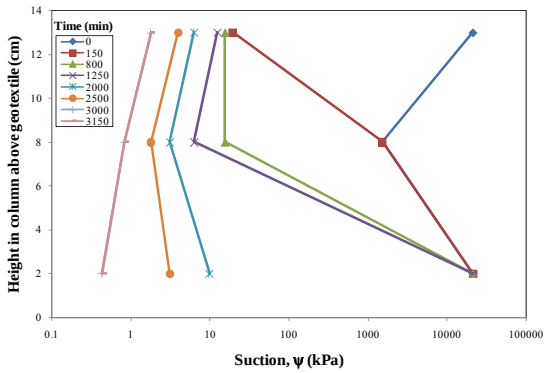

(i)

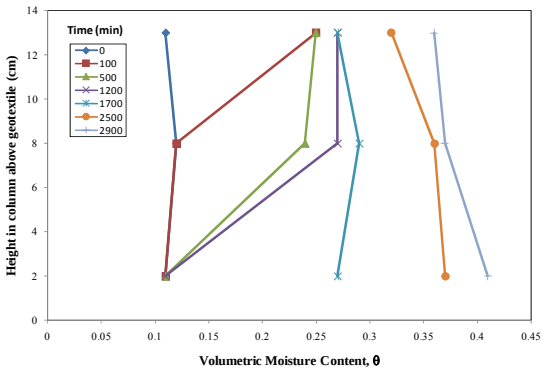

(j)

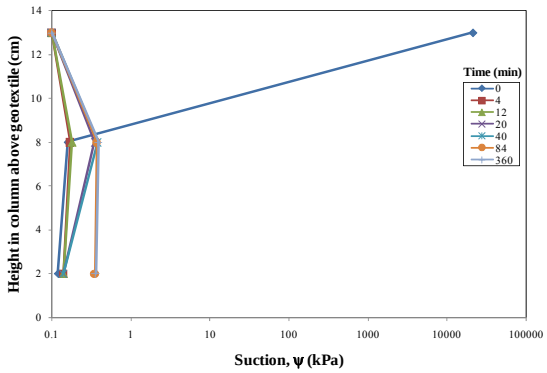

(k)

Figure A.1: Volumetric moisture profiles with time for (a) Test 2, (b) Test 4 Col. 1, (c) Test 4 Col. 2, (d) Test 5 Col. 1, (e) Test 5 Col. 2, (f) Test 6 Col. 1, (g) Test 6 Col. 2, (h) Test 6 Col. 3, (i) Test 7 Col. 1, (j) Test 7 Col. 2, (k) Test 8

References

American Society of Testing and Materials. (2002). "Determination of the Soil Water Characteristic Curve for Desorption Using a Hanigng Column, Pressure Extractor, Chilled Mirror Hygrometer, and/or Centrifuge." *ASTM D6836*. West Conshohocken, Pennsylvania.

American Society of Testing and Materials. (2003). "Standard Test Methods for Measurement of Hydraulic Conductivity of Saturated Porous Materials Using a Flexible Wall Permeameter." *ASTM D5084*. West Conshohocken, Pennsylvania.

American Society of Testing and Materials. (2005). "Standard Test Methods for Liquid Limit, Plastic Limit, and Plasticity Index of Soils." *ASTM D4318*. West Conshohocken, Pennsylvania.

American Society of Testing and Materials. (2006a). "Standard Test Methods for Specific Gravity of Soil Solids by Water Pycnometer." *ASTM D854*. West Conshohocken, Pennsylvania.

American Society of Testing and Materials. (2006b). "Standard Practice for Classification of Soils for Engineering Purposes (Unified Soil Classification System)." *ASTM D2487*. West Conshohocken, Pennsylvania.

American Society of Testing and Materials. (2007a). "Standard Test Method for Particle-Size Analysis of Soils." *ASTM D422*. West Conshohocken, Pennsylvania.

American Society of Testing and Materials. (2007b). "Standard Test Methods for Laboratory Compaction Characteristics of Soil Using Standard Effort (12 400 ft-lbf/ft^3 (600 kN-m/m^3))." *ASTM D698*. West Conshohocken, Pennsylvania.

Bathurst, Richard J., Alvin F. Ho, and Greg Siemens (2007) "A Column Apparatus for Investigation of 1-D Unsaturated-Saturated Response of Sand-Geotextile Systems," *Geotechnical Testing Journal*, Vol. 30, No. 6, pp 1-8.

Bouazza, Abdelmalek, Jorge G. Zornberg, John McCartney, and Hani Nahlawi (2006a) "Significance of Unsaturated Behaviour of Geotextiles in Earthen Structures," *Australian Geomechanics*, Vol. 41, No. 3, pp 133-142.

Bouazza, Abdelmalek, Michelle Freund, and Hani Nahlawi (2006b) "Water Retention of Nonwoven Polyester Geotextiles," *Polymer Testing*, Vol. 25, pp 1038-1043.

Campbell Scientific. (2007). "Instruction Manual—TDR100." Revision: 04/2007. Logan, Utah.

Dell'Avanzi, E., Zornberg, J.G., and Cabral, A.R. (2004) "Suction Profiles and Scale Factors for Unsaturated Flow Under Increased Gravitational Field." *Soils and Foundations*. Vol. 44, No. 3, pp. 1-11.

Gabr, Mohammed A., Brent Robinson, James G. Collin, and Ryan R. Berg (2006) "Promoting Geosynthetics Use on Federal Lands Highway Projects," p 116.

Golder Associates (2008) "Construction Quality Assurance for the Shell Disposal Trenches RCRA-Equivalent Cover Construction," Rocky Mountain Arsenal, Commerce City, Colorado. April 2008. 74 pp.

Henry, K.S. (1996) "Geotextiles to Mitigate Frost Effects in Soils: A Critical Review," Transportation Research Record No. 1534, Transportation Research Board, Washington, D.C., pp. 5-11.

Holtz, R. D., Christopher, B. R., Berg, R. R. (1998) *Geosynthetic Design and Construction Guidelines*, FHWA Technical Report No. FHWA-HI-95-038, Federal Highway Administration, Washington, D. C., April 1998.

Iryo, T., and R. Kerry Rowe (2003) "On the Hydraulic Behavior of Unsaturated Nonwoven Geotextiles," *Geotextiles and Geomembranes*, Vol. 21, pp 381-394.

Iryo, T., and R. Kerry Rowe (2006) "Infiltration into an Embankment Reinforced by Nonwoven Geotextiles," *Canadian Geotechnical Journal*, Vol. 42, No. 4, pp. 1145-1159.

Koerner, R. M. (2005) *Designing with Geosynthetics (4th Ed.)*, Prentice-Hall Book Co., Upper Saddle River, NJ.

Krisdani, Henry, Harianto Rahardjo, and Eng-Choon Leong (2006) "Experimental study of 1-D capillary barrier model using geosynthetic material as the coarse-grained layer," *Unsaturated Soils 2006*. Carefree, AZ: ASCE, pp 1683-1694.

Krisdani, H., Rahardjo, H., and Leong, E.-C. (2008) "Measurement of Geotextile-Water Characteristic Curve Using Capillary Rise Principle," *Geosynthetics International*, Vol. 15, No. 2, pp. 86-94.

Lafleur, J., Lebeau, M., Faure, Y.-H., Savard, Y., Kehila, Y., 2000. Influence of matric suction on the drainage performance of polyester geotextiles. *Proceedings of the 53rd Annual Conference of the Canadian Geotechnical Society: Geotechnical Engineering for the Urban Infrastructures*, Montreal, Canada, pp. 1115–1122.

Ledieu, J., De Ridder, P., De Clerck, P. and Dautrebande, S. (1986) "A Method of Measuring Soil Moisture by Time-Domain Reflectometry," *Journal of Hydrology*, Vol. 88, pp. 319-328.

McCartney, John S. (2007) "Determination of the Hydraulic Characteristics of Unsaturated Soils Using a Centrifuge Permeameter." Diss. University of Texas at Austin, 2007.

McCartney, John, Jeffrey A. Kuhn, and Jorge G. Zornberg (2005) "Geosynthetic Drainage Layers in Contact with Unsaturated Soils," pp 2301-2305.

McCartney, J. S., Villar, L. and Zornberg, J. G. (2008) "Nonwoven Geotextiles as Hydraulic Barriers to Capillary Rise," *GeoAmericas*, Cancun, Mexico, March 3-5, 2008.

Mualem (1976) "A new model for predicting the hydraulic conductivity of unsaturated porous media," *Water Resource Research*, Vol. 12, pp. 513-522.

Noborio, K. (2001) "Measurement of Soil Water Content and Electrical Conductivity by Time Domain Reflectometry: A Review," *Computers and Electronics in Agriculture*, Vol. 31, pp. 213-237.

Richardson, G. (1997) "Fundamental Mistakes in Slope Design," *Geotechnical Fabrics Report*, Vol. 15, No. 2, pp. 15-17.

Steward, J. W., Williamson, J., and Mohney, R., (1977) *Guidelines for the Use of Fabrics in Construction and Maintenance of Low-Volume Roads*, USDA, Forest Service, Portland, OR.

Stormont, John C., and Clifford E. Anderson (1999) "Capillary Barrier Effect from Underlying Coarser Soil Layer," *Journal of Geotechnical and Geoenvironmental Engineering*, Vol. 125, No. 8, pp 641-648.

Stormont, John C., Karen S. Henry, and T. M. Evans (1997) "Water Retention Functions of Four Nonwoven Polypropylene Geotextiles," *Geosynthetics International*, Vol. 4, No. 6, pp 661-672.

Stormont, John C., and Carl E. Morris (1998) "Method to Estimate Water Storage Capacity of Capillary Barriers," *Journal of Geotechnical and Geoenvironmental Engineering*, Vol. 124, No. 4, pp 297-302.

Stormont, John C., and Ramos, R. (2004) "Characterization of a Fiberglass Geotextile for Unsaturated In-Plane Water Transport," *Geotechnical Testing Journal*, Vol. 27, No. 2, pp. 1-6.

Stormont, John C., and Shenxiong Zhou (2005) "Impact of Unsaturated Flow on Pavement Edgedrain Performance," *Journal of Transportation Engineering*, Vol. 131, No. 1, p 8.

Tang, Y. (2009) Unpublished Master's Thesis. University of Texas at Austin.

Topp, G. C., and Reynolds, W. D. (1998) "Time domain reflectometry: A Seminal Technique for Measuring Mass and Energy in Soil," *Soil & Tillage Research*, Vol. 47, pp. 125-132.

Tinjum, J., Benson, C., and Blotz, L. (1997) "Soil-Water Characteristic Curves for Compacted Clays." *Journal of Geotechnical and Geoenvironmental Engineering*, Vol. 123, No. 11, pp. 1060-1069.

Yang, H., Rahardjo, H., Leong, E.C., and Fredlund, D.G. (2004) "A Study of Infiltration on Three Sand Capillary Barriers." *Canadian Geotechnical Journal*, Vol. 41, pp. 629-643.

Zornberg, J. G., and Christopher, B. R. (1999) "Chapter 27: Geosynthetics," *The Handbook of Groundwater Engineering*, CRC Press, Inc., Boca Raton, FL.

Vita

Nathan Evan Thompson was born April 12, 1985 in Bowling Green, Kentucky, to James and Sheila Thompson. He has one sibling, Katherine Grace Thompson, an older sister. After graduating from Warren East High School in 2003, he began his studies in Civil Engineering at the University of Kentucky. Nathan obtained a Bachelor of Science degree in Civil Engineering in May of 2007. In August of 2007, he began his graduate studies in the Geotechnical Engineering group of the Department of Civil, Architectural, and Environmental Engineering at the University of Texas at Austin.

Permanent address: 1579 Mt. Olivet-Girkin Rd
Bowling Green, KY 42101

This thesis was typed by Nathan Thompson.